Final Report On Project

Single-stage Earth-orbital Reusable Vehicle
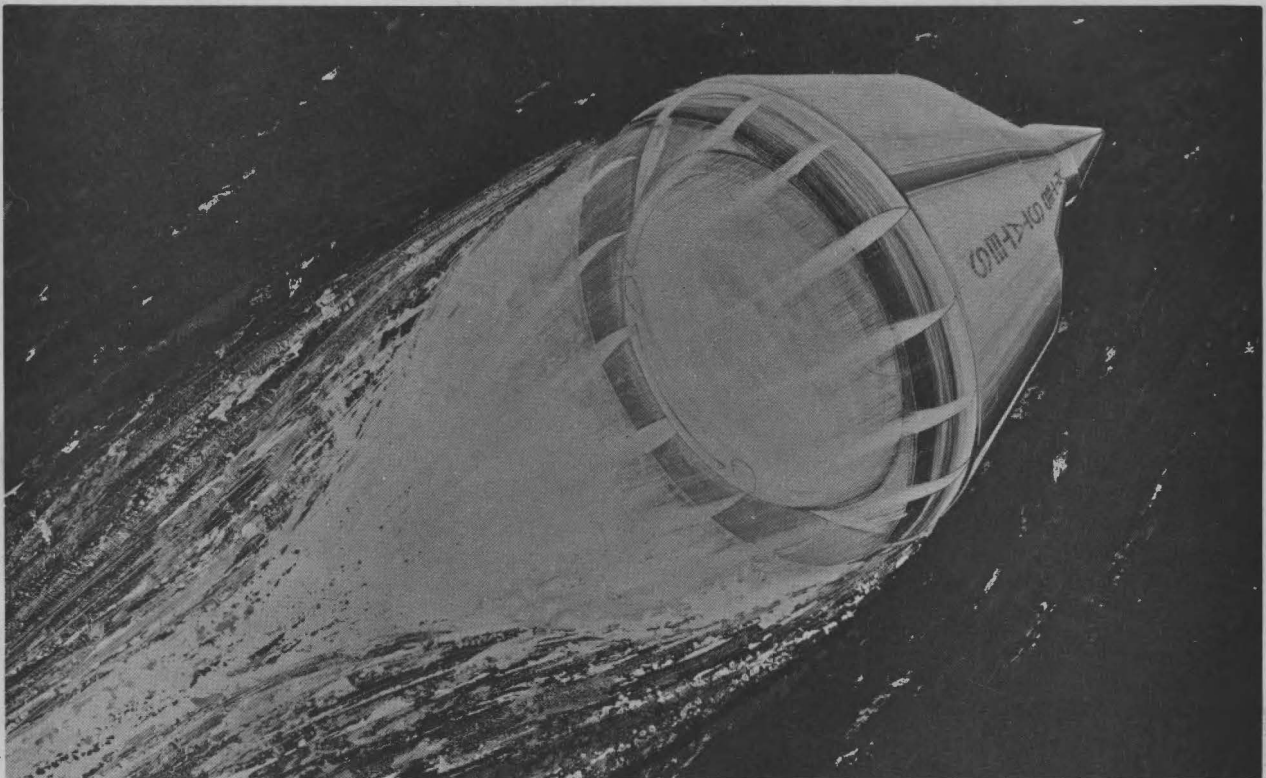
SPACE SHUTTLE FEASIBILITY STUDY

volume 1   contract NAS8-26341

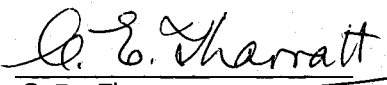summary   june 30, 1971

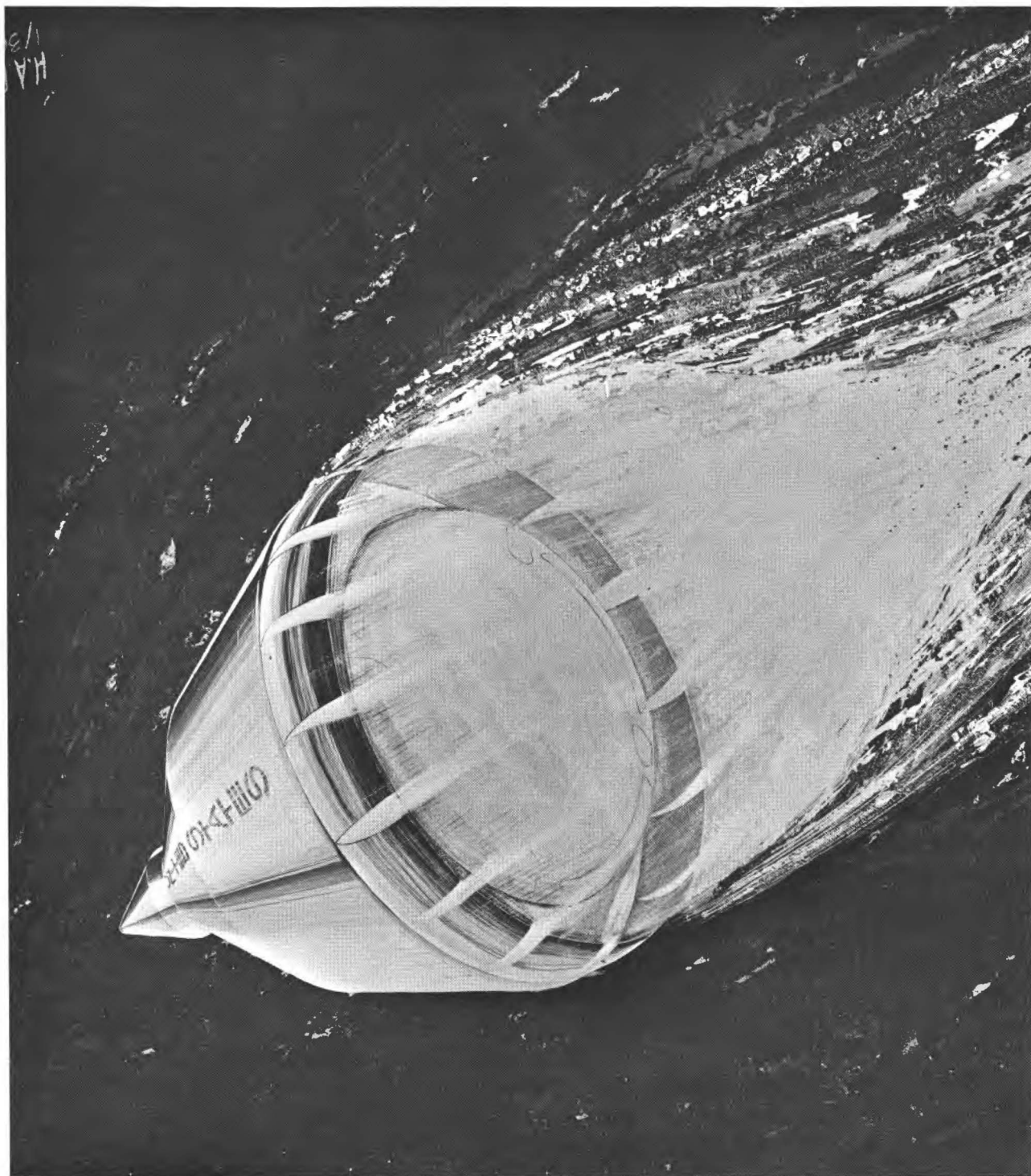Final Report On Project

SINGLE-STAGE EARTH-ORBITAL REUSABLE VEHICLE

SPACE SHUTTLE FEASIBILITY STUDY

volume 1

summary

contract NAS8-26341

june 30, 1971

approved: _C. E. Tharratt_

C.E. Tharratt

Project Manager - SERV

FOREWORD

This volume is one of a 6-volume final report of the Study of a Single-stage Earth-orbital Reusable Vehicle (SERV). The study was conducted by the Chrysler Corporation Space Division (CCSD) for the National Aeronautics and Space Administration, George C. Marshall Space Flight Center under Contract NAS8-26341. The purpose of the study was to evaluate the potential of SERV as the boost element of a candidate space transportation system. To establish the SERV potential, five key technical areas affecting concept feasibility were identified for examination: engine performance, aerodynamic characteristics, thermal protection, subsystem weights, and the landing method. The results of these analyses are published in a final report consisting of the following six volumes:

Volume 1 Summary
Volume 2 Aerodynamic Model Testing
Volume 3 Concept Evaluation
Volume 4 Vehicle Definition
Volume 5 Operations Definition
Volume 6 Resources

Chrysler gratefully acknowledges the cooperation and support of North American Rockwell Corporation, Rocketdyne Division, who under subcontract assisted in the model test, and analyzed the test results of the uniquely integrated SERV engine-to-structure concept. Rocketdyne also generated parametric engine data and designed the SERV aerospike engine. Chrysler also acknowledges the support and technical assistance received from Detroit Diesel Allison Division of General Motors Corporation who provided parametric engine data for advanced technology direct lift gas turbine engines and the AVCO Systems Division who provided design and cost data for thermal protection systems. In addition, acknowledgement is made to the following NASA and DOD agencies for their cooperation during wind tunnel testing: NASA-Ames, NASA-LaRC, NASA-MSFC, and AF-AEDC.

The study was managed and supervised by:

Charles E. Tharratt   Study Manager
William R. Baldwin   Principal Systems Analyst
John H. Wood   Principal Performance Analyst
Arthur P. Raymond, III   Principal Program Analyst

of the Chrysler Corporation Space Division, supported by Robert E. Schnurstein of the North American Rockwell Corporation, Rocketdyne Division. The study was conducted under the direction of Robert J. Davies, NASA study manager.

TABLE OF CONTENTS

LIST OF ILLUSTRATIONS

Section 1
INTRODUCTION

1.0 GENERAL

The potential advantage of the SERV concept could become reality if the feasibility of the concept can be established. Previous Chrysler in-house studies indicated the concept was feasible within the limitations of available data; however, it was recognized that certain technical aspects for determining feasibility required inputs of higher quality data than those available before the concept can progress to a preliminary definition phase. It was planned to obtain the improved data during the course of this study contract.

1.1 STUDY OBJECTIVE AND EXPECTED RESULTS

The study objective was to further assess the feasibility of the SERV concept by selecting an appropriate configuration, determining the feasibility of the large diameter aerospike engine to meet the SERV requirements, and performing a more definitive design and weight analysis to support the necessary single-stage mass fraction requirements.

Study effort was divided into seven tasks, the output of which form the expected results. A brief synopsis of these expected results is as follows:

1) The development of the vehicle configuration to be used as the initial or preliminary baseline for the study, including a detailed comparison with previous single-stage-to-orbit vehicles.

2) Determination of base flow characteristics, and the determination of ascent and reentry static stability and drag characteristics for the baseline vehicle.

3) Substantiation of baseline concept, including the aerospike engine, through trade studies and parametric vehicle sizing analysis.

4) A point design of a selected configuration and its aerospike engine, including concept sensitivities.

5) Minimum definition of operations, project plans, schedules and costs.

1.1.1 PRINCIPAL GROUND RULES

The NASA-approved ground rules were patterned after those of the other shuttle studies wherever possible to ensure the best possible comparison.

Certain revisions requested by NASA were impacted during the latter portion of the study, and these will be discussed later. The principal ground rules were as follows:

1) Fully reusable single-stage-to-orbit vehicle, spacecraft study excluded;

2) vertical take-off and landing;

3) reference mission is logistics resupply of space station;

4) design reference orbit is 270-nm circular by 55-deg inclination from 28.5 degrees north latitude;

5) 25,000 lb of gross cargo to 55-deg 270-nm orbit and return;

6) maximum payload capability to polar orbit and low inclination orbit to be identified;

7) cargo hold sized for a minimum clear volume of 15-ft dia x 60-ft long;

8) baseline ascent main propulsion is an integral aerospike rocket engine;

9) baseline landing propulsion is an array of jet engines using JP-4 fuel;

10) intact abort capability to be provided;

11) peak acceleration and deceleration not to exceed 3g;

12) return to preselected site minimum of once every 24 hours;

13) vehicle life of 10 years and 100 missions.

1.1.2 STUDY SCHEDULE

A summary of the study schedule identifying the critical path is presented in figure 1.1-1.

1.2 BASELINE DEVELOPMENT

Because SERV has unorthodox features, NASA directed that Task 1 of this study be mainly devoted to researching past single-stage-to-orbit (SSTO) studies to ensure that accumulated experience and desirable system characteristics identified in those studies were incorporated in the development of a baseline vehicle. This baseline SERV was to form the starting point of all further study effort. Nine SSTO vehicles, including SERV, were examined (see figure 1.2-1.) They varied from SASSTO to NEXUS; a range in gross liftoff weight of approximately 220 thousand to 24 million pounds. The diverse nature of the nine configurations ranged from the non-recoverable MLLV (most efficient SSTO due to its low drag ascent profile) through several partially recoverable concepts that are not appropriate for current NASA requirements, to several vehicles that could be considered or adapted to be fully reusable.
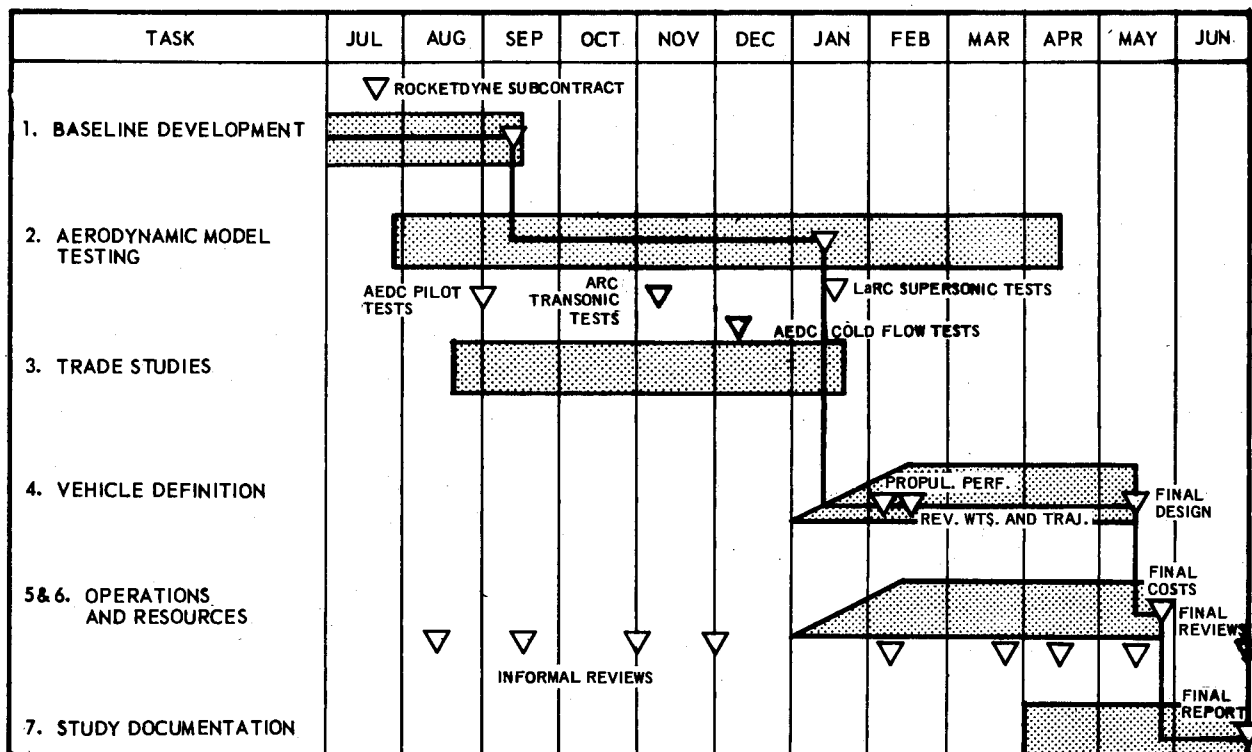
Figure 1.1-1.   Study Schedule Identifying Critical Path
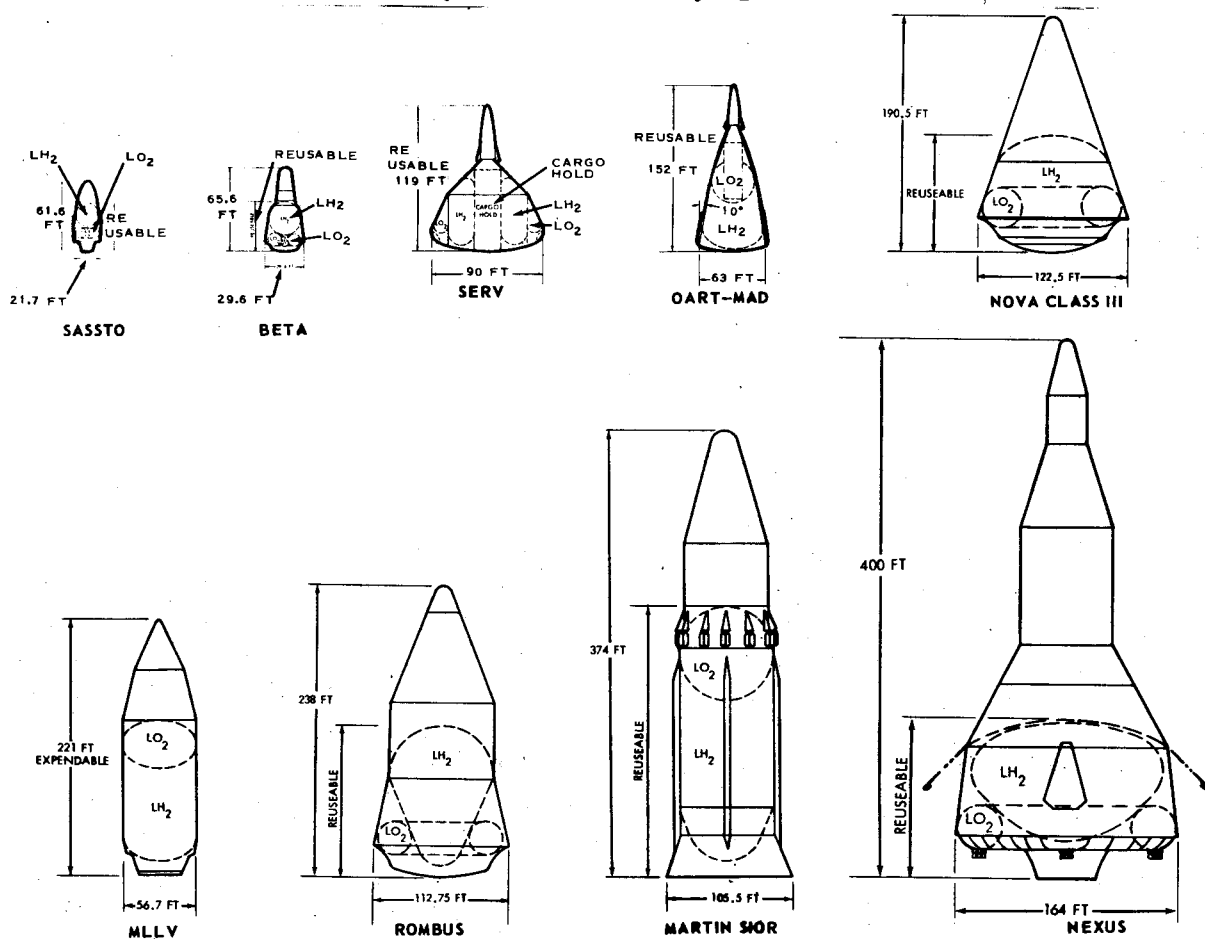
Figure 1.2-1.   Baseline Vehicle Development - Alternate SSTO Characteristics

1.2.1 PRIMARY CONSIDERATIONS

From these investigations, it was established that the most important considerations in vehicle subsystem characteristic selection were the study ground rules, ascent propulsion, reentry and landing mode, external shape and internal arrangement. Of these considerations, study ground rules were the most influential. The SERV study ground rule of 3g maximum deceleration during reentry greatly influenced, or essentially dictated, the external configuration. The characteristics of SERV were recognized as a compromise between ascent and reentry performance; the former, requiring a slim, low drag, ascent profile; the latter a low weight, large frontal area, high drag profile of low reentry ballistic factor $(W/C_D A)$.

The internal arrangement was demonstrated to be greatly influenced by the need to package the ascent and landing propulsion and propellant tanks within the mission-dictated external shape in as small a volume as possible.

The trade study baseline was not changed as a result of these investigations.

1.2.2 TRADE STUDY BASELINE

The baseline vehicle for trade study consideration and aerodynamic model tests is presented in figure 1.2-2. Key features are identified and changes are summarized under trade study results. The baseline vehicle with alternate payload shapes is shown in figure 1.2-3.

The baseline vehicle has a liftoff weight of 4.5 million pounds, a liftoff thrust of 5.4 million pounds, and boosts 88,060 pounds to the baseline mission parking orbit of 100 nautical miles at 55 degrees inclination. Vehicle diameter is 90 ft and the cargo hold dimensions are 23 feet in diameter by 60 feet in length. The 12-module LO_2/LH_2 integral aerospike engine is 88.7 feet in diameter by 8.2 feet in length and has a sea-level and vacuum specific impulse of 346.7 seconds and 469.5 seconds, respectively. An installation of 28, JP-4 fueled turbojet lift engines provides deceleration and landing propulsion.

1.2.3 SERV OPERATION

The baseline SERV is propelled to earth orbit by the thrust of an integral aerospike rocket engine. In operation (figure 1.2-4), the SERV with a spacecraft and a cargo module as its payload takes off vertically from the Kennedy Space Center (KSC) and goes to a 100 nm orbit in the plane of a space station. The spacecraft then extracts the cargo module from SERV and transfers the cargo to the space station in higher orbit. Following a transfer of cargo to and from the space station, the spacecraft returns with the cargo module and docks to SERV in lower orbit. If an optional winged spacecraft is used, the spacecraft disengages after docking the cargo module and returns to earth using swing wings in the lower atmosphere. Due to a relatively high hypersonic L/D, it has a cross range capability of 1800 nm.

SERV remains in low earth orbit until required to reenter and return to KSC. To accomplish this reentry, SERV reorients itself to the familiar Apollo command
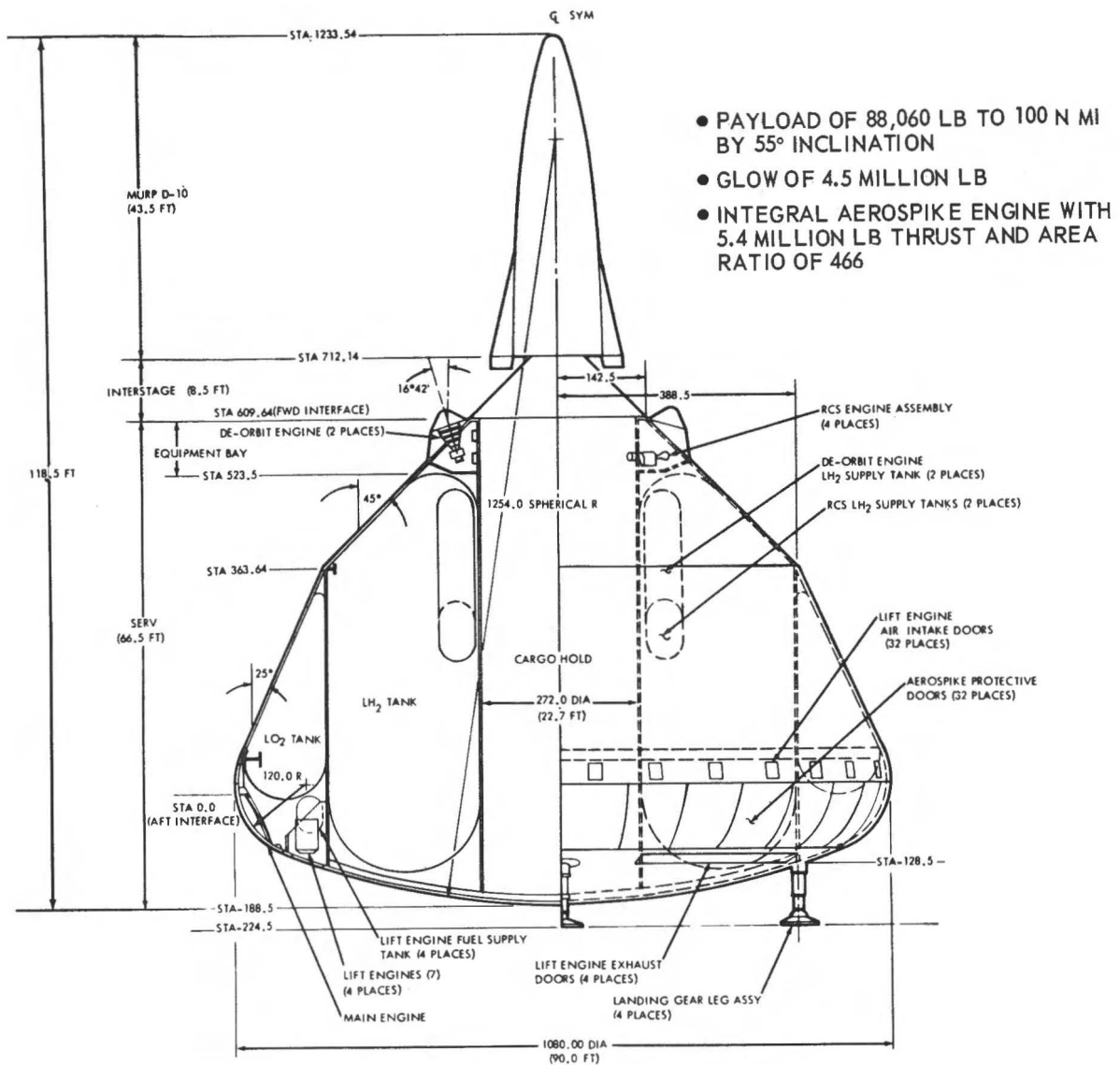
Figure 1.2-2. Baseline Vehicle Arrangement

Labels in figure:

STA 1233.54 — ₵ SYM

PAYLOAD OF 88,060 LB TO 100 N MI BY 55° INCLINATION

GLOW OF 4.5 MILLION LB

INTEGRAL AEROSPIKE ENGINE WITH 5.4 MILLION LB THRUST AND AREA RATIO OF 466

MURP D-10 (43.5 FT)

STA 712.14

INTERSTAGE (8.5 FT)

16°42'

142.5

388.5

STA 609.64 (FWD INTERFACE)

DE-ORBIT ENGINE (2 PLACES)

RCS ENGINE ASSEMBLY (4 PLACES)

EQUIPMENT BAY

STA 523.5

118.5 FT

45°

1254.0 SPHERICAL R

DE-ORBIT ENGINE LH₂ SUPPLY TANK (2 PLACES)

RCS LH₂ SUPPLY TANKS (2 PLACES)

STA 363.64

SERV (66.5 FT)

CARGO HOLD

25°

LH₂ TANK

272.0 DIA (22.7 FT)

LIFT ENGINE AIR INTAKE DOORS (32 PLACES)

AEROSPIKE PROTECTIVE DOORS (32 PLACES)

LO₂ TANK

120.0 R

STA 0.0 (AFT INTERFACE)

STA -128.5

STA -188.5

STA -224.5

LIFT ENGINE FUEL SUPPLY TANK (4 PLACES)

LIFT ENGINES (7) (4 PLACES)

LIFT ENGINE EXHAUST DOORS (4 PLACES)

LANDING GEAR LEG ASSY (4 PLACES)

MAIN ENGINE

1080.00 DIA (90.0 FT)

MODULAR SPACECRAFT

WINGED SPACECRAFT

EXTENDED MODULAR SPACECRAFT

LARGE PAYLOAD (REUSABLE OR EXPENDABLE SERV)

Figure 1.2-3. Alternate Configurations

1-5
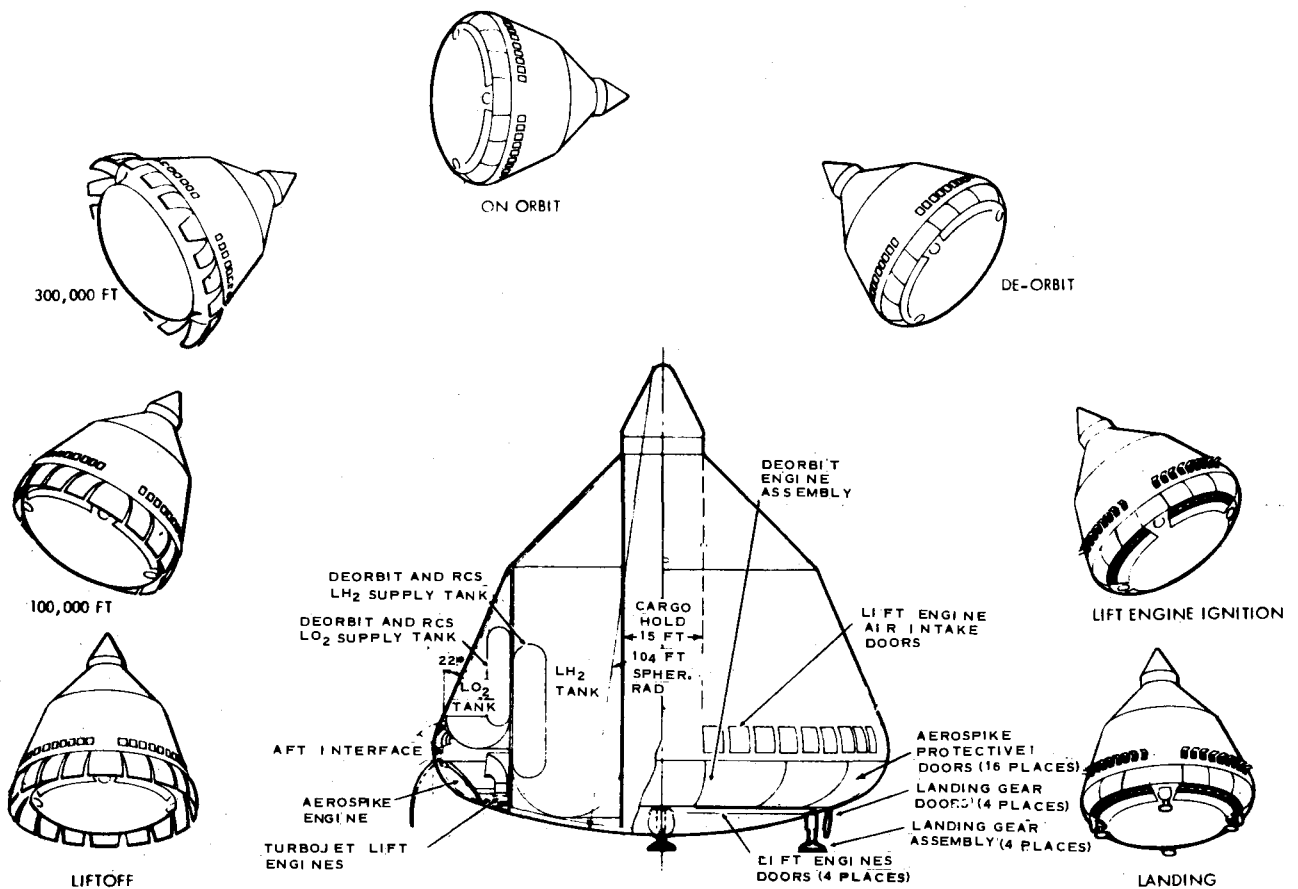
Figure 1.2-4. SERV Operation

module reentry attitude and reenters the atmosphere semiballistically. With SERV, however, the target landing point is on land instead of water, and more specifically, within operational distance of the Vertical Assembly Building (VAB) at KSC. Using current Apollo reentry navigation and guidance technology, SERV will be within 4 miles of the landing pad when it is at 25,000 ft. Prior to this point, SERV will be tracked by radar and a ground based command transmitter will be transmitting landing site coordinate data. At 25,000 ft altitude, air intakes and doors for exhaust efflux open and ignition of four quadrants of direct lift gas turbine engines occurs.

The landing phase begins at approximately 15,000 ft with the gas turbine thrust being used to horizontally translate and decelerate the vehicle to a hover above the landing pad. The landing gear is deployed and a controlled descent to the landing pad is initiated. The final descent and touchdown is similiar in operation to that of a helicopter.

1.3 TRADE STUDY RESULTS

Trade study results were described in detail in the November 30th Status Review and the February 10th Mid-term Review; only a brief summary is presented here.

1.3.1 KEY FEASIBILITY ISSUES

The potential of SERV depends chiefly on the satisfactory solution of six key issues affecting concept feasibility. These issues are arranged in figure 1.3-1 with respect to their affect on the ascent and descent SERV configurations. Engine performance, aerodynamic drag, and subsystem weights have a decisive collective influence on vehicle ascent performance; i.e., the ability to meet mission objectives. The method and type of thermal protection during the reentry environment, descent aerodynamic characteristics and landing method, determine the attractiveness of SERV as a recoverable and reusable space shuttle. These subjects were investigated during the trade study period, with incorporation of results from supporting aerodynamic model tests.

ASCENT CONFIGURATION

DESCENT CONFIGURATION
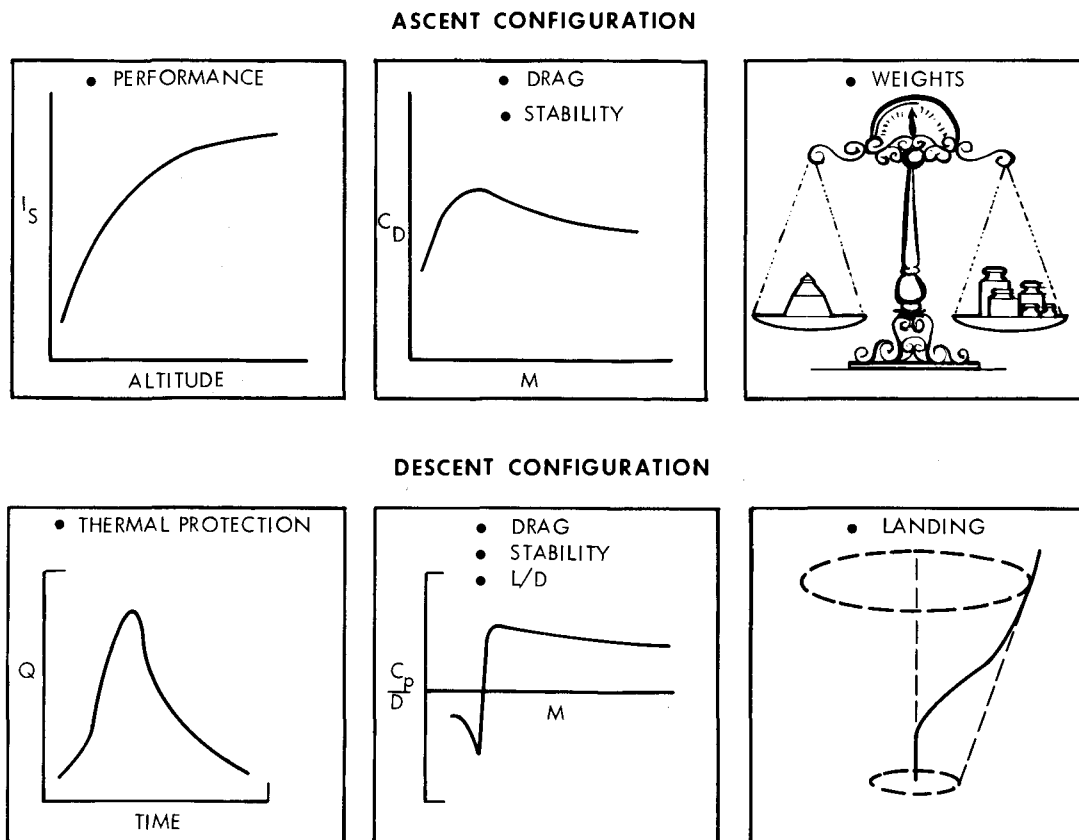
Figure 1.3-1. Key Feasibility Issues

1.3.2 CONCEPT EVALUATION AREAS

Subsystem trade analyses were performed in seven areas, as indicated in figure 1.3-2: ascent configuration, structural and vehicle arrangement, descent configuration, avionics, auxiliary propulsion, ascent propulsion, and landing propulsion. The results of these analyses were reflected as changes to the vehicle dry weight and performance.

ASCENT CONFIGURATION

- ALTERNATE PAYLOAD SHAPES
- AEROSPIKE DOOR SHAPE AND OPERATION
- THERMAL PROTECTION
- VEHICLE SIZING

STRUCTURAL AND VEHICLE ARRANGEMENT

- PRIMARY STRUCTURE ALTERNATIVES
- STRUCTURAL MATERIAL ALTERNATIVES
- AEROSPIKE AND TURBOJET INSTALLATION
- HIGH-PRESSURE BELL ENGINE INSTALLATION
- PROPELLANT TANK INSULATION
- THERMAL PROTECTION DOOR INSTALLATION
- LANDING GEAR INSTALLATION
- BASE HEAT SHIELD INSTALLATION
- VEHICLE SIZING

DESCENT CONFIGURATION

- L/D AND W/C$_D$A CONFIGURATION ALTERNATIVES
- INSULATION MATERIALS
- HEAT SHIELD DESIGN ALTERNATIVES
- HEAT SHIELD DOOR SEALS AND OPERATION
- AEROSPIKE PROTECTION DOOR ALTERNATIVES
- LANDING GEAR ALTERNATIVES
- VEHICLE SIZING

AVIONICS

- GN&C
- POWER
- COMMUNICATIONS

AUXILIARY PROPULSION

- PITCH-YAW CONTROL ALTERNATIVES
- ROLL CONTROL ALTERNATIVES
- DEORBIT ALTERNATIVES

ASCENT PROPULSION

- ENGINE COMPARTMENT ARRANGEMENT
- AEROSPIKE INTERNAL ARRANGEMENT
- AEROSPIKE DUAL COMBUSTOR ALTERNATIVE
- PROPELLANT TANKAGE ARRANGEMENT
- HIGH-PRESSURE BELL ENGINE ALTERNATIVE

LANDING PROPULSION

- TURBOJETS VERSUS TURBOFANS
- LANDING ROCKET VERSUS TURBOJET
- AEROSPIKE RESTART VERSUS TURBOJET
- JP-4 VERSUS HYDROGEN FUEL
- JET INLET AND OUTLET GEOMETRIES
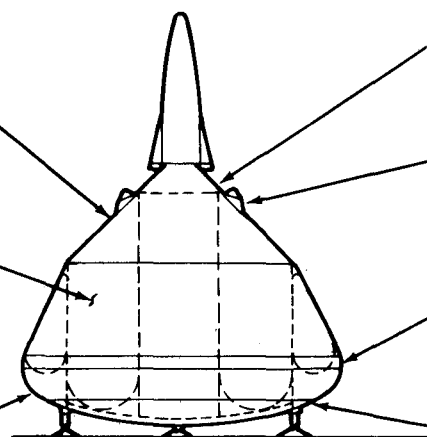
Figure 1.3-2. Concept Evaluation Areas

Section 2

FINAL CONFIGURATION DEFINITION

2.0 GENERAL

In this section the SERV configuration evaluation, sizing criteria and final definition are discussed.

2.1 SERV CONFIGURATION EVOLUTION

Figure 2.1-1 traces the evolution of SERV during the study. The trade studies commenced with a baseline SERV of 90-ft. diameter and a 4.5 million pound GLOW. Incorporation of results obtained from wind tunnel tests to establish the aerodynamic characteristics and to determine the aerospike engine performance, plus more definitive evaluation of structural, mechanical and propulsion subsystem requirements initiated a resizing of the vehicle. During this activity, it was decided to size a SERV capable of transporting a MURP spacecraft plus propulsion adapter and cargo to orbit and returning a personnel module (PM) plus propulsion adapter and cargo to earth. The weights of these ascent and reentry payloads have a significant influence on vehicle size. Thus the 88-ft. diameter hybrid SERV evolved with a GLOW of 4.733 million pounds.

The 88-ft. diameter hybrid SERV, shown in figure 2.1-1, was used as a baseline for point design analyses. During these analyses the LH_2 propellant tank bulkhead was raised to provide additional space for tank sumps, additional thermal protection was incorporated to reduce the effect of thermal gradients across the primary structural shell, the propulsion subsystem weights were revised, and the results of a detailed stress analysis were incorporated. A final sizing of the vehicle was initiated to incorporate these changes. At the same time final aerospike engine performance data were used and the propellant tanks were increased in size to accommodate a minimum CEI performance of the aerospike engine. The output of this final sizing was a revised baseline 96 ft. in diameter and 6.054 million pound GLOW.

2.1.1 PAYLOAD CRITERIA FOR SIZING HYBRID CONFIGURATIONS

Basic dimensions and summary weight breakdowns are given in figure 2.1-2 for the two spacecraft under consideration. These two spacecraft were specified for study to evaluate the effect of long and short cross-range reentry vehicles aboard SERV.

Note that the hybrid SERV configurations are sized by the MURP mission payload during ascent and PM mission payload for landing.
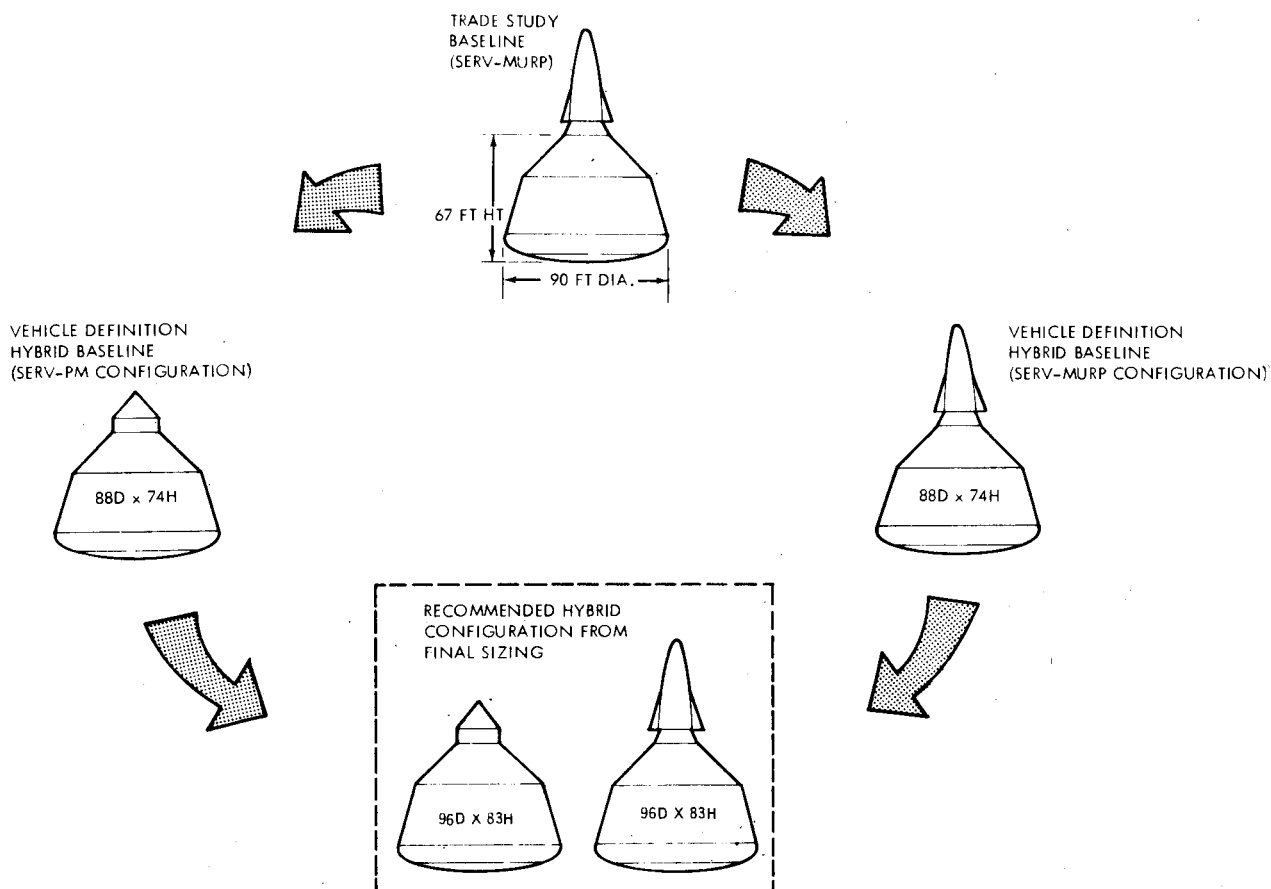
Figure 2.1-1. SERV Configuration Evolution

MURP SPACECRAFT (LB)		50,525
REENTRY VEHICLE	29,800	
PROPULSION ADAPTER	7,700	
ABORT SUBSYSTEM	6,300	
CONTINGENCY (10%)	4,385	
EXPENDABLES	2,340	
MANEUVERING PROPELLANTS		10,775
GROSS CARGO WEIGHT		25,000
TOTAL PAYLOAD (LB)		86,300

PM SPACECRAFT (LB)		21,758
PERSONNEL COMPARTMENT	7,912	
PROPULSION COMPARTMENT	7,668	
ABORT SUBSYSTEM	4,200	
CONTINGENCY (10%)	1,978	
EXPENDABLE (332 LB)	EXPENDED	
MANEUVERING PROPELLANTS		EXPENDED
GROSS CARGO WEIGHT		25,000
TOTAL PAYLOAD (LB)		46,758

Figure 2.1-2. Payload Criteria for Sizing Hybrid Configurations

2.2 MISSION PROFILES

Figure 2.2-1 shows schematically the mission profiles for the two spacecraft concepts being examined. The profiles apply to the 55-degree inclination, space station cargo delivery, reference mission. For both spacecraft profiles the injection altitude is 50 nm.

For the SERV-PM, both the SERV and spacecraft go into a high altitude (260 nm) phasing orbit. Terminal rendezvous and docking of the personnel module and cargo are accomplished using a propulsion system in the personnel module. Upon mission completion, the personnel module, with its return cargo, rejoins SERV. The SERV, plus cargo and spacecraft, reenters and lands as a unit. Alternate mission profiles for SERV-PM that yield higher cargo transfer will be discussed later.

In the SERV-MURP profile, SERV with its payload establishes a circular orbit at a low altitude (110 nm). The MURP, plus cargo, proceeds to the space station while SERV remains in the lower orbit. At mission completion MURP rejoins SERV and transfers the return cargo. MURP then separates, reenters, and lands, while SERV, plus cargo, reenters and also lands.

These mission profiles are not exclusively used by the PM or MURP because alternate modes exist. For instance the SERV-PM profile could be used by SERV-MURP under emergency rescue conditions when additional ascent propellants would be substituted for cargo.

2.3 FINAL VEHICLE SELECTION

Analysis of the alternative configurations for SERV led to the conclusion that the MURP configuration was capable of performing the PM mission except for the return payload requirement imposed by having the PM return on SERV together with the cargo. A composite vehicle was therefore sized with the MURP ascent capability coupled with the PM return requirements. (See figure 2.3-1.) The composite vehicle delivers the required 25,000 lb payload to the Space Station for a MURP mission and can deliver 25,000 lb or 53,200 pounds depending upon the ascent profile for the PM mission.

Key features of the main propulsion subsystem are shown in table 2.3-1.

SERV incorporates an integral aerospike engine comprising 12 interconnected modules for ascent propulsion. A one-turbopump-out capability is provided.

The landing propulsion is provided by turbojet lift engines which operate at a thrust efficiency of 80 percent. A one-engine-out capability is provided.

Major dimensions and key configuration features for the final configuration are shown in figure 2.3-2. The standard vehicle has a PM spacecraft that returns to earth on SERV. The alternate MURP spacecraft is also shown. SERV is designed for fully automatic unmanned operations. For this mode of operation a nose cone of the PM external configuration would be installed in lieu of the spacecraft.

SERV-PM

SERV-MURP

Figure 2.2-1. Mission Profiles
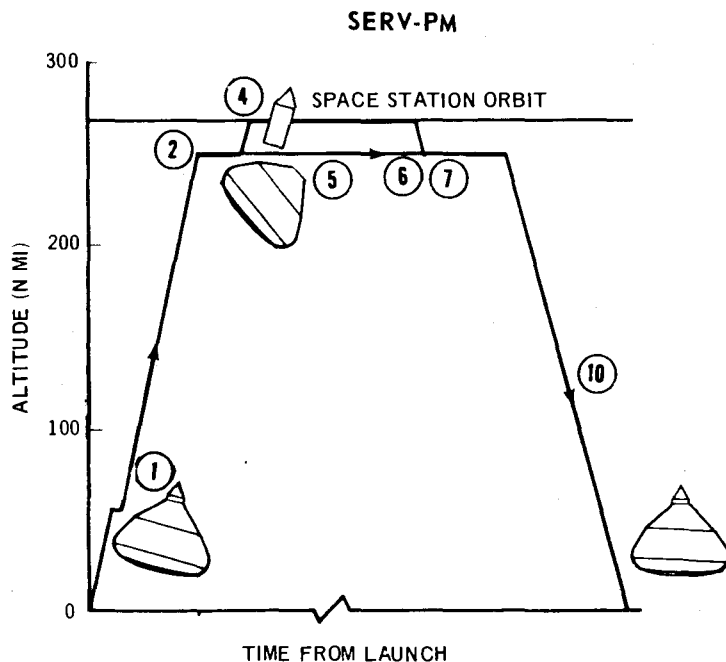
1. LAUNCH FROM KSC INTO PERIGEE OF
   TRANSFER ELLIPSE
2. CIRCULARIZE AT PARKING ORBIT ALTITUDE
3. SEPARATE AND TRANSFER TO 110×260
   PHASING ORBIT
4. RENDEZVOUS AND DOCK WITH SPACE STATION
   AT 270 N MI ORBIT
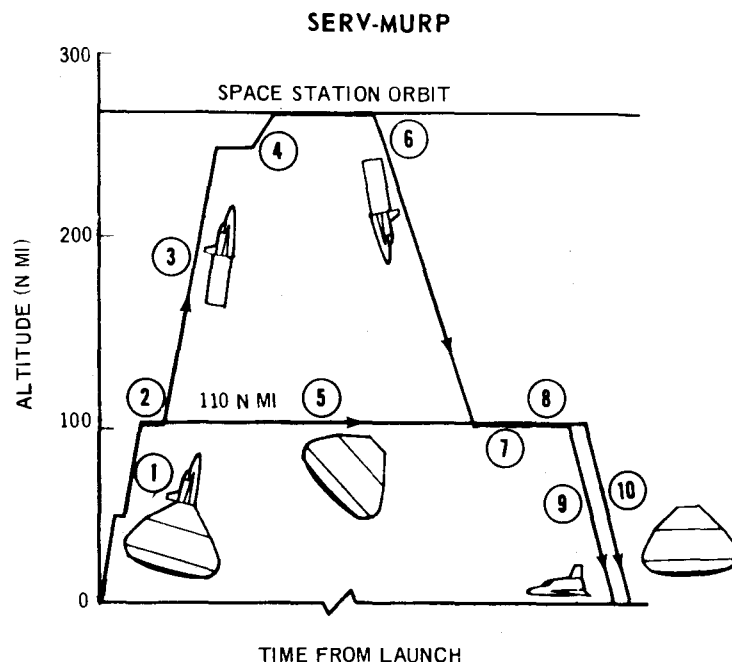
5. MAINTAIN PARKING ORBIT ALTITUDE
6. SEPARATE, CHANGE PLANE AND TRANSFER TO
   PHASING ORBIT
7. RENDEZVOUS AND DOCK WITH SERV
8. TRANSFER CARGO AND SEPARATE FROM SERV
9. DEORBIT AND REENTER (MURP)
10. DEORBIT AND REENTER (SERV OR SERV-PM)

Differential corner radii have been incorporated in the aerospike protection doors on the vehicle maximum diameter. This feature, when combined with a horizontal cg offset, ensures that the desired trim angle of attack and lift to drag (L/D) ratio can be achieved during reentry.

ITEM	SPACECRAFT/PROFILE DESCRIPTION	
	PM (260 x 55)	MURP (110 x 55)
PAYLOAD WEIGHT (LB)	50,900	88,900
CARGO WEIGHT TO 270 x 55 (LB)	25,000	27,300
LIFTOFF THRUST (LB)	7,454,000	7,454,000
GLOW (LB)	6,046,000	6,049,000
VEHICLE DRY WEIGHT (LB)	494,249	
● PRIMARY STRUCTURE	200,018	
● AEROSPIKE ENGINE	110,804	
● TURBOJET ENGINES	48,845	
● THERMAL PROTECTION	24,695	
● ALL OTHER SUBSYSTEMS	64,955	
● CONTINGENCY (10%)	44,932	
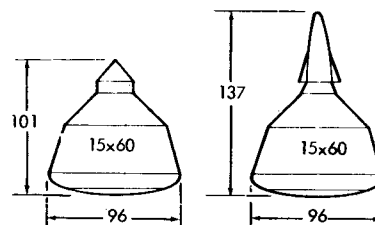
Figure 2.3-1. Final Vehicle Selection

Table 2.3-1. Main Propulsion Subsystems

ASCENT	LANDING
GENERAL: ● 12-MODULE AEROSPIKE ENGINE ● LOX/LH AT 6:1 MIXTURE RATIO ● 2000 PSI CHAMBER PRESSURE ● TURBOPUMP OUT CAPABILITY	GENERAL: ● TURBOJET LIFT ENGINES ● JP-4 FUEL ● F/W RANGE OF 17 TO 20 ● ENGINE OUT CAPABILITY
FINAL CONFIGURATION: ● THRUST OF 7.45M LB SL, 9.72M LB VAC ● I_S OF 348 SEC SL, 467 SEC VAC ● NOZZLE EXPANSION RATIO OF 409	FINAL CONFIGURATION: ● 40 ENGINES ● 20,759 THRUST EACH ● F/W OF 17
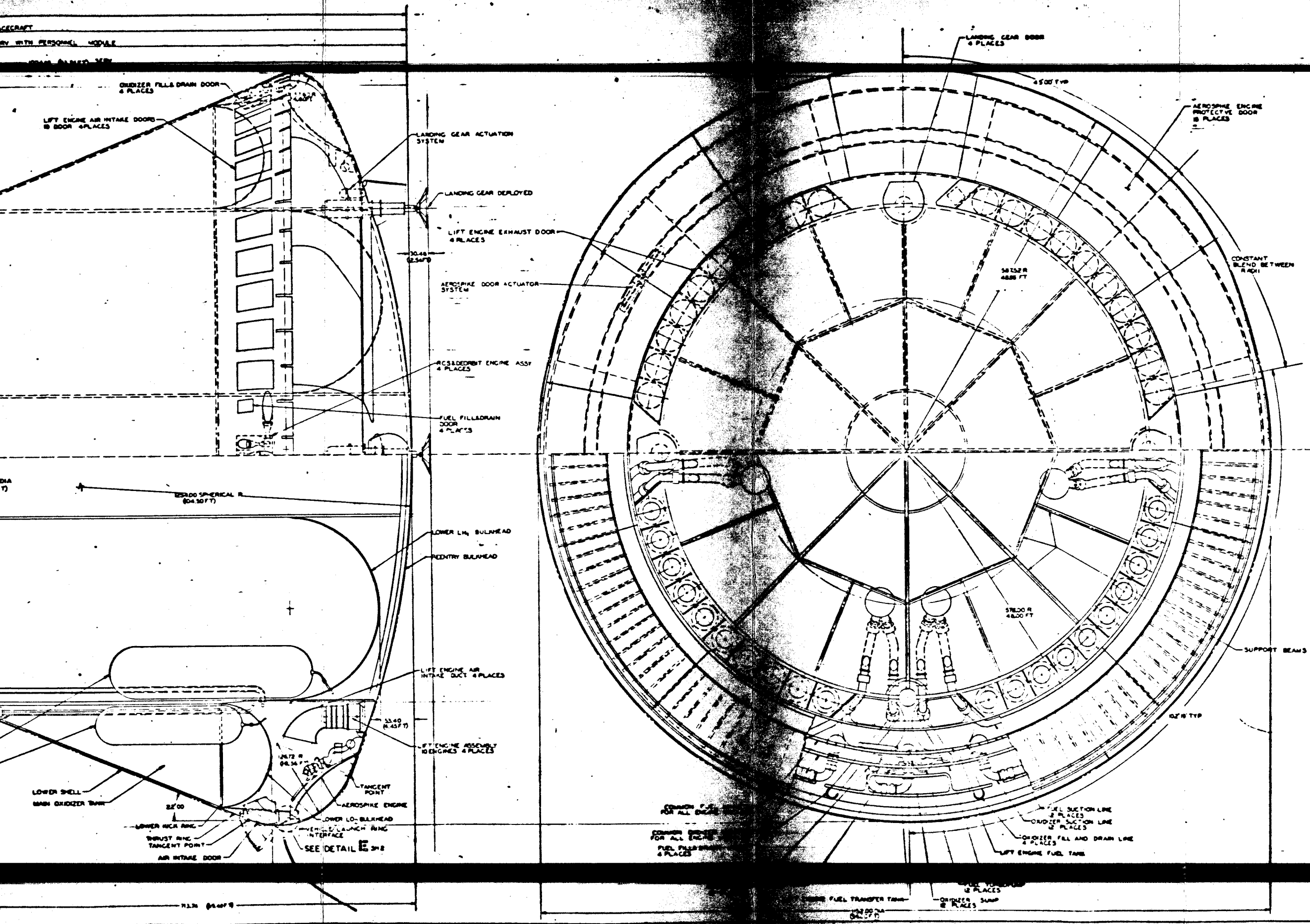
Figure 2.3-2. Final Vehicle Arrangement

2-7/2-8
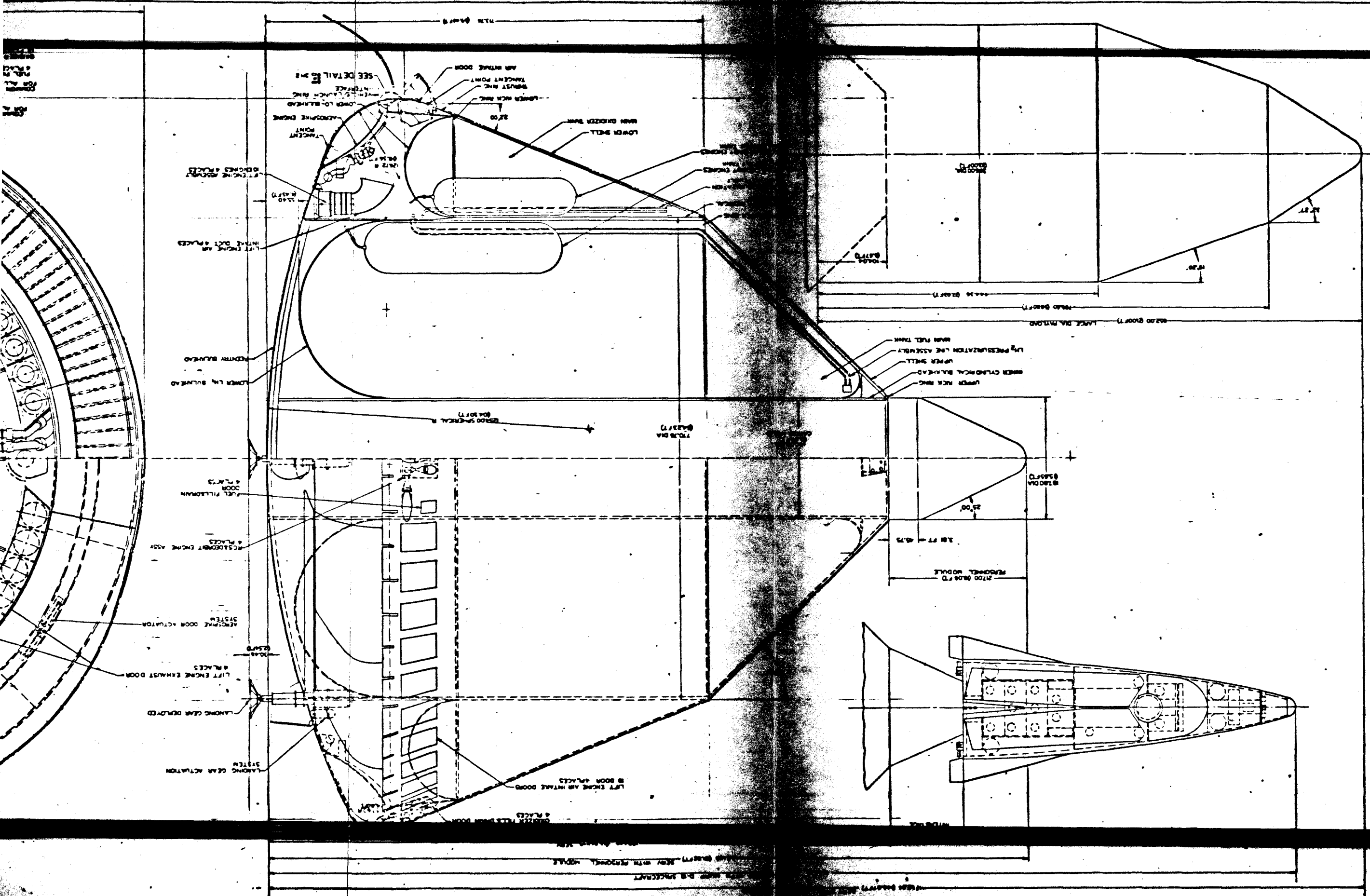
Section 3

FLIGHT TECHNOLOGY ANALYSES

3.0 GENERAL

The results of flight technology analyses are presented in this section. Vehicle flight performance is presented and hazard and abort implications are discussed. The results of cold flow testing of a model SERV are used to examine feasibility and develop aerospike engine performance. The results of wind tunnel tests of ascent and reentry SERV configurations are used to establish the aerodynamic characteristics. Thermal protection requirements are discussed, and the ascent, reentry, and landing control characteristics are outlined.

3.1 VEHICLE FLIGHT PERFORMANCE

The general scope of work for the mission and performance analyses subtask during the vehicle definition phase of the study is outlined in this section. Mission profiles, hazards and abort, final performance, and fixed hardware sensitivities are discussed.

3.1.1 MISSION PROFILES AND TIME LINES

SERV as currently defined is capable of operating in two basic modes (figure 3.1-1). In Mode A, following injection into an elliptical orbit using the mainstage propulsion system, required post-injection maneuvers are accomplished using the SERV auxiliary system only, with the payload (spacecraft plus cargo) as a passive unit. In Mode B, both the SERV auxiliary system and the propulsive capability of the spacecraft are used for on-orbit maneuvering.

The mission profiles for the space station cargo delivery mission using these two modes are illustrated schematically in figure 3.1-1. The required post-injection maneuvers associated with each profile and the mission time lines associated with each mode are indicated in figure 3.1-1.

3.1.1.1   Mode A Mission Phasing Requirements

The central angle of the space station shown on figure 3.1-2 is defined as the angle formed by a line within the plane of the space station orbit from the center of the earth to the ascending mode and a line from the center of the earth to the space station. This angle is measured when the plane of the space station orbit contains the launch site. The total minimum time from launch through landing is presented
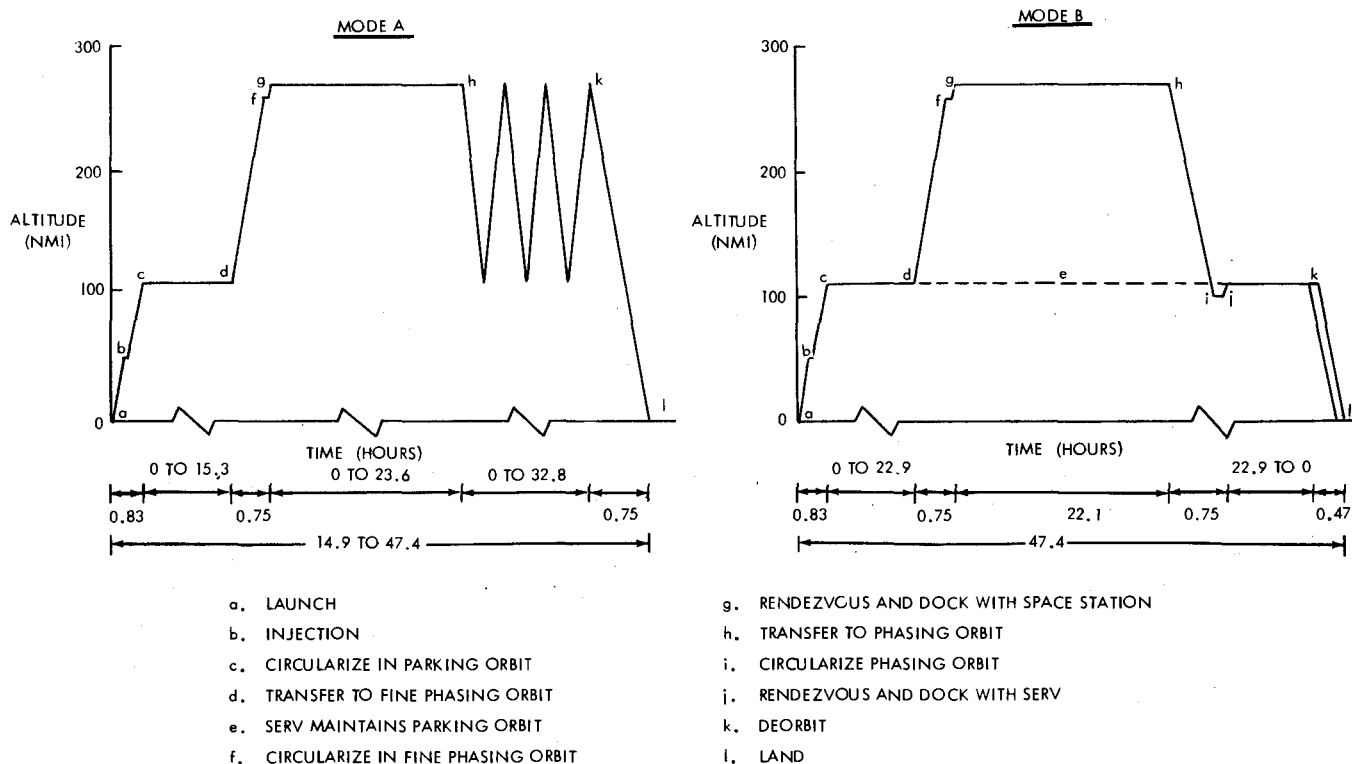
Figure 3.1-1. Mission Profiles and Time Lines

MODE A

a. LAUNCH
b. INJECTION
c. CIRCULARIZE IN PARKING ORBIT
d. TRANSFER TO FINE PHASING ORBIT
e. SERV MAINTAINS PARKING ORBIT
f. CIRCULARIZE IN FINE PHASING ORBIT

g. RENDEZVOUS AND DOCK WITH SPACE STATION
h. TRANSFER TO PHASING ORBIT
i. CIRCULARIZE PHASING ORBIT
j. RENDEZVOUS AND DOCK WITH SERV
k. DEORBIT
l. LAND
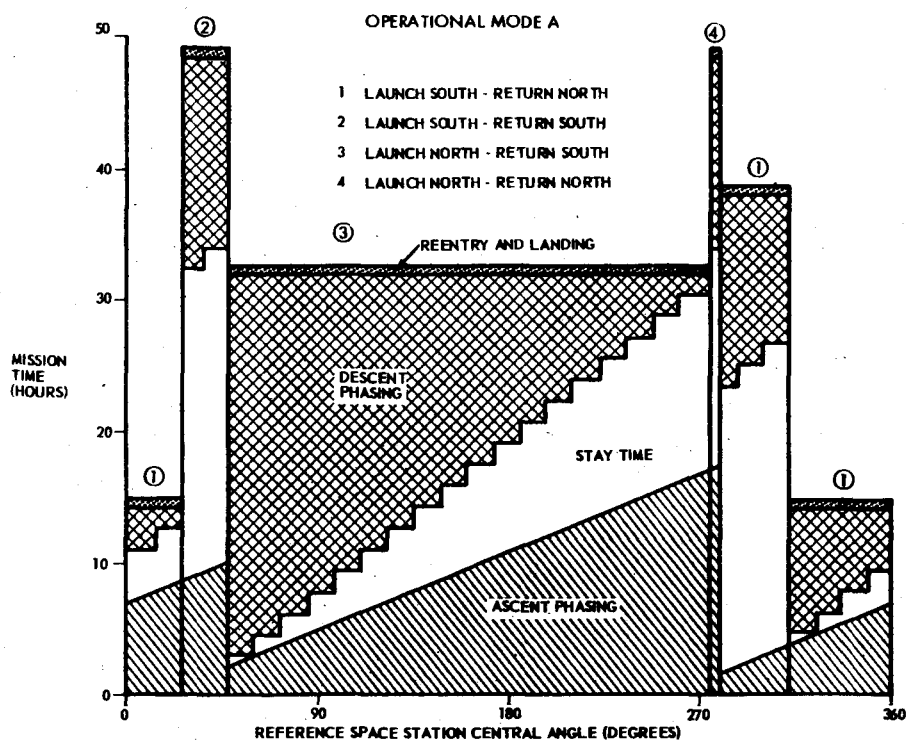
Figure 3.1-2. Mode A Mission Phasing Requirements

3-2

for SERV only, Mode A operation, as a function of space station central angle orientation, on figure 3.1-2. The combination of launch and landing direction yielding the minimum total time for a particular space station central angle region are shown. The total times are made up of four categories relating to the specific operational phases of ascent, orbital stay time available prior to descent phasing initiation, descent and reentry. The times attributable to each phase are identified by different shading patterns. For a specific space station central angle, the stay time shown indicates the time measured from rendezvous when phasing must be initiated. If the required stay time at the orbit for a particular mission exceeds the time shown on this chart, approximately 24 hours or 15 orbits of the space station must pass before an opportunity to return recurs. The mission times that result from this operational mode range from 14.9 to 47.4 hours throughout the space station central angle range. For this profile it would be desirable to orient the space station within the 14.9 hour mission time range to allow minimum reaction time under emergency conditions. The time required in parking orbit for ascent phasing never exceeds 15.3 hours throughout the central angle range. This number is of interest in evaluating the velocity requirements for parking orbit maintenance in the total velocity budget.

3.1.1.2   Mode B Mission Phasing Requirements

For operational Mode B, where SERV remains in the 110 nautical mile parking orbit while the spacecraft proceeds to the space station, the positional orientation in terms of latitude, longitude for deorbit, is independent of the space station central angle at launch. It depends rather on the ascent to orbit characteristics of SERV. It was found that the orbit trace of the selected parking orbit passed through the desired deorbit position once every 16 revolutions of the parking orbit without phasing adjustments. The critical timing associated with this operational mode was related to achieving the rendezvous of the spacecraft with SERV for return. Regardless of the ascent phasing time required for the original rendezvous with the space station, the first opportunity for return to the SERV required a stay time at the station of 22.1 hours after arrival. The total mission time as a function of space station central angle at launch for this mode is presented on figure 3.1-3 for a north launch. A total mission time of 47.4 hours is required for all space station central angles except those from 33 through 41 degrees. For this region, ascent phasing time requirements resulted in missing the first return opportunity. Utilizing a south launch for this region, however, will provide mission times of 47.4 hours throughout the central angle range. For this mode, the difference in regression of the orbital planes of the parking orbit and the space station orbit will require a plane change of 0.7 degrees/day to accomplish the SERV/spacecraft rendezvous. Parking orbit maintenance time for this mode is a minimum of 46 hours and increases with mission duration. If required stay time at the station exceeds the 22.1 hours available for the minimum mission time case, additional return opportunities recur every 22.9 hours thereafter.

3.1.1.3   Deliverable Cargo Variation with Mission Duration

Using the appropriate velocity budgets associated with both Modes A and B coupled with the phasing information on these profiles, the deliverable cargo carrying
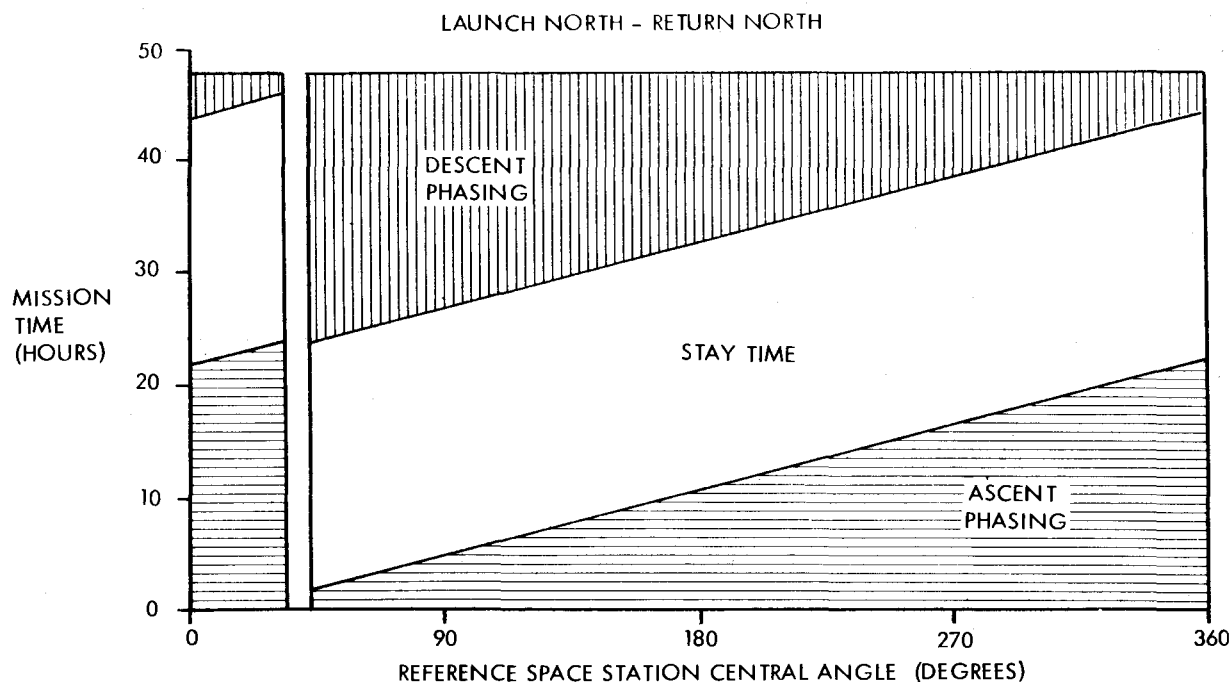
Figure 3.1-3. Mode B Mission Phasing Requirements

capability for the SERV-PM and the SERV-MURP configurations was determined. (See figure 3.1-4.) These results are presented as a function of mission duration. Based on the phasing results, the minimum duration mission for each mode of operation is noted. The cargo carrying capability of the SERV-PM using either mode exceeds the SERV-MURP capability because of the lower spacecraft weight associated with this configuration.

3.1.1.4   Configuration/Profile Assessment

For each payload configuration, the performance and operational characteristics associated with both operational modes were examined and the advantages and disadvantages assessed. The results of this assessment are summarized on table 3.1-1. Generally, both operational modes have desirable characteristics. Mode B provides a performance advantage, while Mode A has advantages related to phasing flexibility. No single selection need be made at this time since the ability to operate in either mode is possible under the current design concept. Indeed, the selection of the operational mode to be used can be made for each mission without penalizing other missions. This capability greatly enhances the flexibility of SERV.

3.1.2   HAZARDS AND ABORT

3.1.2.1   Engine Out Implications

The aerospike engine for SERV consists of 12 modules and each module has a turbopump. The 12 turbopumps which feed into a common manifold, have been designed with an overspeed capability such that should a pump fail the remaining pumps can operate above the nominal operating speed to maintain the required thrust level.
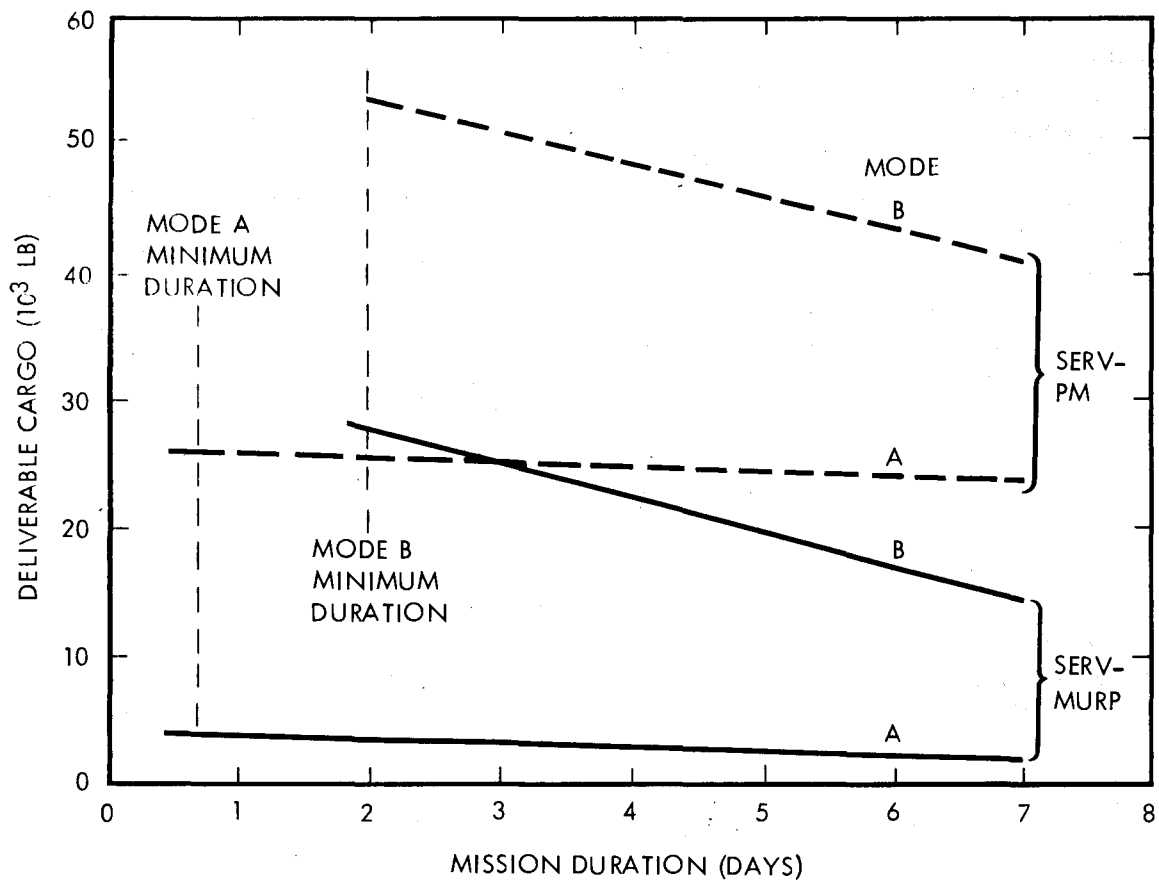
Figure 3.1-4. Deliverable Cargo Variation with Mission Duration

Table 3.1-1. Configuration/Profile Assessment

ITEM	CONFIGURATION AND MISSION PROFILE			
	SERV-PM		SERV-MURP	
	MODE A	MODE B	MODE A	MODE B
PAYLOAD IN PARKING ORBIT (LB)	50,900	86,700	53,600	88,900
CARGO TO SPACE STATION, MIN. DURATION (LB)	25,000	53,200	3,100	27,300
CARGO TO SPACE STATION, 7-DAY MISSION (LB)	23,400	40,900	1,500	14,600
ABILITY TO MEET DESIRED MISSION CHARACTERISTICS:				
• 25,000 POUND CARGO, MIN. DURATION	YES	YES	NO	YES
• 25,000 POUND CARGO, 7-DAY MISSION	NO	YES	NO	NO
• 48-HOUR RESCUE MISSION REACTION TIME	YES	NO	YES	NO
• 1500-NM CROSS RANGE CAPABILITY	NO	NO	YES (MURP)	YES (MURP)

The thrust level, which can be maintained after the failure of one or more turbo-
pumps, is a function of the design overspeed capability of the pumps. This relation-
ship is presented parametrically on the left hand side of figure 3.1-5, which shows the
percent of nominal thrust after failure as a function of percent overspeed in the pump
design for 1, 2 and 3 turbopumps out. Trajectories simulating failures to various
thrust levels occurring at varying times along the ascent trajectory were generated.
From these data the curve of failure time after which a failure to a specific percent
thrust could occur without aborting the mission was determined. These results are
shown on the right hand side of figure 3.1-5. The shaded area indicates the thrust
level, failure time combinations yielding mission abort situations. To the right of
this region is an area of combinations for which the nominal mission can be accompli-
shed utilizing part or all of the flight propellant reserve. This region is bounded on
the right by the nominal thrust level versus time.

The current point design of the turbopumps incorporates a 20 percent overspeed
capability. The dashed line on figure 3.1-5 reflects this capability. Interpreting the
results for this design indicates that the nominal mission can be accomplished with a
failure of one or two turbopumps at any time. The nominal mission can be accomplished
utilizing the FPR with three turbopumps out if the failure of a third pump occurs after
50 sec.
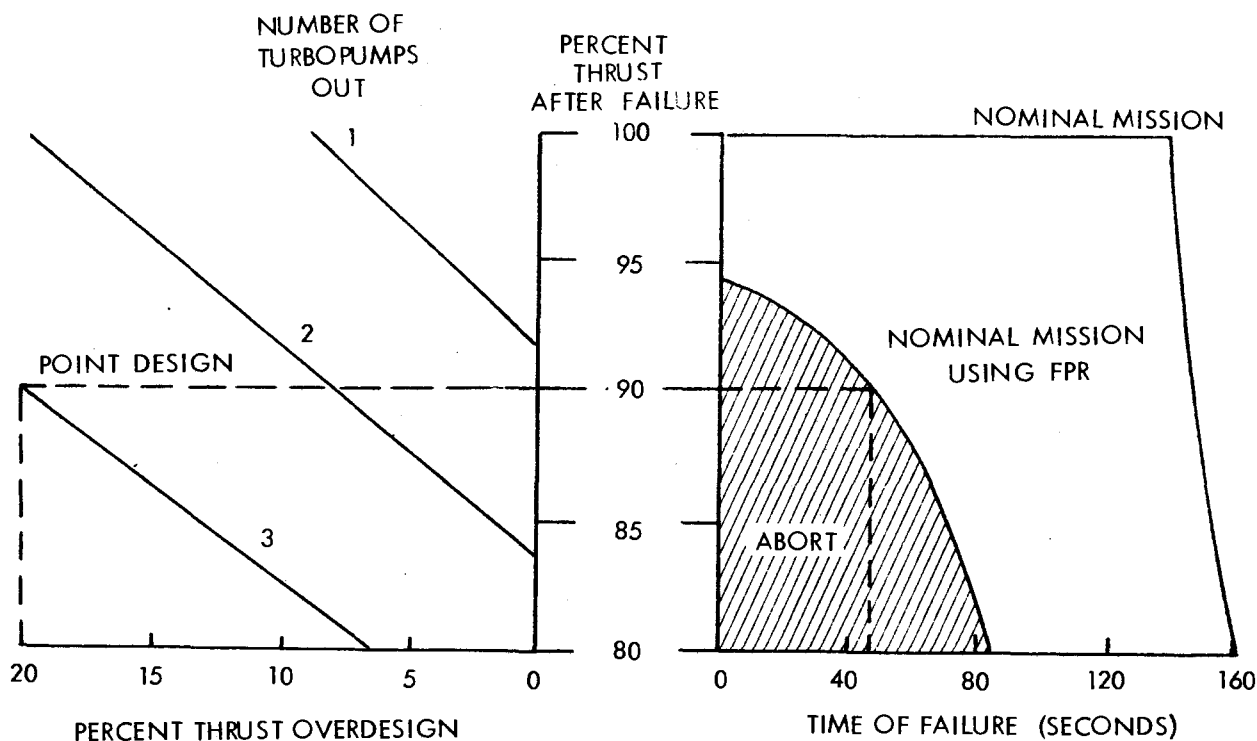
Figure 3.1-5. Engine Out Implications

3.1.2.2 Intact Abort Implications

In the event of a catastrophic malfunction of SERV during ascent, abort capability for both the PM and the MURP spacecraft has been provided. Abort for the PM is provided using eight solid rocket motors, which have been sized to give an initial T/W of 5.7 from SERV with all engines shut down. For SERV failures which precipitate moderate rates to structural breakup, this abort system will be adequate. The PM, once aborted, will traverse a parabolic arc trajectory until it reaches 50,000 in altitude, at which time a sailwing is deployed and the PM sets down on either land or water. Similarly, for the MURP, separation from a malfunctioning SERV is accomplished using solid rocket motors. However, with this spacecraft an aircraft type landing will be used. The abort modes for both the PM and the MURP are shown schematically on figure 3.1-6.

3.1.3 SERV FINAL PERFORMANCE

The capability of the SERV for a spectrum of missions has been determined and is presented on table 3.1-2. The numbers presented are gross payload values (i.e., spacecraft plus cargo). For the space station mission the deliverable cargo weights are shown in parenthesis. For this mission, payload and cargo were examined using the two operational modes.

3.1.4 FIXED HARDWARE SENSITIVITIES

The sensitivity of payload to variations in significant vehicle and mission parameters has been determined for three missions of interest. For the space station cargo delivery mission, cargo sensitivities have also been assessed. These data are presented in table 3.1-3. These are fixed hardware sensitivities and reflect the expected variation in payload which will result from a known variation in a particular parameter on the ground.

3.1.5 REENTRY PERFORMANCE

Figure 3.1-7 shows the reentry corridor for return from the range of orbital altitudes considered for SERV. The entry conditions are referenced to the 400,000 ft interface altitude. As indicated, the maximum deceleration experienced during reentry increases as the entry angle increases. These decelerations were obtained for full-lift trajectories with an L/D of 0.30 and a band of W/C_DA values from 40 to 70 psf.

To maintain aerodynamic maneuvering capability within the 3.0 g deceleration limit, SERV must reenter at entry angles to the left of the 3.0 g band. From a deorbit propellant standpoint, it is further desirable to enter at shallow angles as indicated by the magnitude of the deorbit velocities. However, a skip-out condition will occur for very shallow entry angles. In addition, range sensitivity is a problem in the area of the skip-out restriction. To provide a footprint capability without causing large range sensitivity, SERV is currently restricted to reentry conditions to the right of the 2.5 g deceleration band.
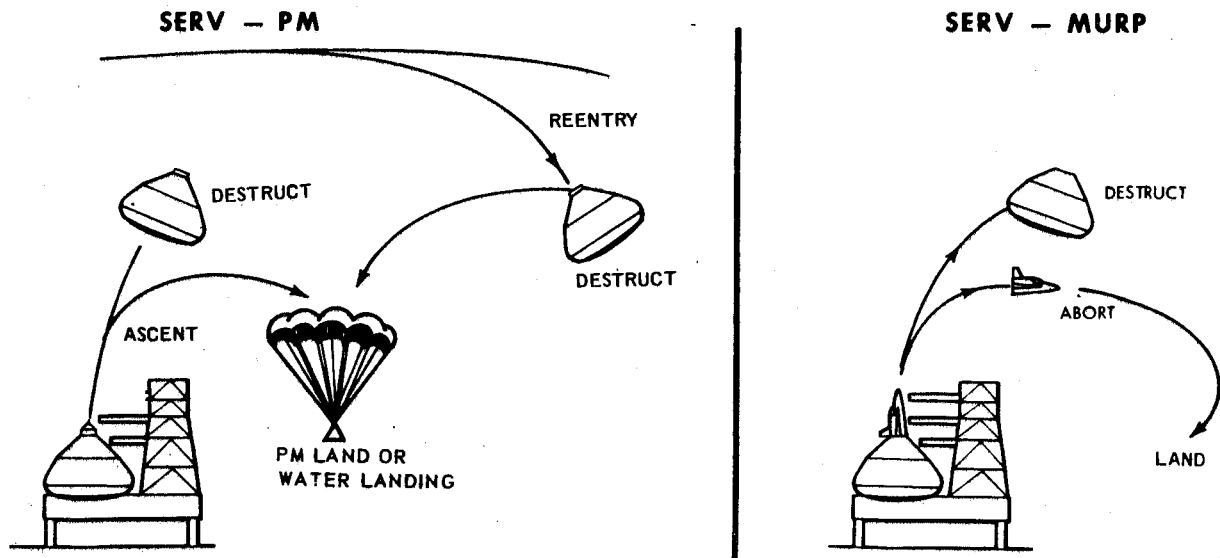
Figure 3.1-6. SERV Abort Modes

Table 3.1-2. SERV Final Performance (Gross Payload Capability)

SPACECRAFT	MISSION ORBIT (PAYLOAD IN POUNDS) (NM CIRCULAR X DEGREE INCLINATION)				
	110 NM X 28.5 DEG	270 NM X 55 DEG MODE A	270 NM X 55 DEG MODE B	100 NM X 90 DEG	100 NM X 104 DEG
MURP	116,439 (65,912)*	53,577 (3,052)	83,370 (27,282)	NA	NA
PM	112,260 (90,170)	50,873 (25,000)	80,697 (53,223)	42,975 (20,885)	25,819 (3,729)
NOSECONE**	112,260	50,873	NA	42,975	25,819
EXTENDED NOSECONE**	125,000	63,000	NA	54,000	36,000

*VALUES IN PARENTHESES ARE CARGO WEIGHTS

**WEIGHT OF NOSECONE AND EXTENSION INCLUDED IN PAYLOAD

Table 3.1-3. Fixed Hardware Sensitivities

MISSION PARAMETER		OPERATIONAL SENSITIVITY*			
		DUE EAST 100 NMI/28.5°	SPACE STATION 110 NMI/55°		RETRO GRADE 100 NMI/104°
		PAYLOAD	PAYLOAD	CARGO**	PAYLOAD
WEIGHTS					
INERT WEIGHT	LB/LB	-1.000	-1.000	-0.875	-1.000
INERT WEIGHT	LB/PERCENT	-6012	-6016	-5264	-6001
DRY WEIGHT	LB/LB	-1.003	-1.004	-0.879	-1.008
DRY WEIGHT	LB/PERCENT	-4,958	-4,962	-4344	-4,982
PROPULSION (PERCENTAGE VARIATIONS)					
SPECIFIC IMPULSE (T CONSTANT)	LB/SEC (VAC)	3,690	3,582	3,134	3,364
SPECIFIC IMPULSE (ẇ CONSTANT)	LB/SEC (VAC)	4,214	4,065	3,557	3,777
THRUST (ISP CONSTANT)	LB/PERCENT	2,175	2,038	1,783	1,715
THRUST (ẇ CONSTANT)	LB/PERCENT	19,570	18,977	16,603	17,632
PROPELLANT LOAD	LB/LB	0.1063	0.1028	0.0899	0.0962
PERFORMANCE					
ASCENT VELOCITY	LB/FPS	-53.7	-51.4	-44.9	-46.2
ON-ORBIT ΔV		-	-		
SERV/ASCENT PAYLOAD	LB/FPS	-52.0	-49.6	-43.4	-45.4
SERV/RETURN CARGO	LB/FPS	-47.4	-47.4	-41.4	-47.4
SERV	LB/FPS	-43.4	-43.4	-38.0	-43.4
DRAG	LB/PERCENT	-724	-697	-610	-640
ORBIT INCLINATION	LB/DEG	-850	-1125	-984	-1200
LAUNCH SITE ALTITUDE	LB/FT	6.33	6.17	5.38	5.47

*MOST SENSITIVITIES ARE NON-LINEAR AND SHOULD BE USED ONLY FOR SMALL DEVIATIONS.
**CARGO DELIVERED TO 270 N MI
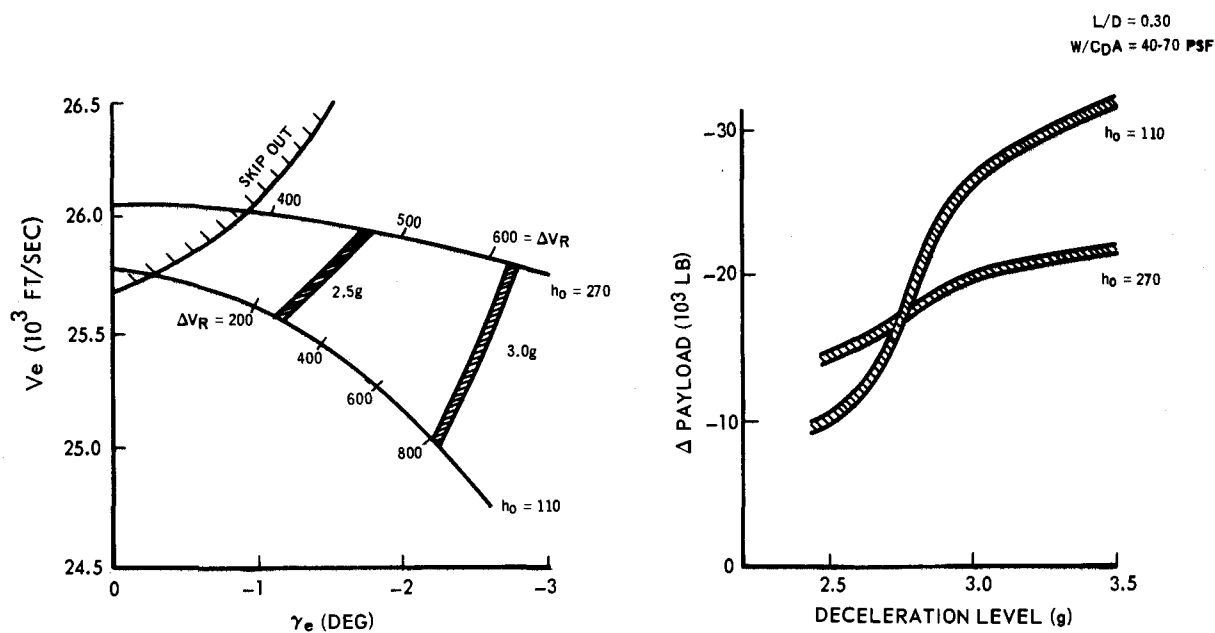
Figure 3.1-7. SERV Reentry Corridor

Figure 3.1-8 shows reentry footprint envelopes for constant L/D reentry from an orbital altitude of 110 nm for a retro velocity increment of 400 ft/sec. Footprint size is shown for L/D values of 0.25, 0.30 and 0.35, and the point at which various deceleration values are reached is shown for each L/D value. For SERV, the maneuvering capability is measured from the point of maximum range to the point where a deceleration of 3.0 g is encountered. As shown, an increase in maneuvering capability above the nominal provided by an L/D of 0.30 could be provided by trimming the vehicle to a higher L/D value, by raising the deceleration limit, or by a combination of both.
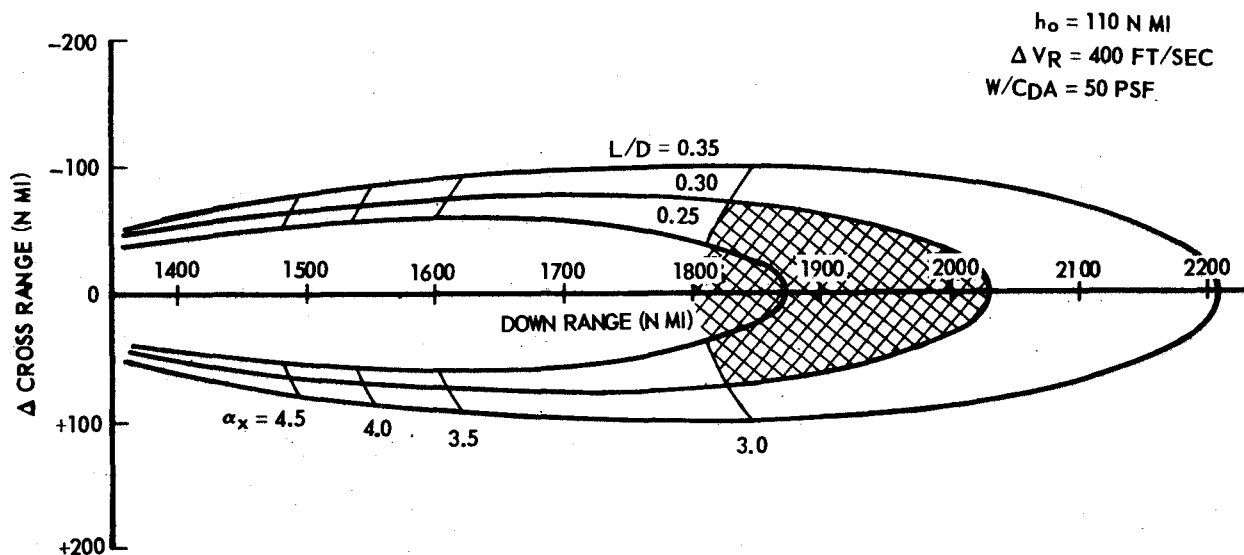
Figure 3.1-8. Reentry Footprint for Constant L/D Reentry

3.2   AEROSPIKE PROPULSION PERFORMANCE

To answer this foremost feasibility issue, a series of cold flow tests were performed on a 27-inch-diameter model of SERV at the Arnold Engineering Development Center. Engine characteristics, test procedures, and test results are presented.

The model design was based on the 90-ft diameter baseline vehicle, having 12 aerospike modules arranged in a ring of 87.4 ft outside diameter. (See figure 3.2-1.) The engine is fully integrated with the SERV, forming the base closure of the vehicle and using the entire base of the vehicle. Each of the 12 interconnected modules have a set of 2-stage, turbine-driven pumps; module interconnection is accomplished by use of a common manifold on the high pressure side of the pumps. Individual modules are controlled by oxidizer and fuel valves downstream of the common manifold. The module turbopumps are capable of emergency operating levels such that in the event of a failure of one of the 12 units, the remaining 11 can maintain all 12 modules at their normal operating level. Protective doors protect the aerospike ramp during reentry operations, as shown in cross section on figure 3.2-1.

INTERCONNECT MANIFOLDS FOR
TURBOPUMP-OUT CAPABILITY

SERV CONFIGURATION (ENGINE
PROTECTIVE DOORS NOT SHOWN)

ENGINE MODULE

INTEGRAL
AEROSPIKE
ENGINE

DOORS
REENTRY POSITION

ENGINE FIRING
POSITION FOR
LOW ALTITUDE
(OPENS FURTHER
AT HIGH ALTITUDE)

VIEW A-A
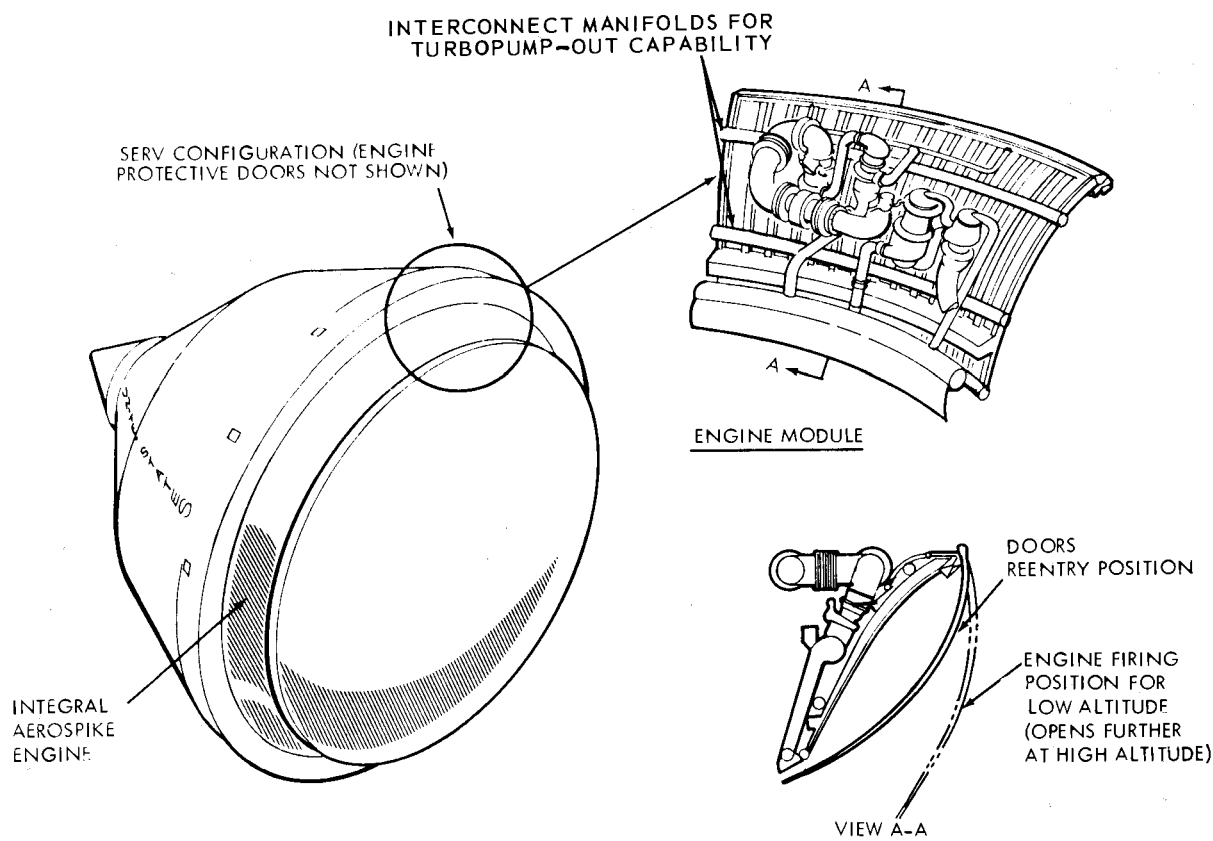
Figure 3.2-1. Aerospike Engine Integrated with SERV

Data for the baseline engine were supplied by Rocketdyne and subsequently resub-
mitted to reflect a revised integration with SERV. This integration resulted in an
engine with a larger overall diameter, a higher area ratio (483), and interconnected
modules to allow turbopump-out capability. Rocketdyne also incorporated an improved
turbopump in the system. The resultant engine specific impulse was improved by 3.2
sec at vacuum conditions and 1.4 sec at sea level, while engine weight increased by
7,345 pounds. The weight increase was due primarily to module interconnection
plumbing and the increase in diameter (1.3 ft). The revised data were used as the
baseline for subsequent trade study tasks.

Although the engine area ratio changed from 465 to 483 during the design integration,
the fabrication schedule of the cold flow model dictated use of the earlier baseline
engine at ϵ of 465.

3.2.1 COLD FLOW MODEL TESTING

A summary of prior aerospike nozzle testing is shown plotted in normalized form
in figure 3.2-2. Note that different area ratios (ϵ), nozzle lengths (%L), gas
properties (γ), and secondary flow rates (W_s/W_p) are presented. The range of
interest for SERV is shown in the lower left corner. Although the data appear to
scatter, it must be emphasized that it is a basic characteristic of the aerospike

nozzle to follow a "humping" or "roller coaster" type curve during recompression at low pressure ratios. Thus, the data spreading shown is the result of superimposing the recompression characteristics of many different configurations.

NORMALIZED AEROSPIKE THRUST COEFFICIENTS 329-692 11-70
COLD-FLOW AND HOT-FLOW, WITH SECONDARY FLOW

SERV RANGE OF INTEREST

REDUCED NOZZLE EFFICIENCY $C_T/C_{T_{des.}}$

LEGEND:

SYMBOL	ϵ	%L	γ	$\dot{w}_S/\dot{w}_P$ (%)	SYMBOL	ϵ	%L	γ	$\dot{w}_S/\dot{w}_P$ (%)
△	50	30	1.4	1.00	○	76.8	25	1.4	1.03
□	44	15	1.4	1.00	⊕	76.8	15	1.4	1.00
◇	25	16	1.4	1.00	◈	150	10	1.67	1.00
▽	24.54	12	1.4	1.00	●	25.2	20	$H_2 O_2$	(0.75-0.85)
◁	24.2	27.9	1.4	1.02					
▷	24.6	7.3	1.4	1.01	■	26.1	10	NTO/50/50	1.00
○	40.8	29.5	1.4	0.93					
○	40.3	10.1	1.4	1.02	▲	52.95	20	LOX/H_2	(0.50-1.00)
○	110.4	9.3	1.4	1.02					

REDUCED PRESSURE RATIO, $(P_c/P_a)/(P_c/P_a)_{des.}$

Rocketdyne
North American Rockwell

Figure 3.2-2. Status of Aerospike Testing Prior to SERV Cold-Flow Testing

It is readily apparent from the indicated range of interest that insufficient information was available for accurate prediction of the SERV engine performance. In addition, no test information existed for slipstream operations with blunt bodies and high nozzle expansion ratios. Hence, a cold-flow test program was implemented to provide this information.

The objective of the cold flow test was to determine performance and base flow characteristics of a high area ratio (465) aerospike engine at flight Mach number and simulated altitude conditions. A cold flow (air) test model was selected to minimize model cost, minimize test cost, and maximize geometric model accuracy. The final status of model design, fabrication, and test is as follows:

1) Designed jointly by Chrysler and Rocketdyne (completed 8-22-70)
2) Fabricated, assembled, and static checked by Rocketdyne (completed 11-10-70)
3) Tested at AEDC 16T PWT on 12-1-70 through 12-8-70.

The model scaling method used was by direct scaling of the aerospike engine area ratio ($AR_{FS} \approx 465$; $AR_{MS} \approx 417$) and an isentropic compression ramp designed for air ($\gamma = 1.4$).

The essential part of the procedure for predicting hot-firing performance from cold-flow tests lies in the normalization procedure indicated in figure 3.2-3. The relative simplicity of the technique belies the amount of theoretical and experimental effort expended to prove its usefulness. Shown at the top of the figure are the performance curves for two nozzles with different design pressure ratios and design point thrust coefficients. These values can be different because parameters such as area ratio, gas properties, nozzle length, or contour shape are generally different. If the thrust coefficient and pressure ratio for each case is divided (normalized) by its respective design point value, then both curves tend to map onto a single curve as shown in the lower figure. The inverse of this procedure, that is, mapping from a normalized curve to a hot-flow curve was applied in this test program.

Thus the procedure used for the data analysis was as follows. For each Mach number:

1) Values of model C_T versus pressure ratio were obtained from test data and correlated with respect to C_{T_∞}, $C_{T_{BV}}$, and $C_{T_{BVO}}$.

2) Using these data, normalized curves of $C_T/C_{T_{DESIGN}}$, versus $(P_c/P_\infty)/(P_c/P_\infty)_{DESIGN}$ were prepared; model and full scale performance were then correlated by this relationship.

3) Finally, C_T and I_S versus pressure ratio were obtained for the full scale engine using the normalized C_T - pressure ratio relationship.
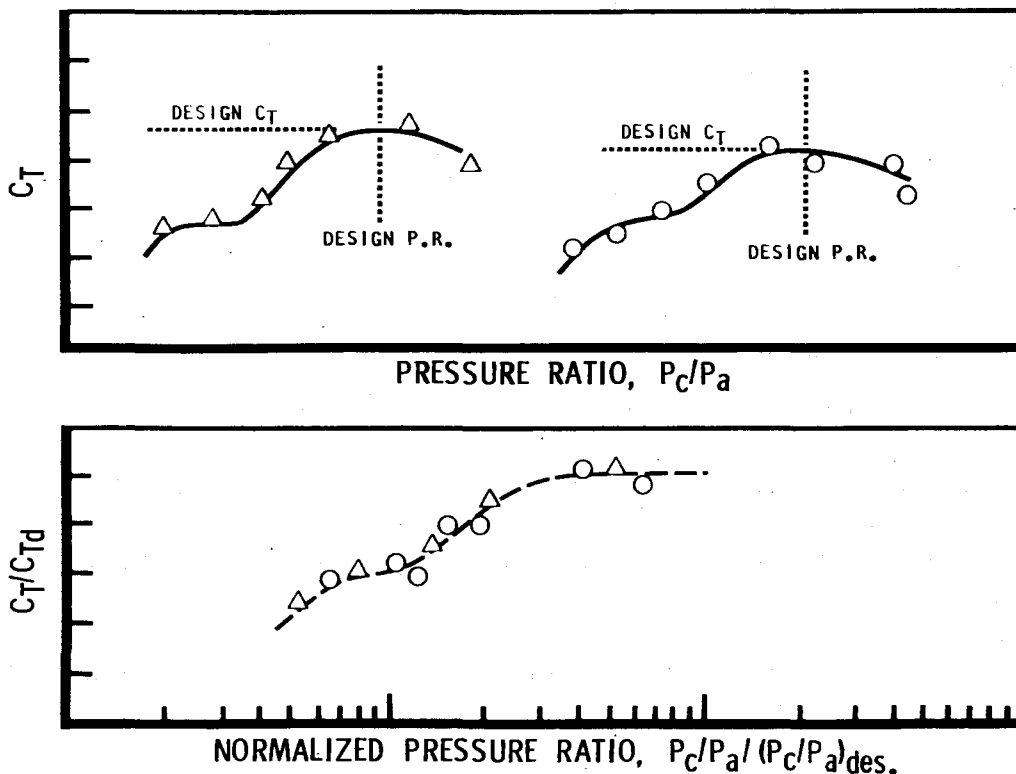
Figure 3.2-3. Normalizing of Aerospike Thrust Coefficients

3.2.1.1 Propulsion Wind Tunnel Installation

Figure 3.2-4 shows the 2-1/2 percent model (approximately 27 inches in diameter) and figure 3.2-5 shows it installed in the 16-foot Transonic Propulsion Wind Tunnel at the Arnold Engineering Development Center. The model was forward-strut-mounted to eliminate obstructions and disturbances in the base region. Four tether cables were secured to the forward sting to prevent dynamic buffeting. The minor aerodynamic disturbances in the base flow created by forward protuberances were well within the accuracy of the measured test data.

Prior to shipping to AEDC, static checkout of the model was performed in the Rocketdyne Rocket Nozzle Test Facility (RNTF). (See figure 3.2-4.) There, the model pressure system was certified to 1080 psi and system leak and proof tests were performed.

3.2.1.2 Test Conditions and Data

The scaling procedure developed by Rocketdyne dictates that the model geometric area ratio should be approximately equal to the full-scale geometric area ratio. Contours on the nozzle expansion surface are then designed for the corresponding ratio of specific heats of 1.4 for cold flow and 1.2 (approximately) for hot flow. Test conditions and test data are summarized as follows:

1) P_c for the model was 400 psia.

2) P_c/P_∞ was varied from 100 to 1000.

3) M_∞ was varied for a range of values: 0, 0.6, 0.8, 0.9, 1.1, and 1.25.

4) Data taken were:

    a) Force for engine-on and engine-off conditions.

    b) Static pressure on forebody, doors, cowl, ramp, base.

    c) Engine primary and secondary flow rates.

A typical Schlieren to illustrate test operation is shown in figure 3.2-6. Test conditions were: doors off, pressure ratio of 600, and Mach number of 0.9. For a more complete description of test operations there is a motion picture which further documents the cold-flow test.

The installed nozzle efficiency is a measure of nozzle performance including the effect of the nozzle on the vehicle drag:

$$C_{T_I} = C_{T_\infty} - \Delta C_{T_D}$$

2.5 PERCENT COLD FLOW MODEL
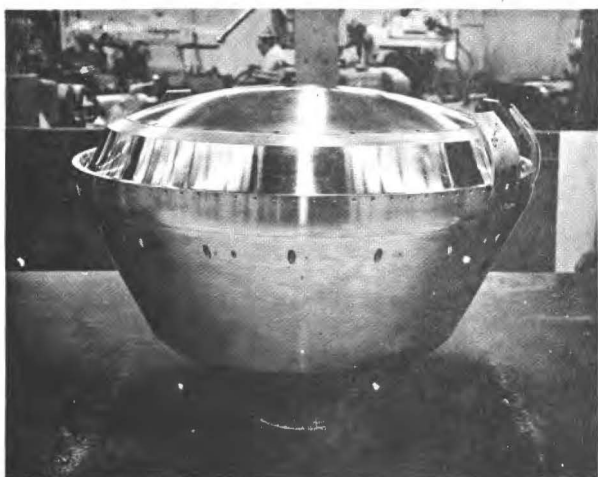
RNTF STATIC TEST
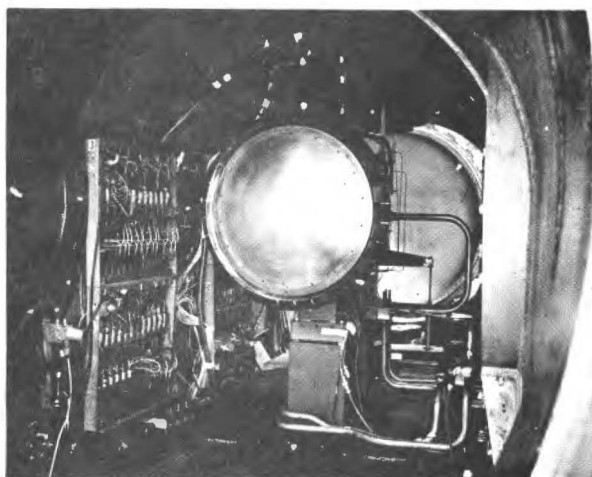
Figure 3.2-4. Model Design and Fabrication
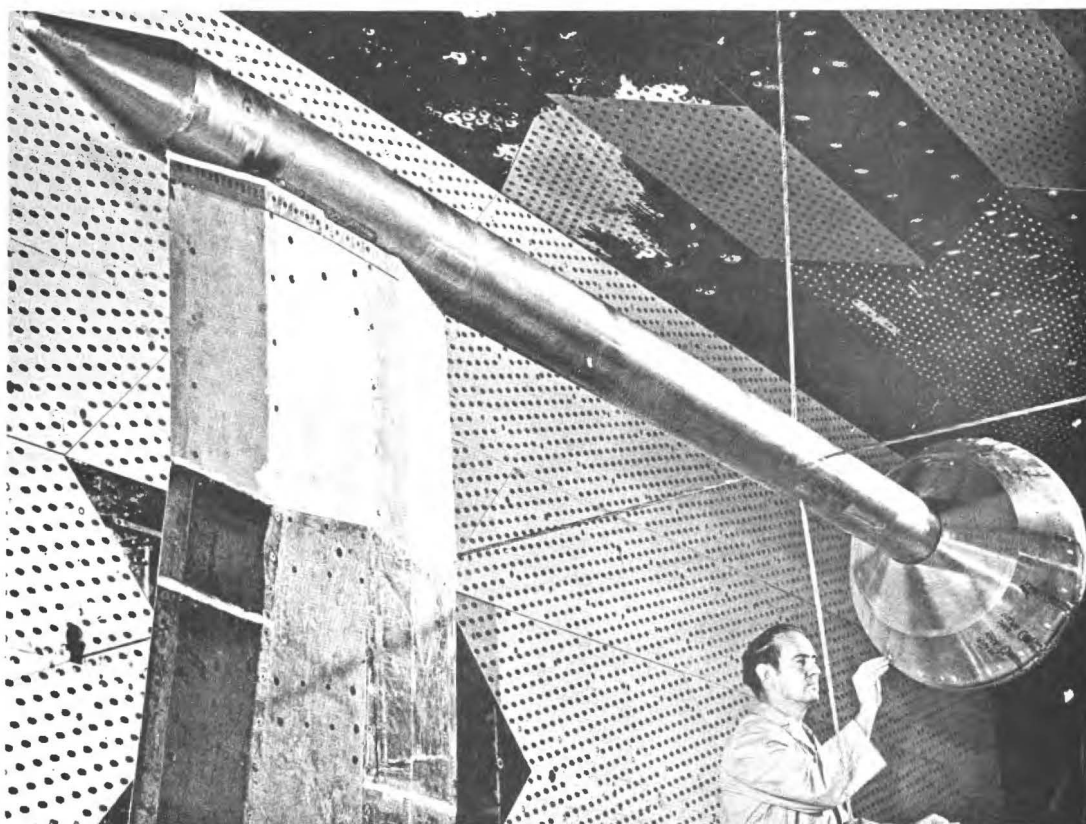
Figure 3.2-5. Propulsion Wind Tunnel Installation
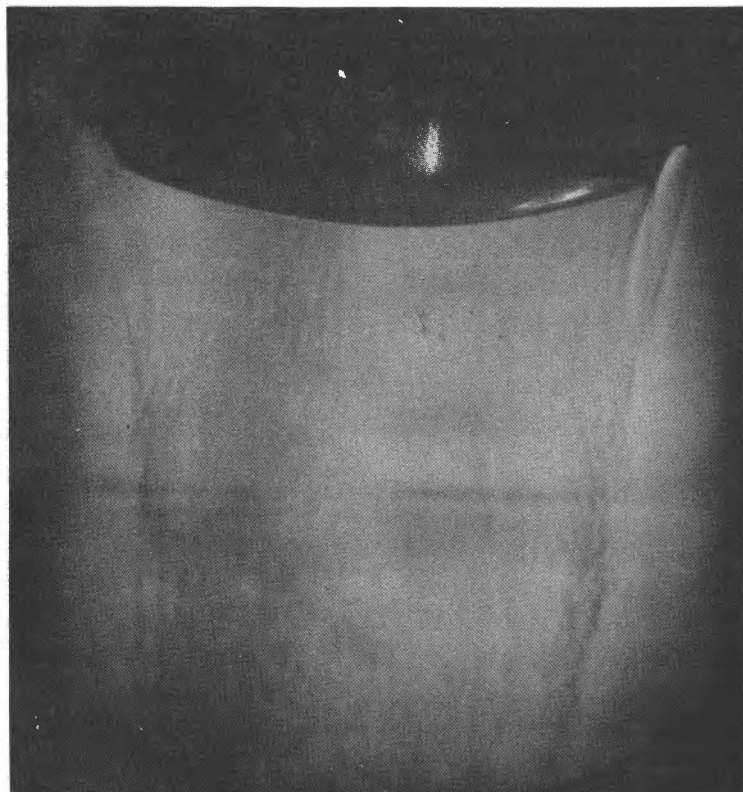
Figure 3.2-6. Schlieren of Cold Flow Test Run (Doors off, Pressure Ratio = 600, Mach = 0.9)

For high pressure ratios, net effect of the protection doors was a decrease in installed nozzle efficiency. The particular door configuration selected for the model tests did not behave as predicted. The results from these tests, figure 3.2-7, indicate that optimization of the door configuration has the potential for a significantly improved installed nozzle efficiency.

Consequently, only doors-off performance was used; but in vehicle design analysis, the door drag was incorporated as a part of the total aerodynamic drag, and the mechanical design of the doors included a means for ventilating the inside cowl region, if required after further investigation.

3.2.1.3   Full Scale Nozzle Efficiency from Model Data

Having located the point of departure from the uncompensated curve for each flight Mach number, the C_{T_∞} data were extended to the range of pressure ratios corresponding to the SERV operating conditions. The installed efficiency C_{T_I} was computed (C_{T_∞} minus ΔC_{T_D}) for the same conditions, the ΔC_{T_D} (drag due to engine operation) being extrapolated from the model data. The full scale installed efficiency, figure 3.2-8, was then computed:

$$C_{T_I} \text{ FULL} = (C_{T_I} \text{ MODEL}) \frac{C_{T \text{ DESIGN, FULL}}}{C_{T \text{ DESIGN, MODEL}}}$$
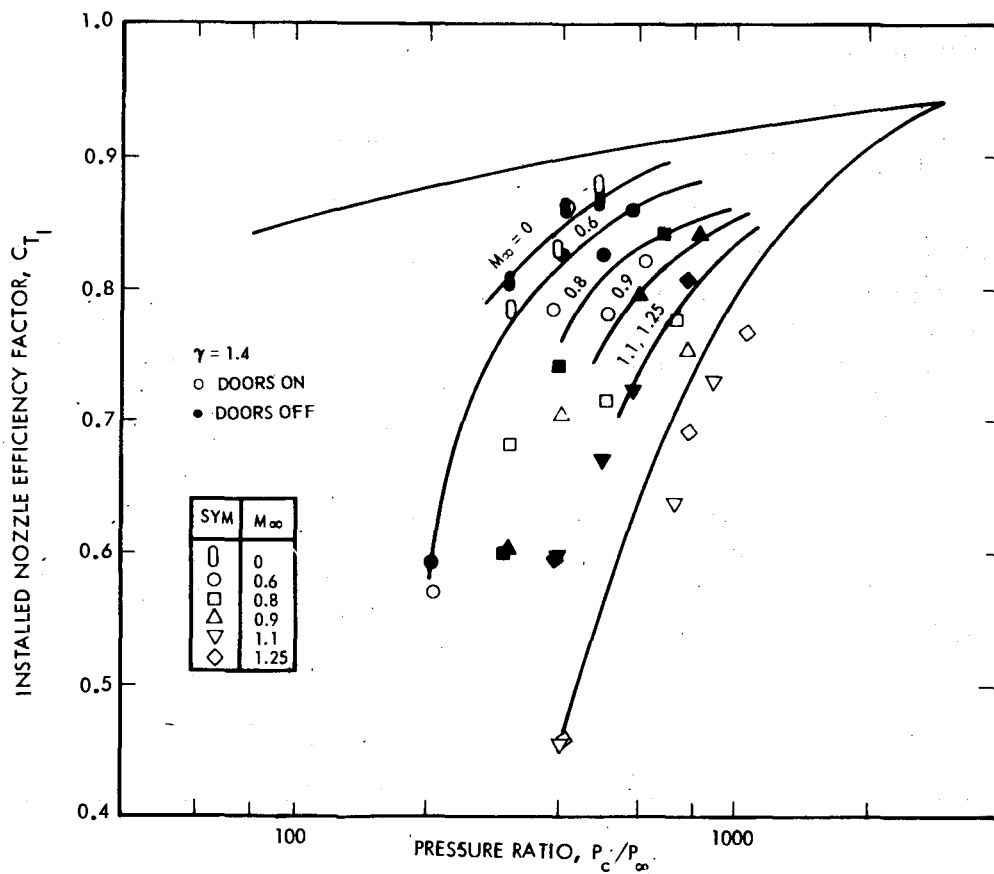
Figure 3.2-7. Model Installed Nozzle Efficiency
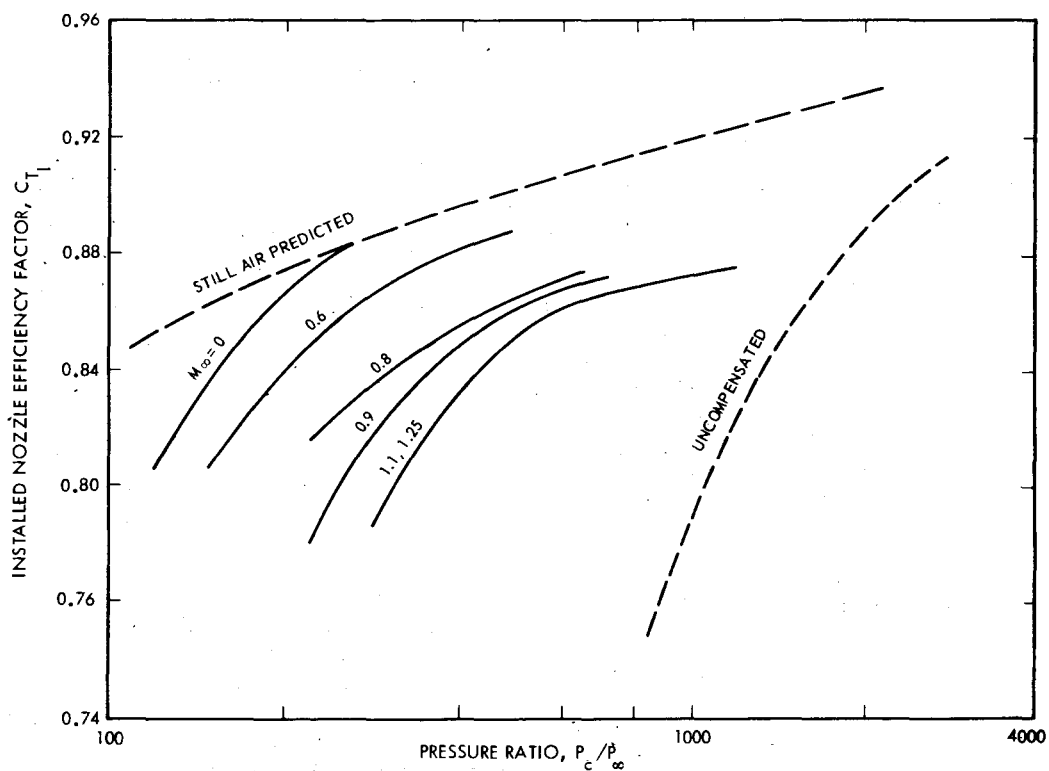
Figure 3.2-8. Full-Scale Nozzle Efficiency from Model Data

at the full scale pressure ratio:

$$PR_{FULL} = (PR_{MODEL}) \frac{PR_{DESIGN, \ FULL}}{PR_{DESIGN, \ MODEL}}$$

The range of pressure ratios covers the expected range of pressure ratio and Mach number operating conditions for the SERV mission.

Specific impulse versus altitude, figure 3.2-9, follows directly from the C_{T_I} versus pressure ratio data:

$$I_s = C_{T_I} \cdot \eta_{c*} \cdot I_{s_{IDEAL}}$$

For $P_c = 2000$ psia, ambient pressure (P_∞) is obtained from pressure ratio, P_c/P_∞, and altitude is known, having P_∞.
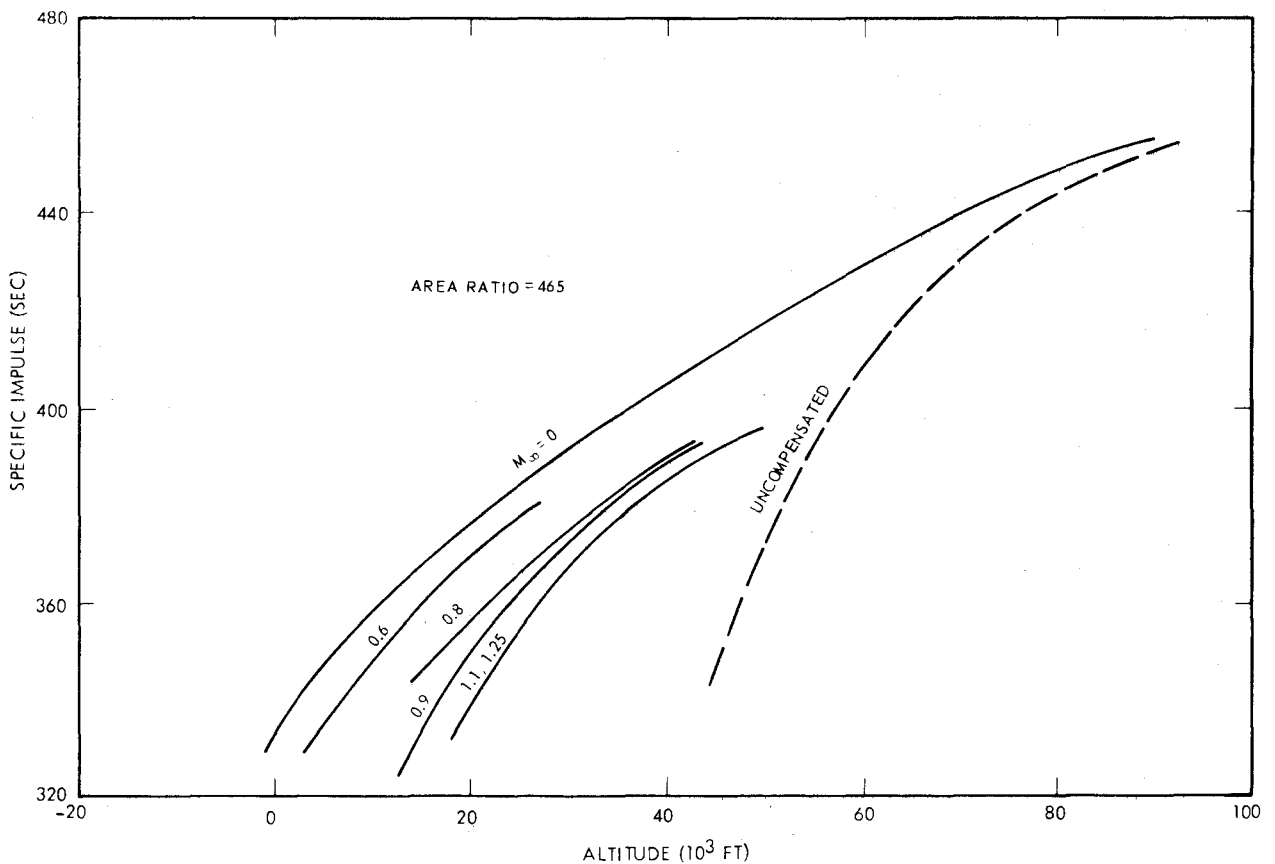
Figure 3.2-9. Full-Scale Engine Performance Based on Model Data

3.2.2 INTEGRATED ENGINE PERFORMANCE

Nominal performance of the point design engine developed by Rocketdyne in the latter portion of the study is shown in figure 3.2-10. This performance also makes use of the model test data as did the performance presented in figure 3.2-9. The values of specific impulse as a function of Mach number and altitude shown were input to the sizing program to perform final configuration sizing. The performance values for a typical SERV trajectory are indicated by the dashed line on the carpet plot.
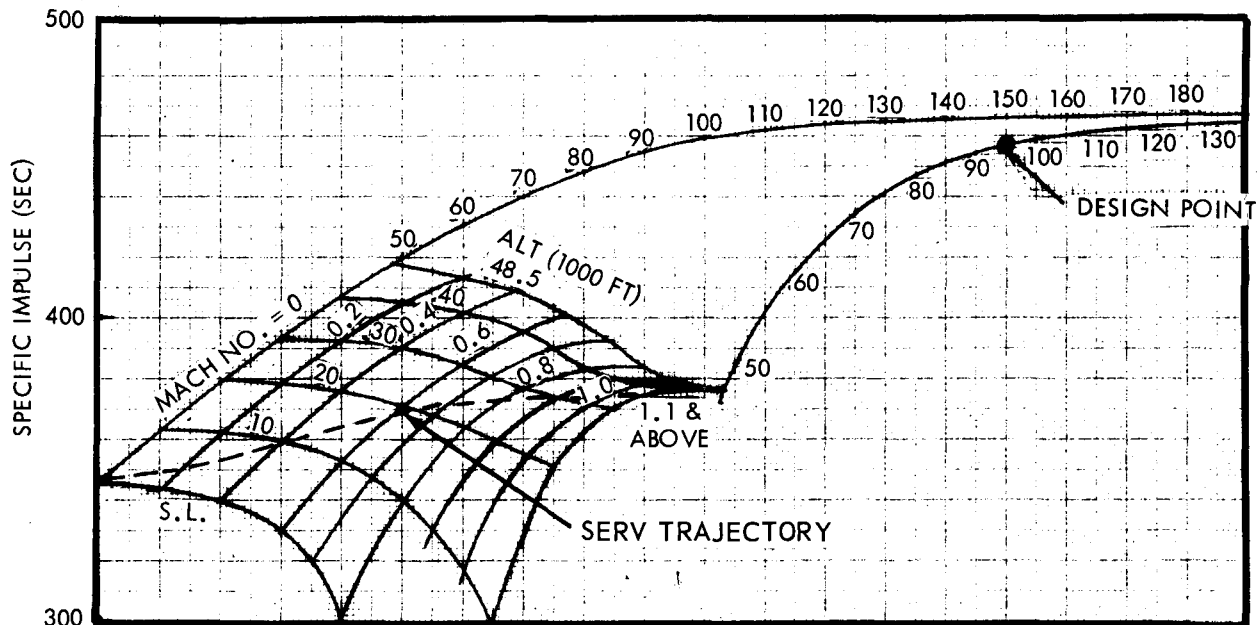
Figure 3.2-10. Nominal Performance of Point Design Engine
(Area Ratio = 433.7)

3.2.3 CONCLUSIONS

Three principal conclusions may be drawn from the analysis:

1) The behavior of the SERV aerospike nozzle was as expected. The base pressures were lower than anticipated but the integrated SERV-aerospike performance was as predicted. No fundamentally new phenomena were observed.

2) Feasibility has been demonstrated within limitations of current tests.

3) Further optimization of engine/vehicle geometry should be explored to improve performance.

3.3 AERODYNAMIC CHARACTERISTICS

This section describes drag and stability characteristics for both the ascent configuration and the descent configuration. In addition, reentry trim angle of attack and lift-to-drag ratio are described for the descent configuration.

3.3.1 ASCENT CONFIGURATION

To resolve this feasibility issue, four major tasks of aerodynamic analysis and testing were completed:

1) Investigation of sensitivity of aerodynamic performance to geometric parameters.

2) Definition of preliminary stability and drag characteristics by analytical methods.

3) Performance of preliminary wind tunnel test programs:

   a) Aerospike engine and base flow tests at the AEDC 16-foot Transonic Propulsion Wind Tunnel for a Mach range of 0 to 1.25 (completed 12-8-70).

   b) Force tests at the ARC 6-foot Supersonic Wind Tunnel for a Mach number range of 0.4 to 2.0 (completed 11-10-70).

   c) Force tests at the LaRC 4-foot Unitary Plan Wind Tunnel for a Mach number range of 2.6 to 4.64 (completed 1-12-71).

4) Application of wind tunnel data for definition of full-scale characteristics.

3.3.1.1   Net Axial Force

Net axial force during ascent flight is defined by three force components acting on the vehicle. (See figure 3.3-1.) These are:

1) Forebody drag composed of pressure and friction drag over the forward surfaces of the vehicle from the payload nose apex rearward to include the outside of the engine doors.

2) Base drag exerted over the inside of the engine doors and exterior flange inward to the engine nozzle, determined by the pressures acting over these surfaces with main stage propulsion on.

3) Effective aerospike engine thrust including compression ramp and base heat shield pressure forces.

The first two of these force components are typically expressed in aerodynamic coefficient form as a function of the flight Mach number at altitude.
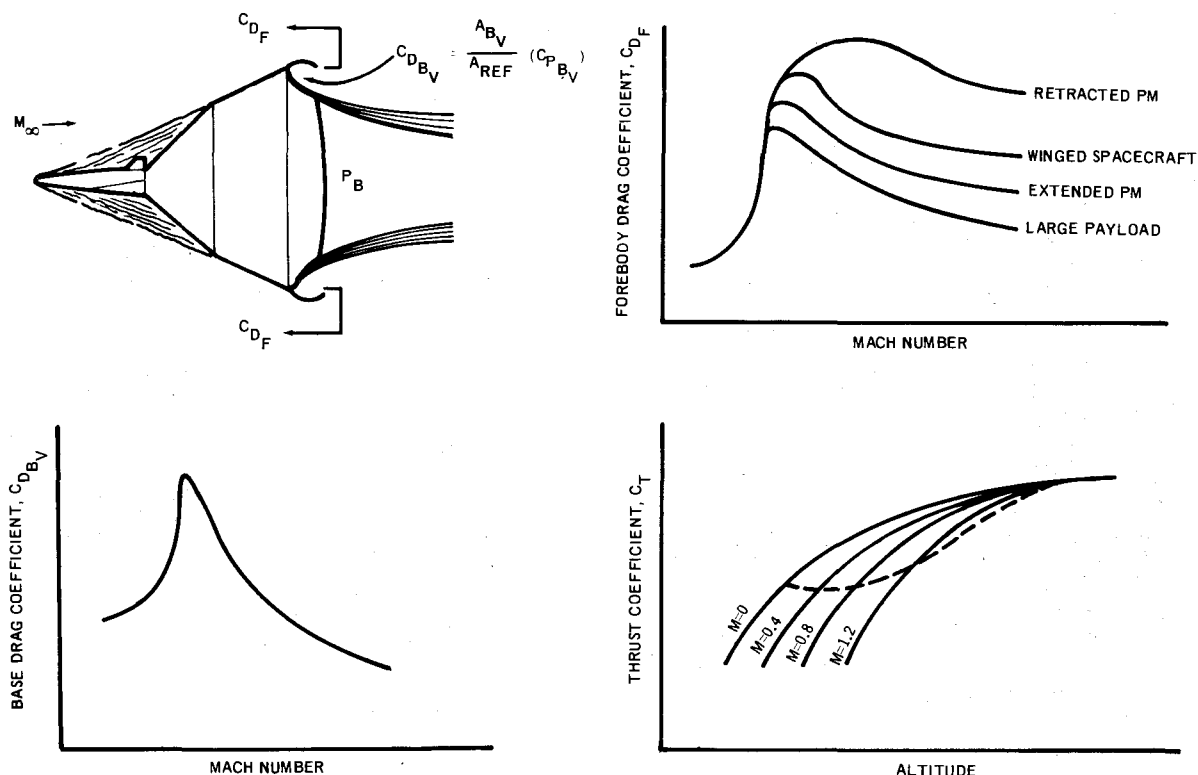
Figure 3.3-1.   Net Axial Force = Thrust - Forebody Drag - Base Drag

3.3.1.2   Flow Field Schlierens

Wind tunnel tests of ≥ 0.55 percent scale models were conducted at the NASA Ames Research Center and Langley Research Center to define preliminary values of the forebody aerodynamic drag and stability forces for the SERV ascent configuration with various payload geometries.

Shown in figure 3.3-2 are typical schlieren photographs of the aerodynamic flow around the various payload/vehicle configurations from an Ames transonic test. Test conditions are freestream Mach number of 1.4 at zero degrees vehicle angle-of-attack.

3.3.1.3   Aerodynamic Drag

Vehicle forebody and base drag coefficients are defined in figure 3.3-3 as a function of flight Mach number. The solid curves present data evaluated from the various scale model wind tunnel tests, compared to the preliminary predicted values presented by the dashed cures. The reductions in forebody drag for the various payloads are a result of the aerodynamic spike effect of the longer and larger payloads. Such payloads produce more conical flow pressure fields over the forebody surface as opposed to the high pressure blunt body level of the retracted personnel module configuration. The increase in drag of the winged payload above Mach 2 is caused by a decrease in the separated region and oblique shock attachment on the 45-degree cone. These trends are influenced by local Reynolds number.
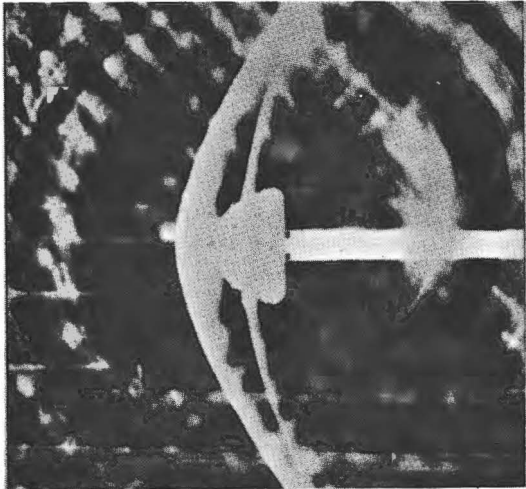
RETRACTED PERSONNEL MODULE (PM-2)
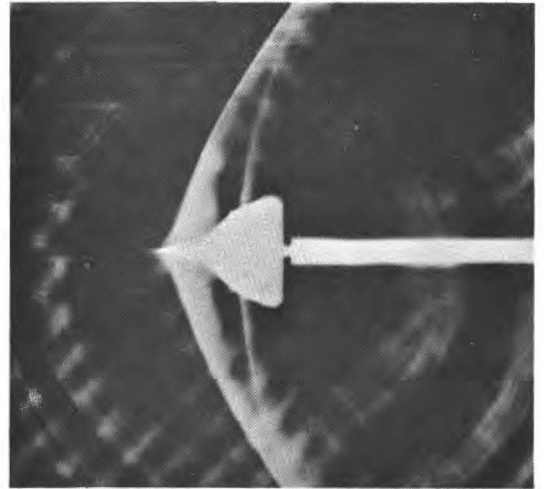
WINGED SPACECRAFT (WP-1)
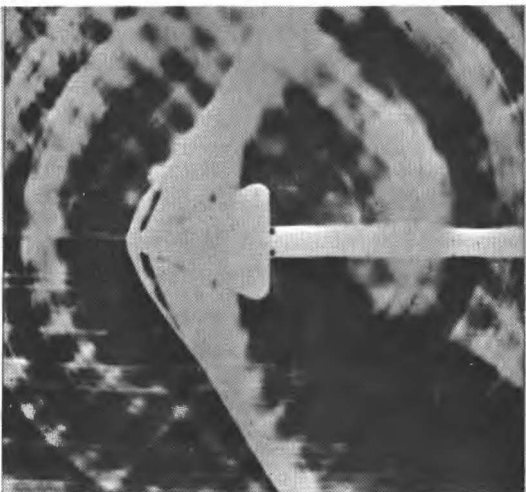
EXTENDED PERSONNEL MODULE (PM-1)
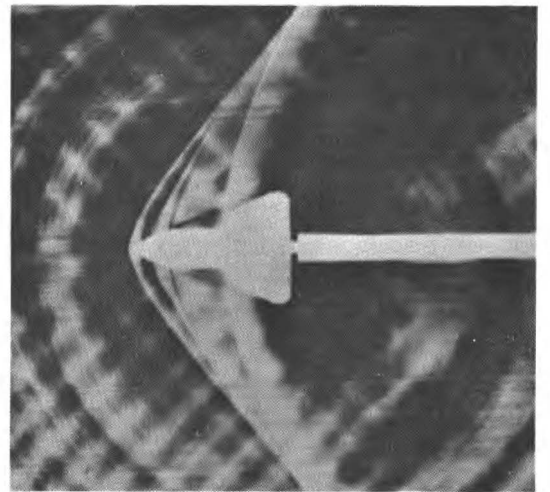
LARGE PAYLOAD (LP-1)

Figure 3.3-2.   Flow Field Schlierens at Mach 1.4 and $\alpha = 0$
(From Arc Transonic Test 66-552)
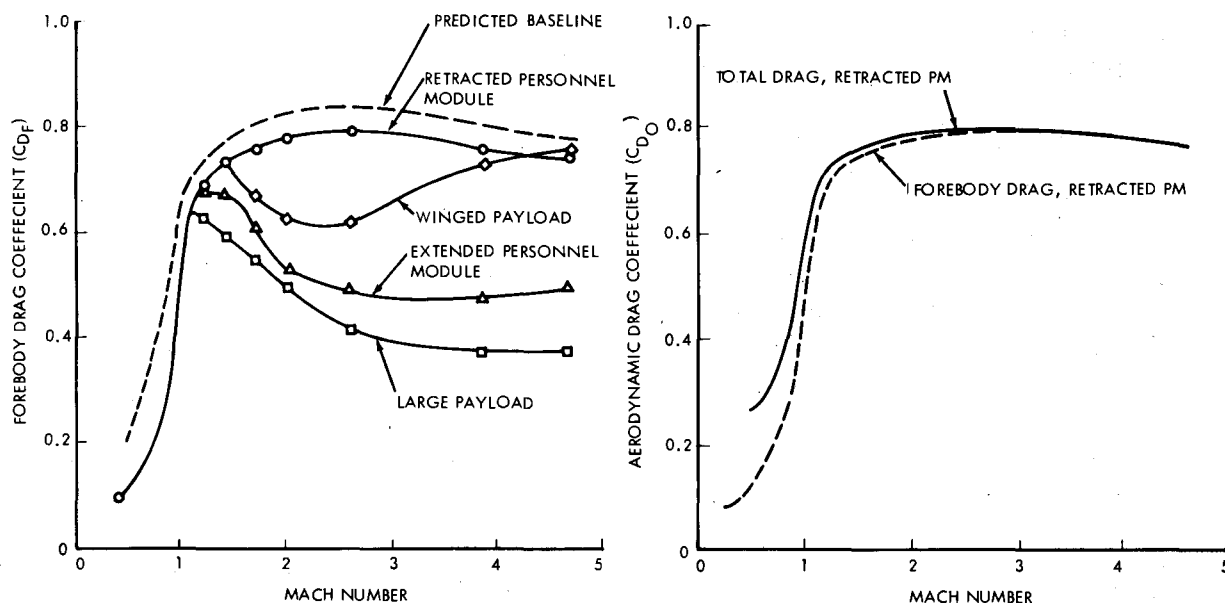
Figure 3.3-3. Aerodynamic Drag

The base drag coefficient includes base pressures acting on the engine doors and base cowl area outside of the engine nozzle perimeter. This incremental term provides a total drag coefficient for the vehicle with the correct engine door opening angle consistent with the definition of installed thrust performance previously presented.

3.3.1.4 Stability Characteristics

Aerodynamic stability characteristics, as determined from the scale model wind tunnel force tests, were compared with the preliminary predictions. The various payload configurations are not all statically stable (i.e., aerodynamic center of pressure (CP/D) aft of the center of gravity); however, the centers of aerodynamic moment are sufficiently close to the nominal center of gravity to not require excessive control forces for directional steering and attitude stability.

3.3.1.5 Conclusions - Ascent Aerodynamics

In summary, for the ascent vehicle, the retracted payload configuration demonstrates high forebody drag characteristics typical of blunt bodies.

The extended payload configurations have lower characteristic drag due to the induced flow separation and equivalent conical flow fields over the forebody above Mach 1.2.

The aerospike engine doors are approximately 10 percent of the total aerodynamic drag. Base drag is induced both by the ambient slipstream flow and the aerospike engine jet exhausts.

All payload configurations have sufficient neutral stability from the standpoint of minimum control force requirements.

3.3.2 DESCENT CONFIGURATION

SERV descent characteristics were first estimated by preliminary design analytical methods utilizing available Apollo data. These characteristics include reentry drag, stability, trim angle of attack, and lift-to-drag ratio. A minimum-scope preliminary wind tunnel test program was then defined to verify the predicted characteristics and determine those characteristics in the transonic and subsonic Mach range for which prediction methods are not adequate.

The test program consisted of testing a 0.55 percent (6-inch diameter) scale model of SERV parametric configurations through the deceleration Mach range of 4.64 to 0.4. It was concluded from indications of the reference Apollo data that the high Mach number aerodynamic data could be extrapolated to the reentry hypersonic Mach range with adequate accuracy for this feasibility study.

High Mach range tests were conducted in the 4-foot supersonic leg of the Langley Unitary Plan Wind Tunnel and were completed on January 12, 1971. Testing in the lower subsonic and transonic Mach range was completed in the Ames 6-foot Supersonic Wind Tunnel on November 10, 1970. These data were then analyzed to define the full scale hypersonic reentry and deceleration characteristics.

3.3.2.1 Reentry Trim Aerodynamics

The SERV reenters with heat shield forward and with a negative wind angle of attack to achieve the required lift-to-drag ratio (similar to the Apollo spacecraft). To obtain static trim at this negative angle of attack, a center of gravity offset from the vehicle geometric centerline may be employed. Figure 3.3-4 shows the static trim angle of attack (α_T) and the lift-to-drag ratio (L/D) at trim angle of attack for the SERV baseline reentry vehicle, with and without engine doors. These values are presented as a function of CG offset in feet for reentry flight Mach numbers varying from 9.0 to 0.4. As defined in the legend, the solid lines represent predicted values for the SERV baseline vehicle with engine doors. These predictions were determined by empirical application of Apollo reference data. The data symbols reflect SERV wind tunnel test data acquired in the Ames Research Center and Langley Research Center scale model force tests. By application of Apollo data trends, these values can be extrapolated to the hypersonic reentry Mach range with adequate accuracy for this level of feasibility study.

Removal of the aerospike reentry protection doors lowers α_T and respective L/D by approximately 30 percent below that with doors on. These data show that an approximate 3 to 4-foot CG offset will be required for the SERV baseline with engine doors to statically trim at an angle of attack in the hypersonic Mach range sufficient to attain an L/D of 0.3. With this constant CG offset, the static trim angle of attack and respective L/D will increase and then decrease as the vehicle decelerates through the supersonic and transonic Mach ranges.
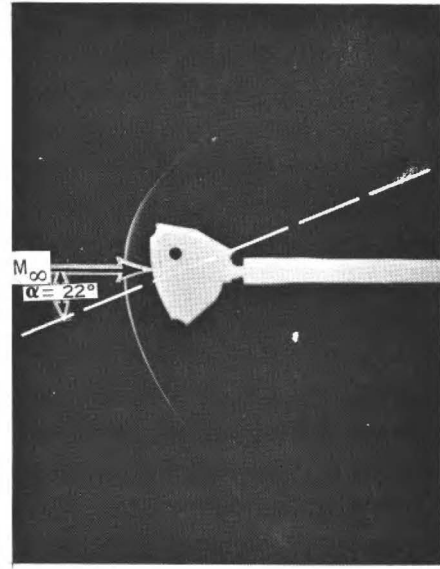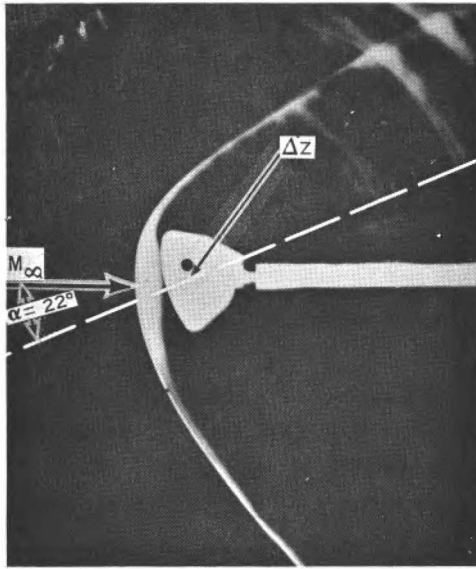
ARC TEST FLOW SCHLIERENS AT $M_\infty = 2.0$
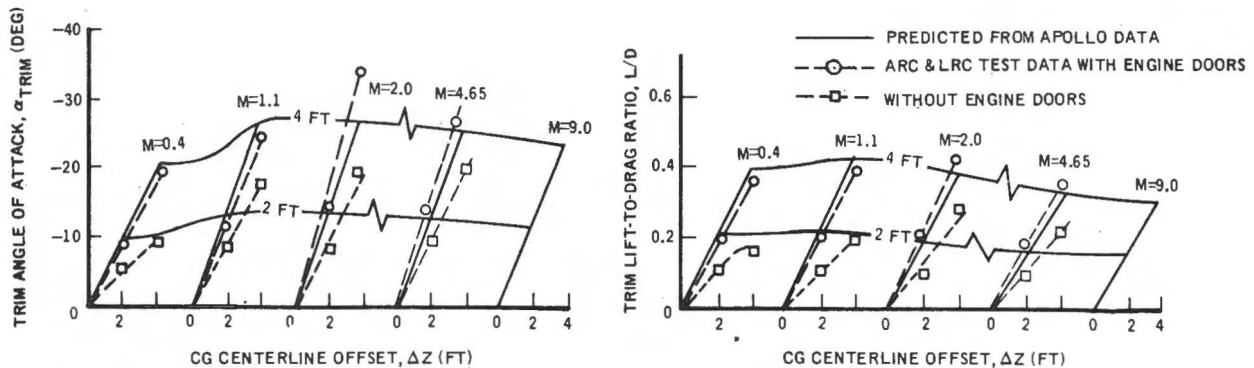
Figure 3.3-4. Reentry Trim Aerodynamics

Also illustrated in figure 3.3-4 are Schlieren photographs showing the aerodynamic flow around the two configurations at M = 2.0 and α = -22 degrees; these are typical of the photographs taken during the ARC and LaRC tests.

3.3.2.2   Stability and Drag

Employing a vehicle CG offset above the vehicle geometric centerline will result in the vehicle aerodynamically trimming at a heat shield facedown angle of attack.   For each Mach condition, the static aerodynamic trim angle of attack is that point at which the aerodynamic pitching moment is equal to zero.   The continuous near-linear negative slope characteristic of the pitching moment with angle of attack of the SERV indicates that the reentry configuration is stable within ± 10 degrees of the trim angle of attack and will have a favorable restoring moment when disturbed by winds.

The aerodynamic drag coefficient at α_T is nearly constant from hypersonic reentry through supersonic deceleration for a specific offset of the CG from the vehicle geometric centerline. The values decrease below Mach 1.0, following the trend expected for a hemispherically blunt body such as SERV.

Aerodynamic lift-to-drag ratio (L/D) at trim angle of attack increases with decreasing deceleration Mach number down to Mach 1.5 and becomes irregular through the transonic speed regime.

3.3.2.3   Configuration Trim Characteristics

Descent vehicle static aerodynamic trim characteristics are very sensitive to the reentry heat shield corner geometry. Illustrated in figure 3.3-5 are the trim angle of attack (α_T) and lift-to-drag ratio at α_T for four different corner geometries at Mach 4.64 as a function of lateral center of gravity position for a specific longitudinal location. There is no appreciable change in α_T by decreasing the heat shield corner radius from the baseline 11 percent to 5 percent, but there is an approximate 10 percent increase in L/D at trim angle of attack. Removing the aerospike engine thermal protection doors results in a 20 percent reduction in α and over a 30 percent decrease in the trim L/D. A very favorable increase in both α_T and $(L/D)_T$ is obtained by reducing the corner radius on just the lower side of the heat shield. A 11 percent to 5 percent combination was tested, which indicated that at this Mach number a trim angle of attack of 10 degrees and a trim lift-to-drag ratio of 0.15 could be obtained with no lateral CG offset, and for all feasible CG locations there would be a sizable increase in the trim lift-to-drag ratio primarily due to the increase in α_T.

NOTE:
- LOGITUDINAL CG LOCATION, X/D = 0.2459 REFERENCED TO VEHICLE STA (O)
- ΔZ REFERENCED TO VEHICLE CENTERLINE (FT)
- $M_\infty = 4.64$

——— 11% HEAT SHIELD CORNER RADIUS
– – – 5% HEAT SHIELD CORNER RADIUS
— — 11% UPPER, 5% LOWER HEAT SHIELD CORNER RADIUS
—·— NO DOORS
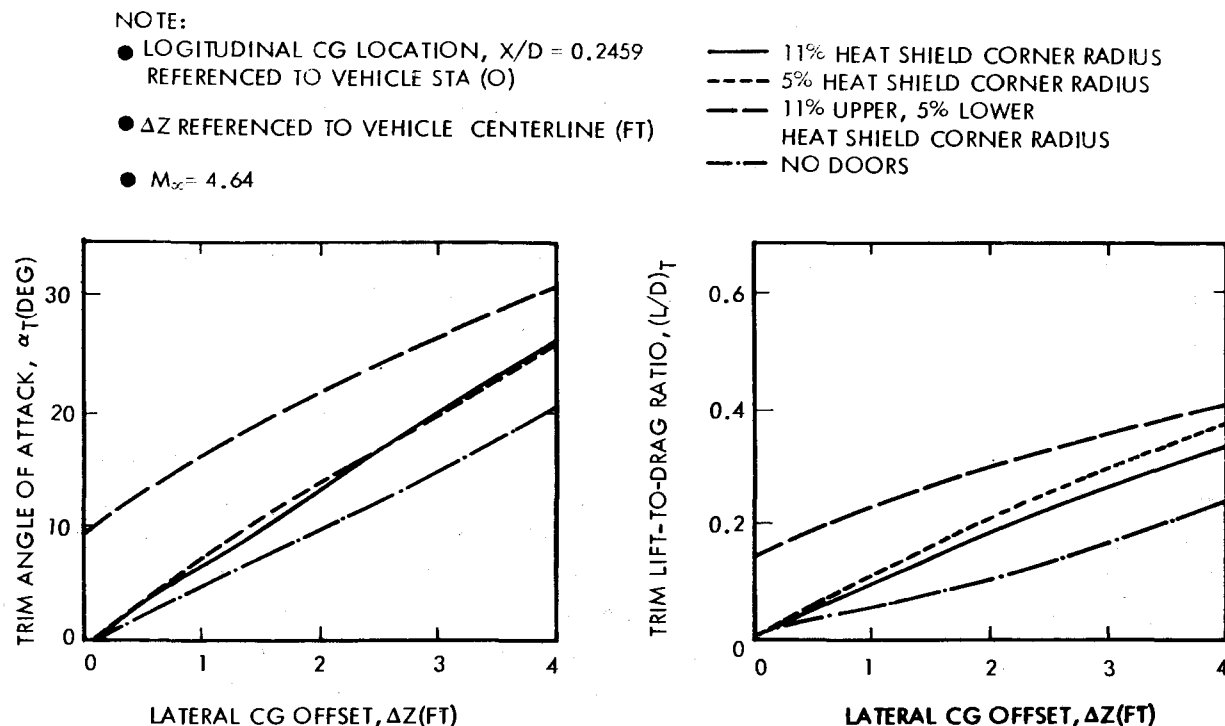
Figure 3.3-5. Configuration Trim Characteristics

3.3.2.4 Recommended Vehicle Descent Aerodynamic Trim Characteristics

To achieve the desired reentry L/D of 0.3 with minimum CG offset requirement, it was recommended that aerodynamic trim augmentation be utilized by employing different corner radii on the upper and lower perimeter of the heat shield. Figure 3.3-6 illustrates trim conditions that the recommended vehicle, having an upper corner radius of $(r/d)_u$ = 0.11 and a lower corner radius of $(r/d)_L$ = 0.05, would fly from reentry through supersonic deceleration. The vehicle is statically stable throughout this range and continues to be stable through transonic and subsonic deceleration.

Reentry trim angle of attack would be held to less than the afterbody angle to minimize afterbody heating. This will be accomplished by decreasing the lateral CG offset if necessary. A resultant α_T of approximately -22 degrees would adequately provide the reentry L/D of 0.3 desired. Both α_T and $(L/D)_T$ would increase with decelerating Mach number in the supersonic range below the flight regime of maximum aerodynamic heating.

The differential corner radii can be achieved by contouring the upper three quarters of the heat shield circumference to the larger radius and employing the smaller corner radius on only the lower quadrant. Effects of this heat shield corner radiusing would hardly be significant to the ascent aerodynamic characteristics of the vehicle, particularly if the radii are confined to the aerospike engine protection doors, which are open during ascent flight.

- $A_{REF} = \dfrac{\pi D_{REF}^2}{4}$
- $D_{REF} = D_{MAX}$
- CG LOCATED AT $\Delta X/D = 0.28$, $\Delta Z/D < 0.028$
- $(r/D)_U = 0.11$
  $(r/D)_L = 0.05$
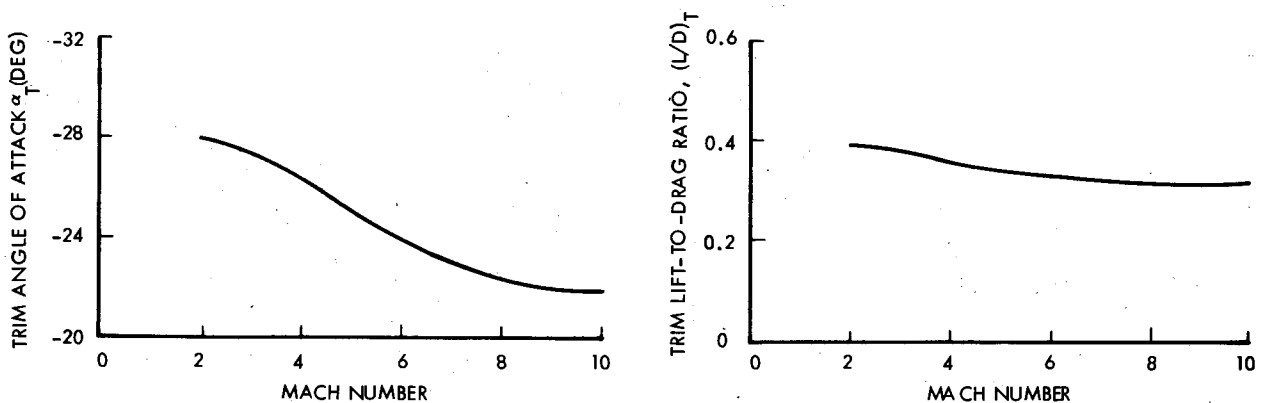
Figure 3.3-6. Descent Aerodynamic Trim Characteristics for Recommended Vehicle

3.3.2.5   Conclusions - Descent Aerodynamics

The desired hypersonic reentry trim L/D of 0.3 can be obtained for the baseline
vehicle with a CG offset of approximately 4 feet. Trim angle of attack would be
approximately -22 degrees. The vehicle is statically stable within ± 10 degrees of
the trim angle of attack from hypersonic reentry through transonic deceleration.

Removal of the aerospike engine thermal protection doors would result in over a
30 percent reduction in reentry trim L/D. This is due to both the reduction in
reentry trim angle of attack and L/D at angle of attack.

Differential corner radiusing of the heat shield is incorporated to minimize CG offset
required to achieve the desired trim lift-to-drag ratio.

3.4   THERMAL PROTECTION CHARACTERISTICS

The thermal environment and protective requirements for ascent and reentry are
presented and the effect of cryogen boiloff is discussed.

SERV reenters the atmosphere at an attitude very similar to the Apollo spacecraft.
Because the SERV shape is also similar to, though larger than Apollo, extensive use
was made of Apollo experimental and flight data in the SERV reentry heating pre-
dictions.

3.4.1   CONICAL FOREBODY

The ascent trajectory of SERV would result in lower aerodynamic heating than the
trajectories flown by the Saturn IB vehicles . (See figure 3.4-1.) However, the aero-
dynamic flow field caused by SERV's 45°0´ and 22°40´ frustums results in higher
aerodynamic heating than the smaller frustum angles on the Saturn IB. Convective
thermal environments that occur on the SERV frustums are compared with Saturn IB
heating rates in figure 3.4-1. It is seen that the heating rates on the upper and lower
frustums of the SERV structure are more severe than the Saturn IB heating rates on
the 9° LEM shroud.

The ascent thermal environment on these structures, assuming no thermal protection,
will result in temperatures of the exposed surfaces that are well below the temperature
limit of Inconel 718, which is approximately 1250° F. However the temperature
differential across the basic honeycomb panels during ascent and reentry were not
acceptable from a structure design standpoint. Therefore, methods of reducing the
temperature differentials were investigated. On the 45 degree frustum, maximum
temperature gradients will occur at a location that is an integral part of the hydrogen
tank. The gradients are, therefore, the result of extremely cold (-420°F) hydrogen
on one side of the honeycomb, ambient air on the other side of the honeycomb, and
the excellent insulative properties inherent in a honeycomb structure.

Figure 3.4-2 presents the SERV tank arrangement and the structural configuration in
each area. The external wall configurations for the 45°0´ and 22°40´ frustum consist

3-28

of a double honeycomb. The inner honeycomb is a structural load carrying component; the exterior honeycomb is lightweight and non-load carrying, and is designed to reduce the temperature gradient across the primary honeycomb.

Temperatures for each face of the double honeycomb configuration are presented on the left of figure 3.4-3. The outer face of the TPS panel reaches a maximum temperature of 890°F at 185 sec. The inner face of the TPS honeycomb reaches 160°F at 300 sec. The inner face of the structural panel is in contact with LH_2 prior to liftoff and, because the honeycomb panel is a good insulator, it remains very cold during ascent. Figure 3.4-3 presents the transient temperature differential across both the TPS panel and the structural panel for the 45-degree frustum. As shown, a maximum differential of 910°F occurs across the 2.0-inch TPS panel at 185 sec. Since this panel will not be a load carrying member, a differential of this magnitude is acceptable. A maximum differential of 540°F is shown across the 4.0-inch thick structural panel at 300 sec after liftoff. At this time, aerodynamic loads are negligible and the magnitude of this differential is also acceptable. A similar analysis was conducted on the 22°40′ frustum. The outer face of the TPS panel reached a temperature of 650°F. The maximum temperature gradient for the structural panel was 400°F.
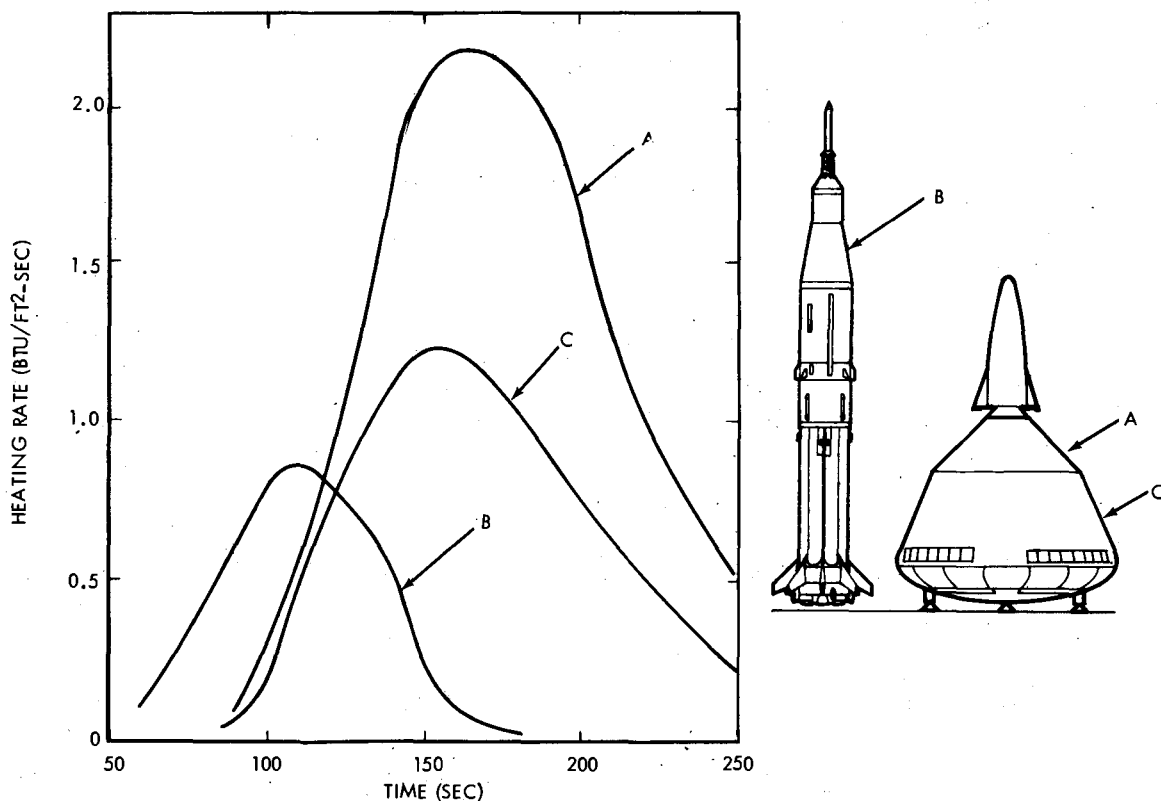
Figure 3.4-1. Ascent Heating Rate Comparison
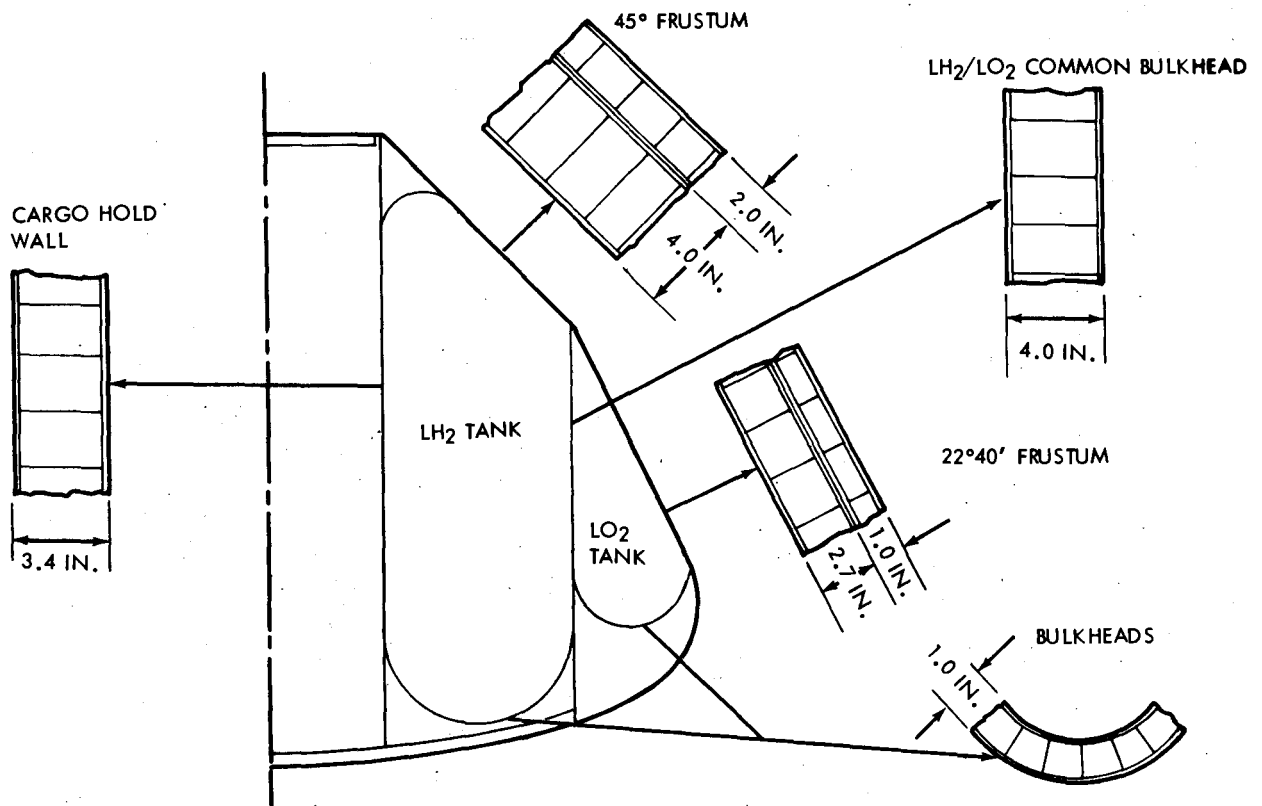
Figure 3.4-2. Cryogenic Tank Thermal Protection
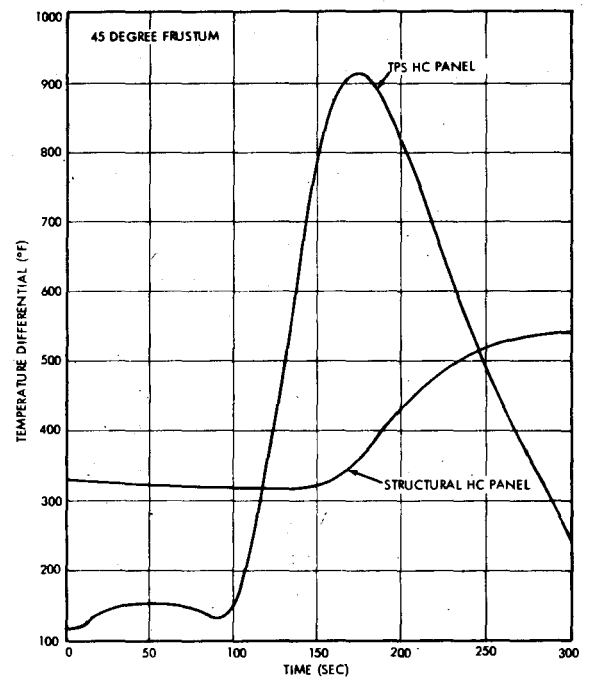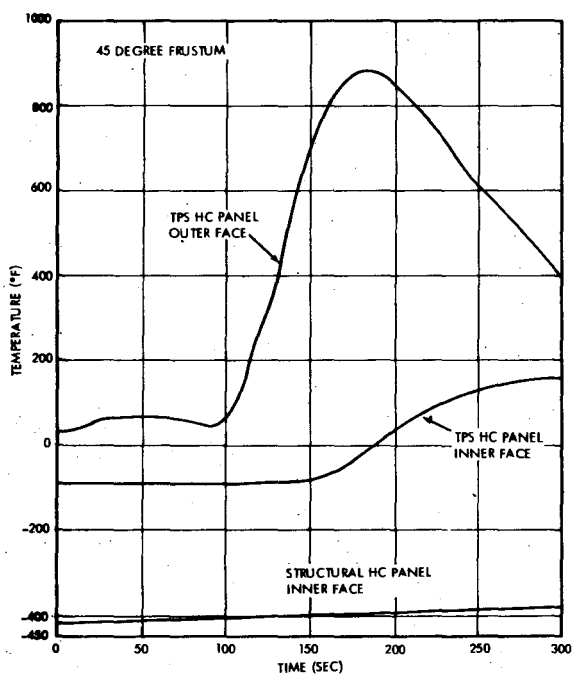
Figure 3.4-3. Ascent Temperature Histories

Heating rates and the outer face structural temperatures on the 45-degree frustum will be lower during reentry than during ascent. Figure 3.4-4 shows transient temperatures for all faces of the double honeycomb panel configuration at the point of maximum heating on the 45-degree frustum. The temperature of the exterior face of the TPS panel is seen to reach 800°F. Peak temperatures of the innerface of the TPS panel and the inner face of the structural panel is 385°F and 170°F, respectively. The maximum temperature gradient across the TPS panel and the structural panel are 600°F and 280°F, respectively. These temperature gradients are much lower than during boost because there is no temperature gradient at start of reentry; whereas, there is a large gradient prior to liftoff due to the LH_2 being in contact with the inner wall. A similar analysis was conducted for the 22°40´ frustum during reentry. The peak temperature on the outerskin of the TPS honeycomb was 1420°F.
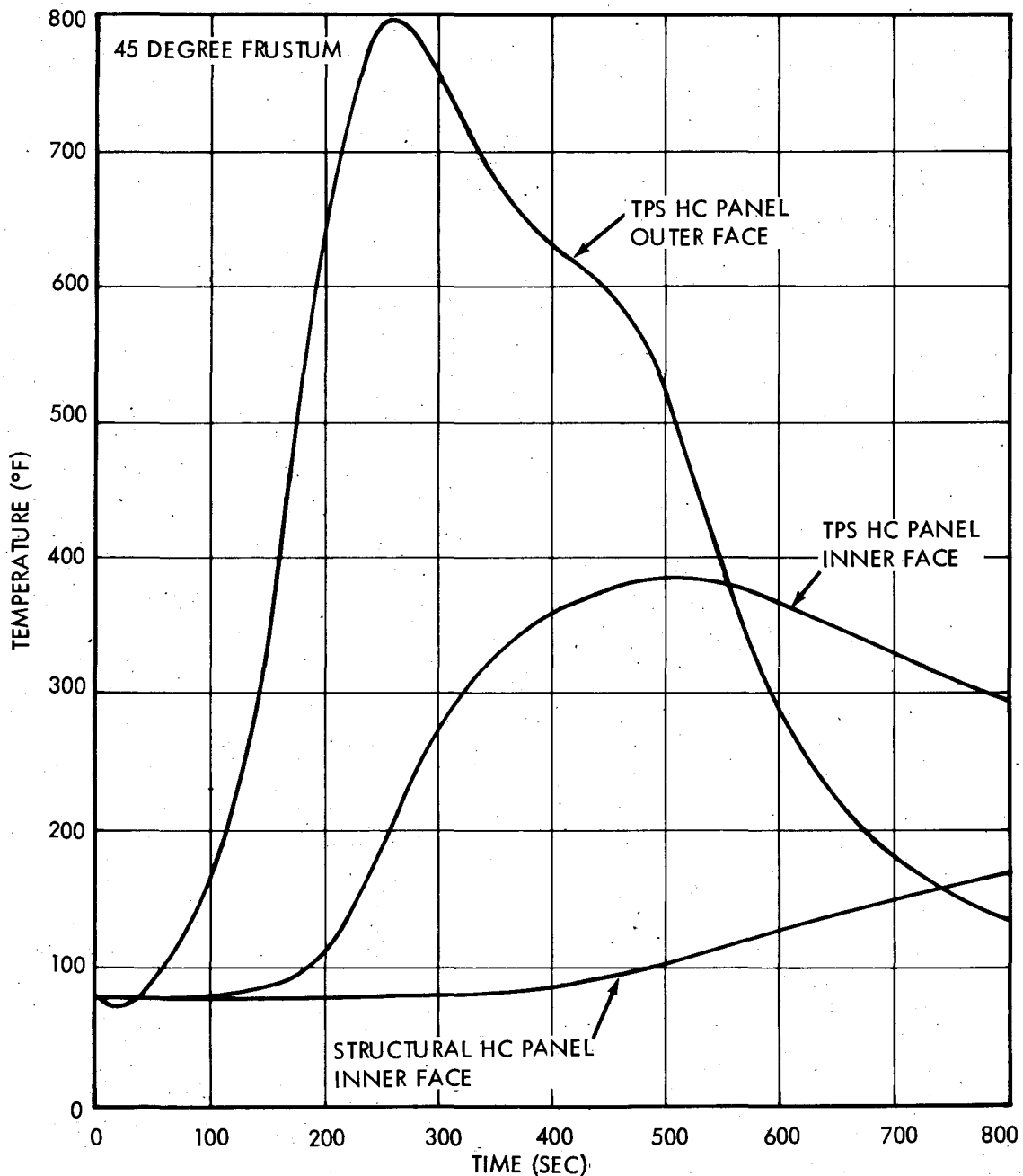
Figure 3.4-4. Reentry Temperature Histories

3.4.2 BASE HEAT SHIELD

The aerodynamic heating on the SERV heat shield during reentry is the dominant factor in establishing the ablative material requirements and substructure temperature. Reentry aerodynamic heating rates on the heat shield were calculated at the maximum heating location (S = 60 feet) and at the stagnation point (S = 0 feet). (See figure 3.4-5.) This was performed for both the maximum peak heating trajectory and the maximum total heating trajectory. The aerodynamic heating rates for these locations resulting from the maximum total heating trajectory are shown as a function of time.

Figure 3.4-5 also shows the variation in thermal environments on the heat shield, expressed as radiation equilibrium temperatures for the maximum total heating trajectory. It is seen that highest heating rates and, consequently, maximum ablative thickness will be required approximately 60 ft from the stagnation point.
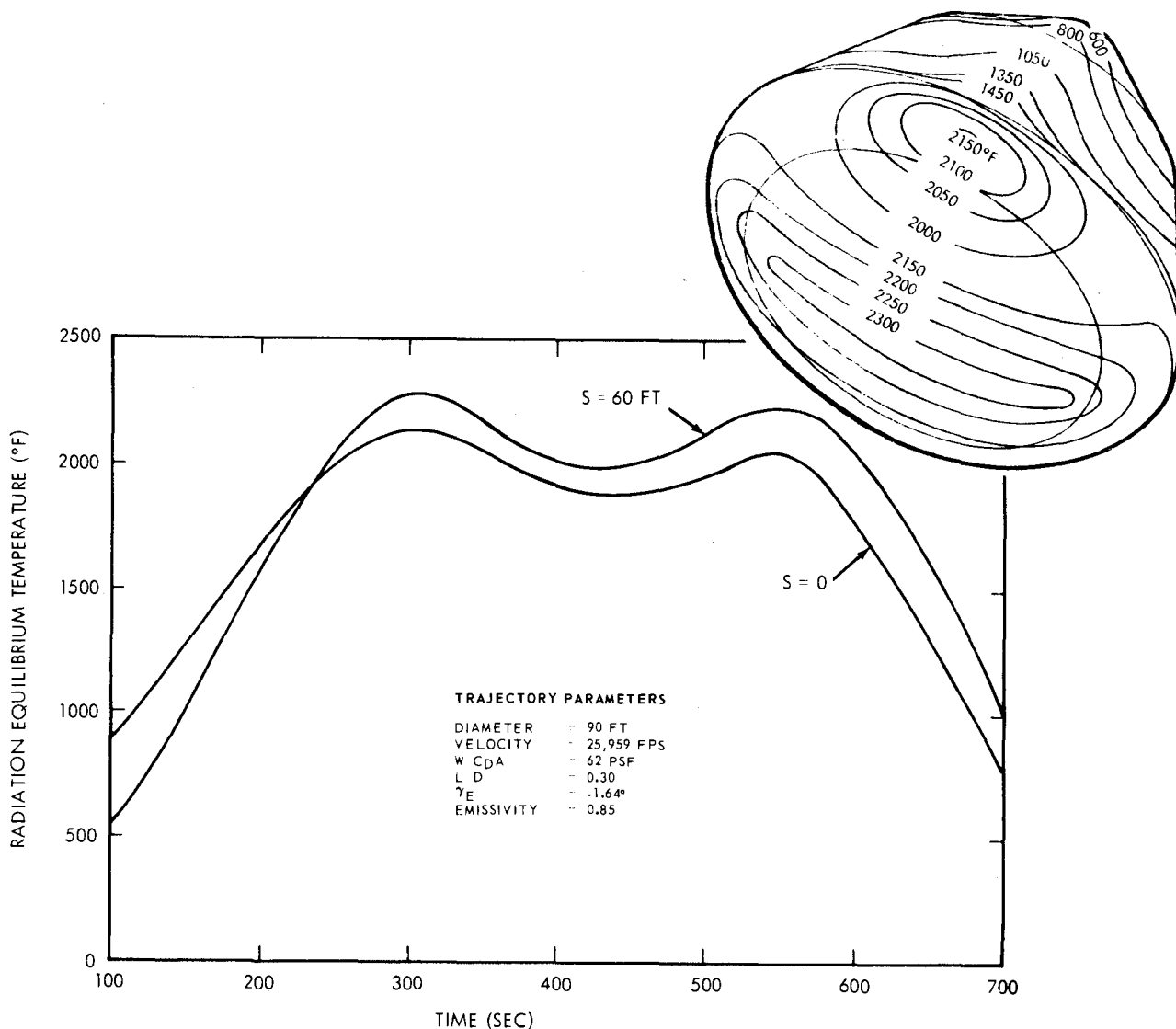
Figure 3.4-5.   Reentry Heat Shield Thermal Environment
(Maximum Total Heating Trajectory)

The adiabatic model depicted by Configuration A in figure 3.4-6 will result in the most conservative estimate of required ablation material. To determine the influence of a non-adiabatic backside honeycomb constraint, the two additional configurations, B and C were analyzed. A low density silicone elastomer was analyzed using these models. Ablator-honeycomb interface temperatures and structural honeycomb backside temperatures are determined.
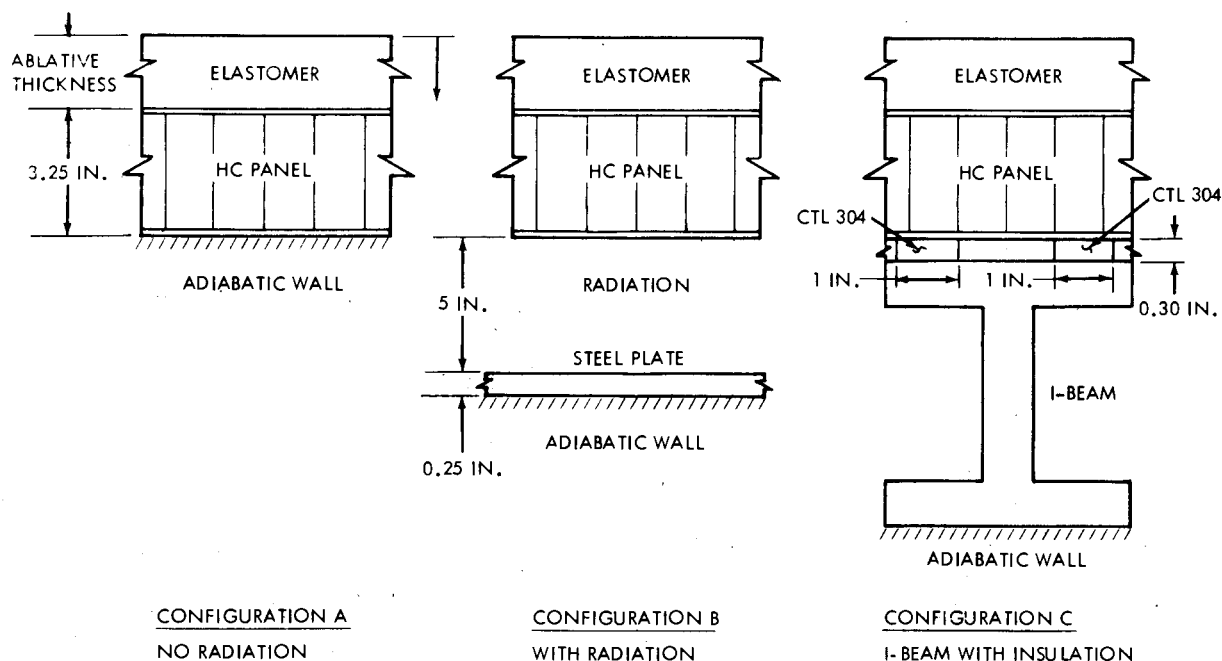
Figure 3.4-6. Ablation Heat Shield Configuration

The influence of internal structure on elastomer-honeycomb interface temperature and honeycomb backside temperature is shown in figure 3.4-7. As can be seen from these curves, the presence of internal structure decreases the maximum temperatures and increases the structural honeycomb temperature gradient. Peak interface and backside temperatures for the three configurations are shown in table 3.4-1.

3.4.3 CRYOGEN BOILOFF

Heat will enter the LH_2 tank from the 45-degree conical outer wall, the LH_2 /LO_2 common bulkhead, the cargo hold wall, and the upper and lower bulkheads. Heat transferred through each of these structures was calculated and the net heat entering the LH_2 tank determined.

The total boiloff rate is 5,161 lb/hr of LH_2. The total weight of LH_2 in SERV at liftoff is 604,517 pounds. Therefore, the boiloff rate per hour expressed as a percentage of loaded weight is 0.85 percent.
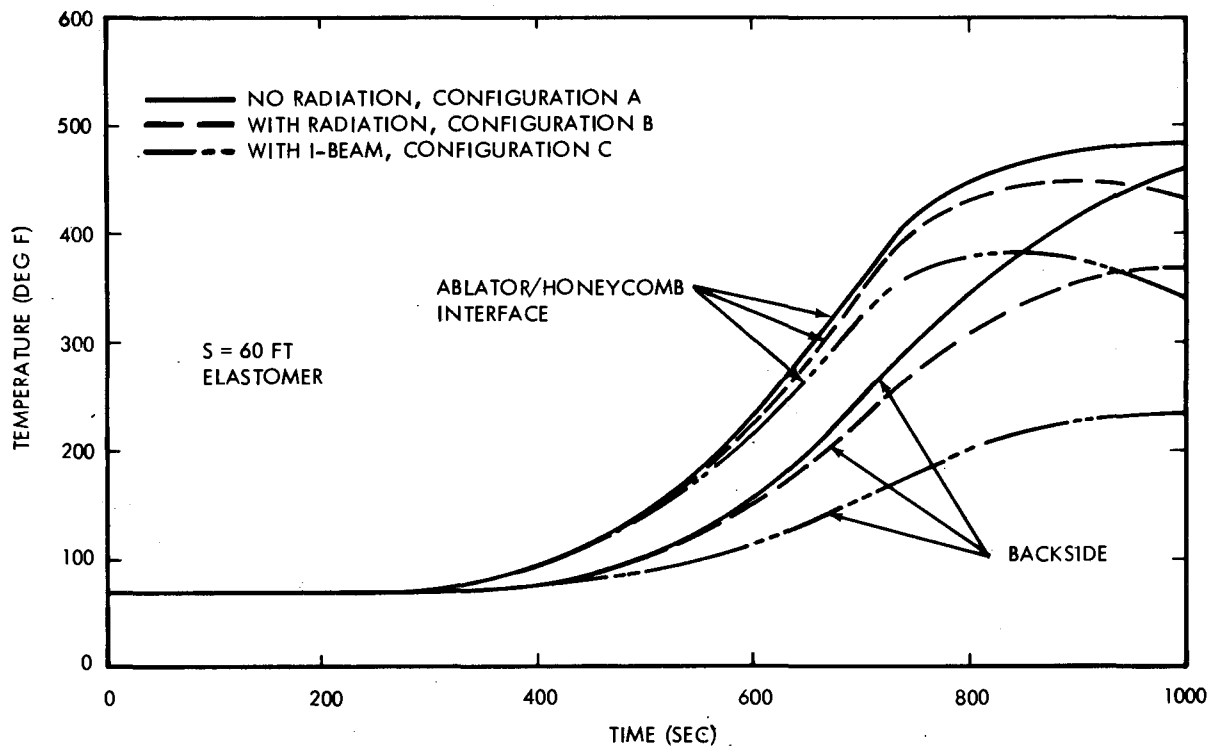
Figure 3.4-7. Influence of Substructure on Primary Structure Temperature

Table 3.4-1. Peak Interface and Backside Temperatures for Silicone Elastomer

For Maximum Total Heating Trajectory and an Elastomer Thickness of 0.8 inch	Configuration		
	A	B	C
Peak Ablator/honeycomb Interface Temperature (°F)	480	445	380
Peak Structural Honeycomb Backside Temperature (°F)	455	370	230

For comparison purposes, a loaded S-IBV stage includes 44,300 pounds of LH_2 and the boiloff rate on the pad is approximately 2,700 lb/hr, for a percentage rate per hour of 6.09 percent. SERV has a much lower percent boiloff due to the honeycomb panel being a better insulator than the polyurethane foam, which is used on the side walls of the S-IVB, and because of the good area-to-volume ratio permitted by the large SERV size.

Heat will enter the LO_2 tank from the 22°40´ lower frustum wall and the lower bulkhead. In addition the LO_2 will be cooled by the LH_2, but this effect is small and was not considered in the analysis. An analysis was made for each structure similar to that described for the hydrogen tank. The total boiloff rate for the LO_2 tank is 10,047 lb/hr, or approximately 0.30 percent of the total loaded LO_2 weight.

For comparison purposes the LO_2 boiloff from the S-IB stage is approximately 28,470 lb/hr or 4.5 percent of the loaded LO_2 weight. The LO_2 tanks on the S-IB stage are uninsulated aluminum and have poor surface-area-to-volume relationship and, therefore, a higher percent boiloff.

Table 3.4.2 presents a comparison of cryogenic boiloff for SERV with existing Saturn stages. Total boiloff and percent boiloff are compared.

Table 3.4-2. Cryogen Boil-off Comparison

LOX			LH_2		
Quantity Stage	S-IB	SERV	Quantity Stage	S-IVB	SERV
Total Boiloff Lb/Hr	28,470	10,047	Total Boiloff Lb/Hr	2,700	5,161
Total LOX Lb	630,000	3,628,655	Total LH_2 Lb	44,300	604,517
Percent of Total Boiloff/Hr	4.5	0.3	Percent of Total Boiloff/Hr	6.09	0.85

3.5 FLIGHT CONTROL

The major phases of ascent, reentry and landing are shown in figure 3.5-1.

3.5.1 ASCENT CONTROL

Vehicle attitude control during ascent is achieved through a combination of differential throttling of selected quadrants of the aerospike engine and RCS roll control thrusters. A block diagram of the pitch/yaw ascent attitude control system is shown in figure 3.5-2.
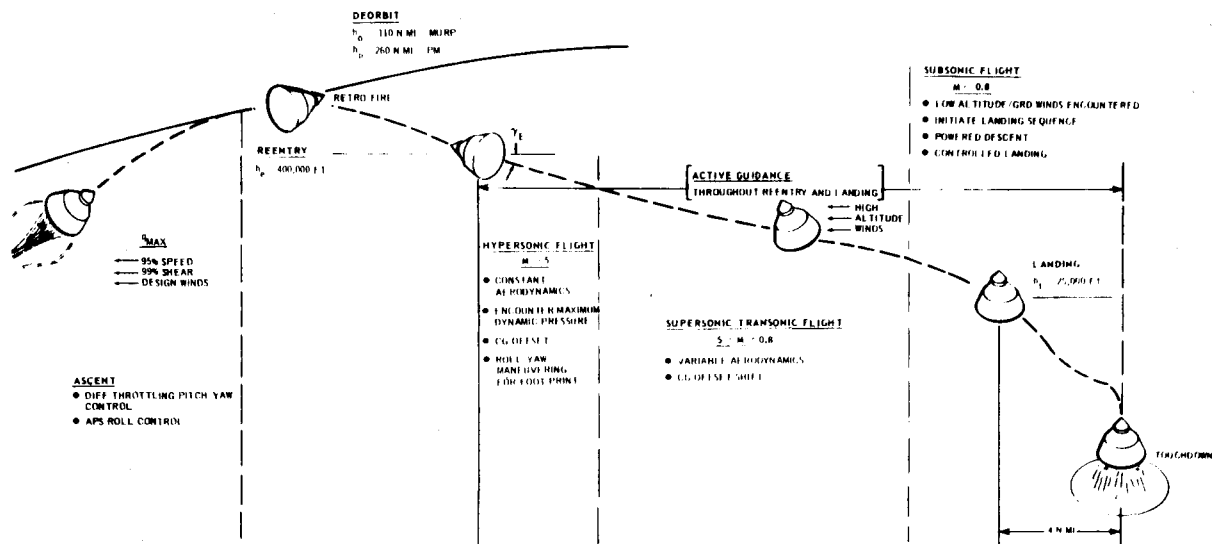
Figure 3.5-1. Major Phases of Ascent, Reentry and Landing Control
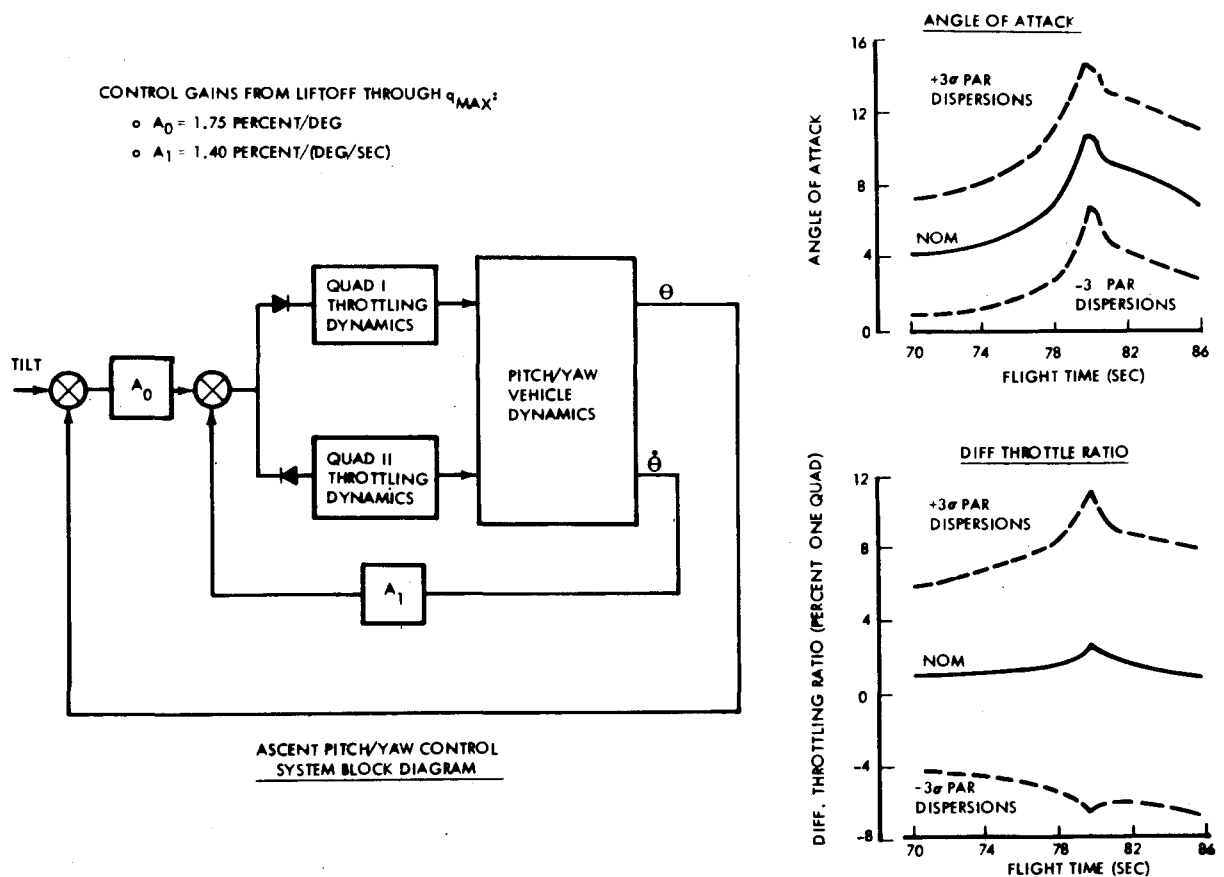
Figure 3.5-2. Ascent Pitch/Yaw Attitude Control

Control is generated from attitude and attitude rate signals. An attitude error gain of 1.75 percent/degree and an attitude rate gain of 1.40 percent/(deg/sec) provide a control frequency of approximately 2.0 rad/sec and a damping ratio of 0.7 at q_{max}. The control torque is generated by throttling an appropriate quadrant of the aerospike engine, thereby producing a moment due to the resultant thrust imbalance. Only one quadrant of the engine is throttled for a given control signal polarity (per axis) as symbolized by the diodes in the diagram. The controllability characteristics of SERV in the q_{max} region are also shown. A worst case condition was simulated by flying the vehicle through a 95 percent speed, 99 percent shear synthetic wind profile peaking at q_{max} and acting in the yaw plane. Parameter dispersions were also considered in evaluating the controllability characteristics. A six degree-of-freedom simulation of the vehicle was used to compute the nominal responses and a convariance propagation routine was used to establish the effects of parameter dispersions. The resultant angle of attack and control throttle ratio in response to the wind, are shown along with the corresponding dispersion envelopes due to the parameter dispersions. Note that the peak control throttle ratio requirement for both wind and parameter dispersions is 11.5 percent; the maximum available is 15 percent.

The roll control system for SERV during ascent employs an auxiliary propulsion system (APS) for providing the roll control torques in conjunction with a time optimal control law to minimize the response time during roll maneuver. A one degree deadzone in the switching logic is incorporated to provide a compromise between fuel consumption and an acceptable limit cycle amplitude. Response time and fuel consumption for various roll maneuver attitudes is shown on figure 3.5-3 along with a typical response to a 45-degree roll maneuver.

A sloshing analysis during ascent was performed. Due to the difficulty of predicting analytically the sloshing characteristics of partitioned annular tanks, the analysis was conducted for a worst case condition where no partitions are used. The resultant rotational symmetry made it possible to calculate the sloshing characteristics analytically. The results of this analysis revealed a strong LO_2 mode instability. This instability was as anticipated and results from the strong interaction of the fundamental LO_2 mode and the rigid body. Instability is attributed to the very large slosh mass and the very low sloshing frequency of the unsectored LO_2 tank. It is expected that the eight partitions which have already been designed into the tanks will lower the effective mass and raise the frequency of the LO_2 sloshing mode, thus substantially reducing or eliminating the sloshing instability. Additional damping if required may be provided by incorporating ring baffles. Further analysis of the sloshing characteristics of the partitioned annular tanks is recommended, supported by an experimental test program.

3.5.2 REENTRY GUIDANCE AND CONTROL

Depending on the SERV mission with either a MURP or PM payload, reentry is by deorbit from either a 110-nm orbit or a 260-nm orbit. Conditions of entry angle and velocity at the 400,000-foot entry interface are determined by constraints imposed by such factors as heating environment, acceleration limits, and the reentry footprint.

The major phases of reentry and landing are shown in figure 3.5-1.
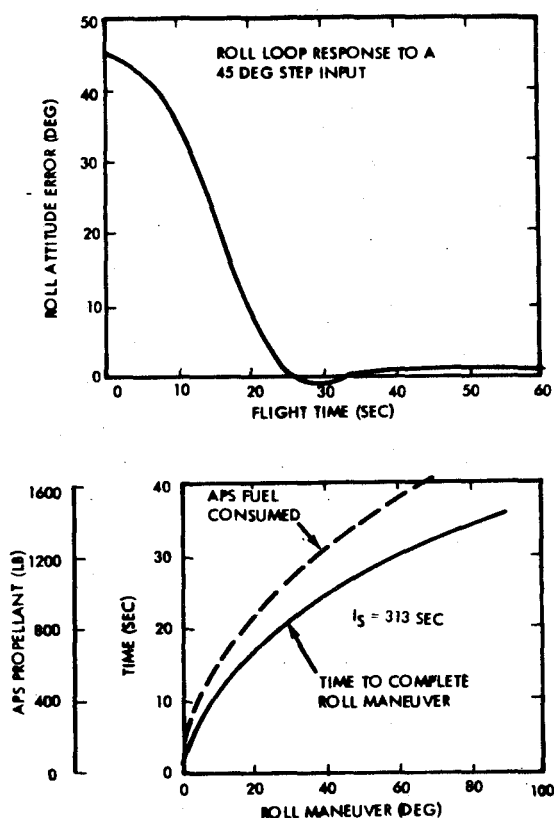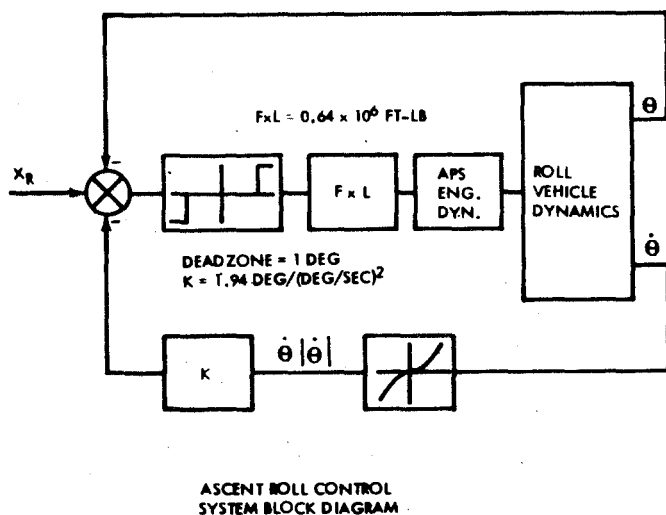
Figure 3.5-3. Ascent Roll Control

During the hypersonic region of flight, maximum dynamic pressure and peak heating temperatures are experienced and vehicle maneuvering is initiated to maintain the desired descent trajectory. The required L/D characteristics for maneuvering are achieved by a vehicle center of gravity (CG) offset of approximately 40 inches.

Because studies of the final vehicle configuration revealed that the maximum attainable CG offset was 36 inches, differential corner radius were incorporated as shown in figure 2.3-2. The radii were selected so that only a 30 inch CG offset was required thus providing a 6 inch margin. This margin can be increased by varying the radii ratio.

High altitude winds are encountered in the supersonic/transonic region of flight. During this regime the CG offset is reduced by the transfer of landing propulsion fuel. These factors combine to produce significant dynamic conditions for consideration in the design of the guidance and control systems.

In the subsonic region the landing sequence is carried out with particular attention given to the landing engine operational constraints, winds, and guidance and control requirements to obtain the necessary range with minimum fuel consumption.

The reentry attitude control subsystem (ACS) for SERV employs the same basic principles and type of hardware utilized in the Gemini and Apollo spacecraft. The basic

system, figure 3.5-4, is composed of a sensing system, signal conditioners and a set of reaction control thrusters which function in an automatic mode to provide the necessary three-axis stabilization of SERV from deorbit, through reentry, and down to the landing interface. The system is activated prior to the deorbit maneuver to orient the vehicle in its correct deorbit attitude. Attitude control is maintained throughout the deorbit maneuver. When the vehicle penetrates the atmosphere, the pitch and yaw attitude reference loops are opened to allow the vehicle to attain its aerodynamic trim state induced by an offset CG. Rate feedback is maintained in all three axes to damp oscillations which may be started due to perturbations in the trajectory.
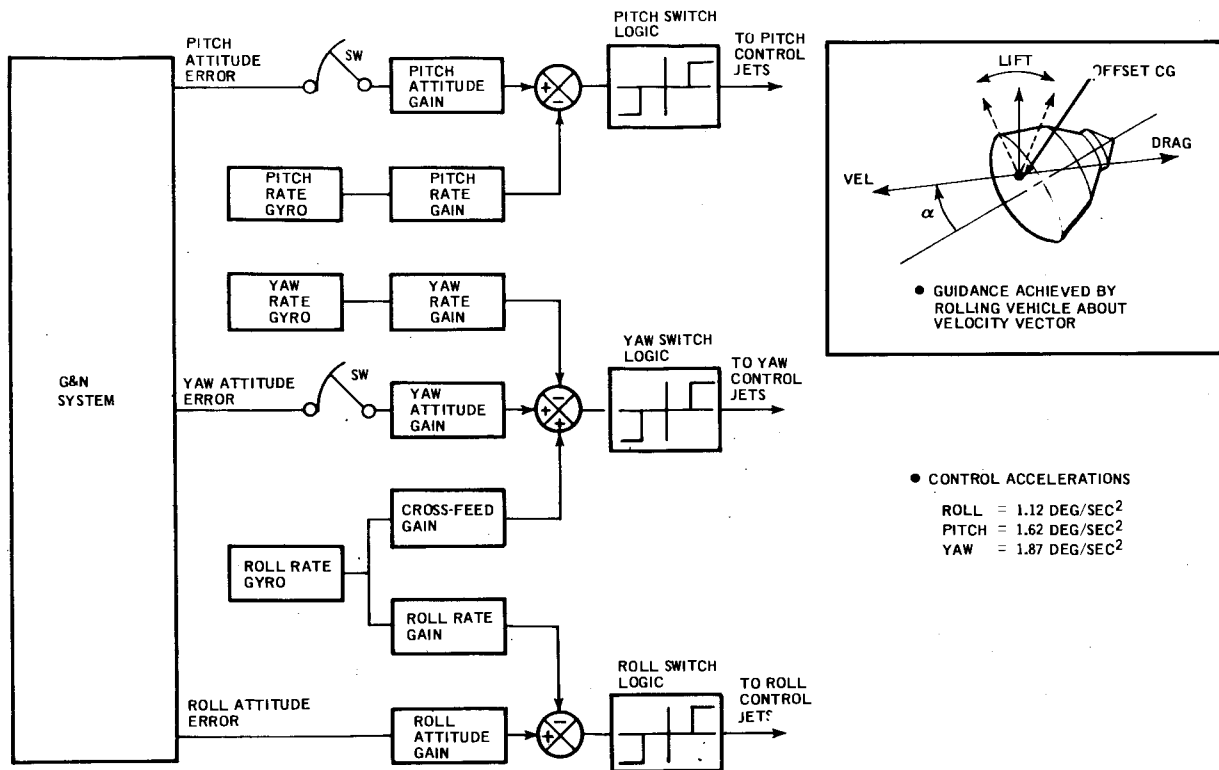
Figure 3.5-4. Reentry Attitude Control

Guidance of SERV is achieved by rolling the vehicle about the velocity vector to distribute the direction of the lift vector such that the proper reference trajectory is maintained. To minimize side slip, a portion of the roll rate signal is introduced into the yaw channel to effectively coordinate the turn.

The controllability of the vehicle in response to winds was assessed by investigating the attitude response characteristics for a family of 95 percent speed, 99 percent shear buildup and backoff wind shear profiles peaking in the altitude range between 46,000 to 26,000 ft. Results of the wind response analyses are summarized in figure 3.5-5, which shows the nominal no wind angle of attack along with superimposed responses to representative cases of the wind profiles considered. The envelope of peak wind induced angles of attack indicates that the maximum deviation from that of

the no wind case is approximately 7 degrees. This occurs for a wind profile peaking at approximately 28,000 feet. Also shown is the stability boundary for allowable angles of attack in the worst case direction (nose down). It is concluded from the results that the vehicle has adequate stability margins for the assumed trim condition and that higher trim L/D in the transonic/subsonic regions can be allowed if more maneuver capability is required.
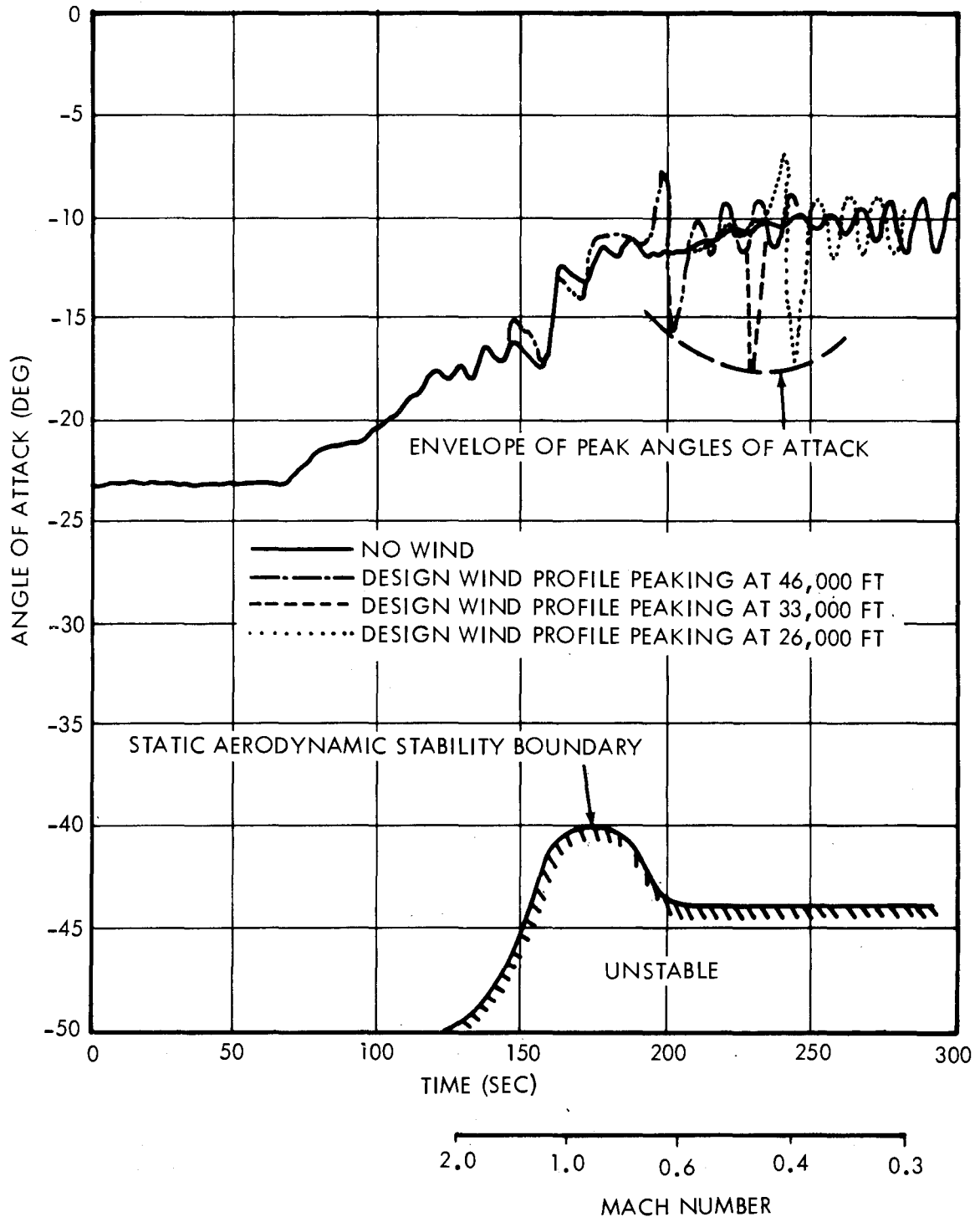
Figure 3.5-5. Summary of Reentry Wind Response Analysis

Pitch attitude and trajectory time histories for the nominal maximum lift condition resulting from a zero roll angle is shown in figure 3.5-6. These time histories represent the vehicle response characteristics starting at an altitude of 159,000 feet down to the landing interface at 25,000 ft. The CG shift trim maneuver starts at approximately 66 sec (at which time the Mach number is 5.5) and is completed at 116 sec (Mach 2.5). The responses to the trim maneuver are smooth and well damped. Maximum activity occurs during the transonic region. This region is characterized by highly varying aerodynamic characteristics that produce the relatively high amplitude oscillation between 120 and 220 sec. The oscillations, however, are maintained within the control deadbands.

Control of the reentry trajectory for SERV is achieved by modulating the L/D about the vehicle velocity vector. Modulation of L/D in the pitch plane controls the range, while modulating the lift vector in the roll plane controls crossrange. The maneuver commands in the form of roll commands are generated by the guidance and navigation subsystem. The control system accepts the roll commands and translates them directly into roll body axis commands, achieving turn coordination by crossfeeding roll rate into the yaw damper loop.

Typical responses of the vehicle to maneuver commands were obtained for the hypersonic/supersonic region and for the transonic/subsonic region. (See figure 3.5-7.) Step inputs of 20 degrees roll command were assumed in the hypersonic/supersonic region to simulate the vehicle response to typical bank angle commands generated by the guidance and navigation subsystem for the purpose of maintaining a reference trajectory. The responses are smooth and well damped. Good turn coordination is achieved by the crossfeed method by observing that the yaw angle of attack (sideslip) remains small during the response.

Response in the transonic/subsonic region shows a constant roll rate command of 10 deg/sec from Mach 3 down to approximately Mach 0.65. The constant roll rate is employed to effectively average out the lift so that an effective ballistic trajectory is maintained in this region. The purpose of doing this is to provide equal maneuver capability in any direction for controlling drift due to winds. The roll rate for this example is commanded to stop at approximately Mach 0.65, at which time the commanded roll angle is 90 degrees to represent a typical crossrange error correction. Just before reaching the landing interface, the roll angle is commanded to zero to illustrate the roll loop response characteristics for a typical landing preparation maneuver. In general the responses, like that in the hypersonic/supersonic region, are shown to be well damped and the limit cycle amplitude is small. Here again it is seen that good coordination of the roll maneuvers is provided by observing that the yaw angle of attack remains small during the response.

3.5.3 LANDING CHARACTERISTICS

The landing mode of SERV, figure 3.5-8, is initiated when SERV approaches an altitude of 25,000 feet, at which time its velocity is approximately 325 ft/sec. At that point in the trajectory the lift engine doors are opened and the engines started, with the ignition sequence taking approximately 8 seconds of an available 40 seconds. The vehicle will

INITIAL CONDITIONS:
- ALTITUDE = 159,313 FT
- MACH = 10.504
- FLIGHT PATH ANGLE = -2.1612 DEG
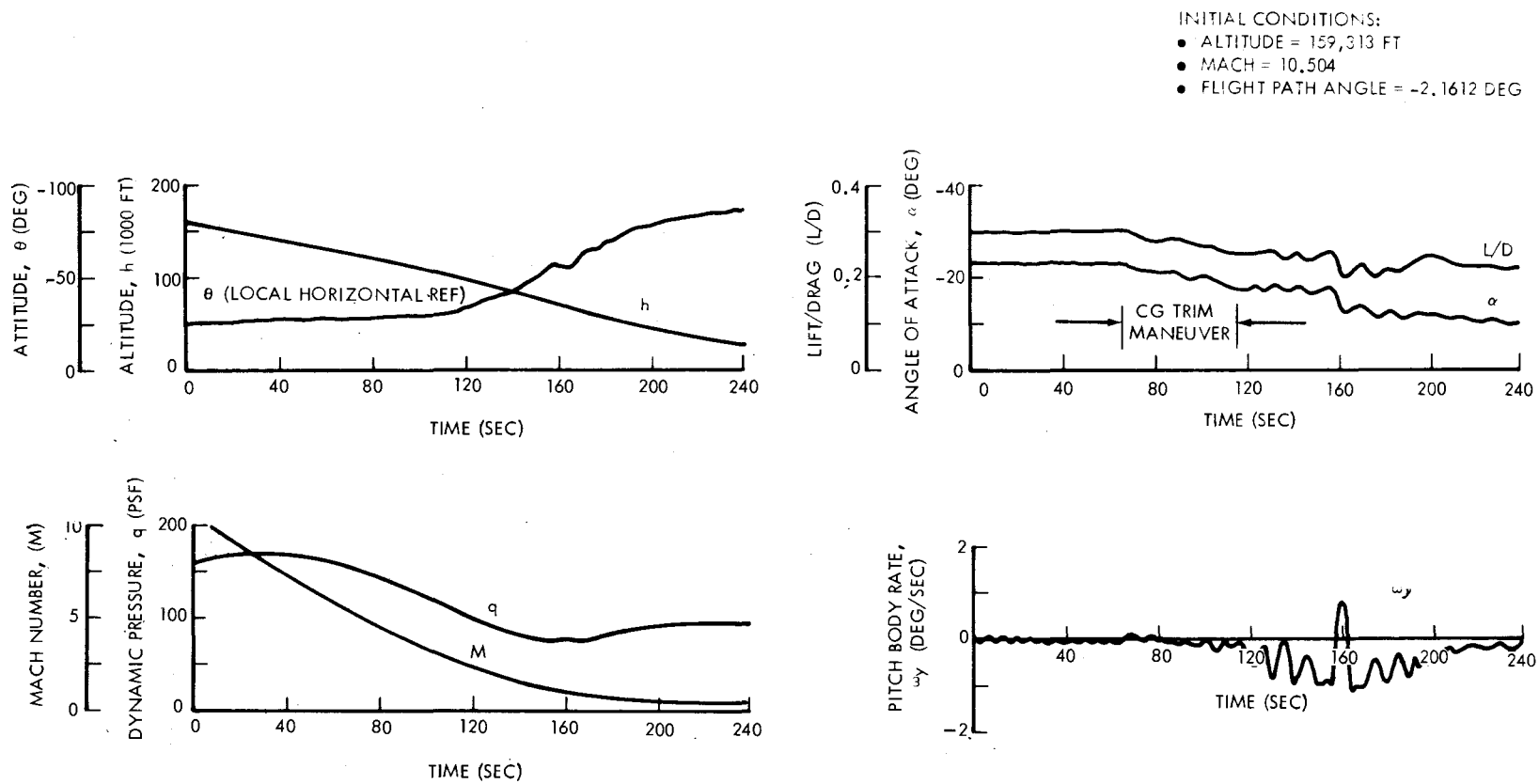
Figure 3.5-6. Reentry Attitude and Trajectory Time Histories
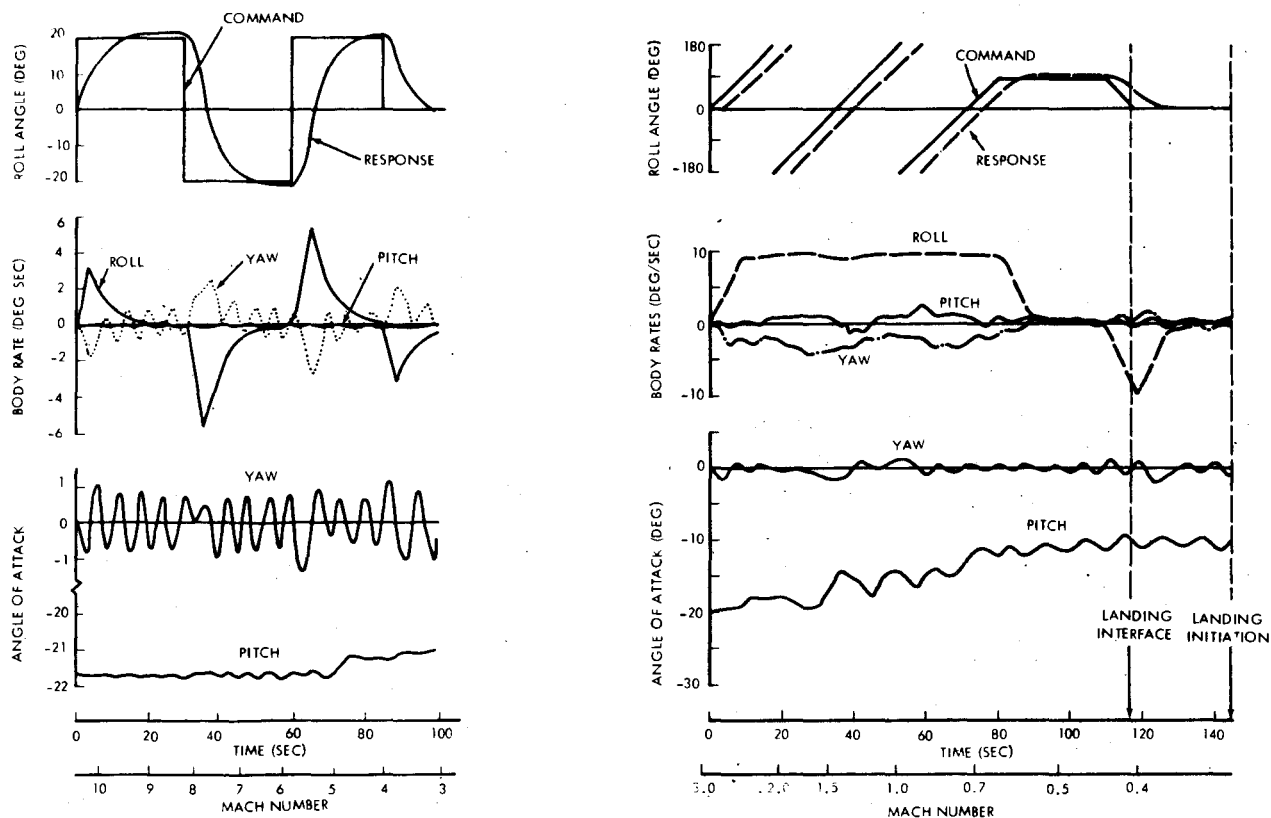
Figure 3.5-7. Response Characteristics to Roll Commands
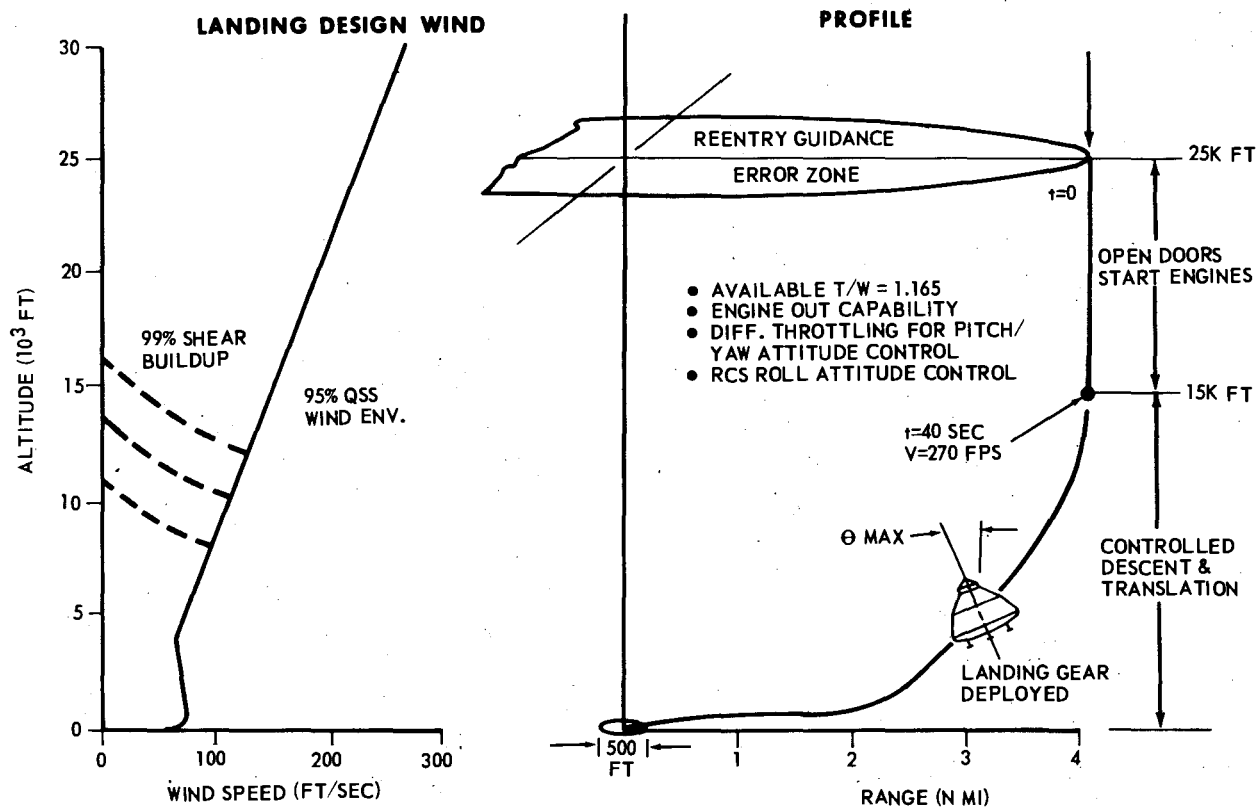
Figure 3.5-8. Landing Control Requirements

continue to descend with the propulsion subsystem at idle thrust (approximately 20 percent of maximum), down to 15,000 ft altitude, at which point the controlled descent is initiated.

The controlled descent is achieved by an automatic system capable of landing SERV at the preselected landing site from any point within a 4 nm radius. The landing system is sized to safely land SERV through a 95 percent speed, 99 percent shear wind and with one engine out. Translation control is achieved by simultaneously pitching the vehicle and throttling the propulsion subsystem. Attitude control in the pitch/yaw planes is provided by differentially throttling the landing propulsion subsystem,, and roll control by the same reaction control subsystem used during reentry.

To provide the maximum safety for a manned landing, a manual override capability will be added to the fully automatic system. Manual override will be used in an emergency mode in the event that SERV fails to reach the vicinity of the primary landing site due to improper reentry. During the manual mode the pilot will utilize an optical display system along with an onboard navigation system to select an alternate site for landing without hazard to life.

Because of the complex nature of the landing control dynamics, it was necessary to develop a detailed landing simulation in order to adequately design and evaluate a functional system. The simulation, which was developed on a digital computer, computes the motion of the vehicle in three coupled degrees of freedom: vertical translation, horizontal translation, and rotation; also included is an uncoupled roll degree of freedom. The simulation contains a detailed representation of the propulsion system and incorporates nonlinear aerodynamics. (See figure 3.5-9.)

The primary landing concept for SERV employs a fully automatic landing guidance and control (G&C) system which controls the descent of the vehicle to the preselected landing site. Inputs to the system consist of a set of measurements of the vehicle status obtained from an onboard navigation subsystem which is augmented by a set of suitable ground based navigation aids located near the landing site.

A functional diagram of one plane of the landing subsystem is shown in figure 3.5-10. There are three basic loops: altitude, range, and attitude. The altitude loop controls the vertical descent by commanding an latitude rate issued by the guidance subsystem. The commanded altitude rate is compared to the sensed altitude rate to form the error signal. This signal is then processed to form the control command that is routed to the propulsion subsystem. In a similar manner the range is controlled by commanding a range rate, also issued by the guidance subsystem. This signal is compared to the sensed range rate to form an error signal which is then processed to form an attitude command. The attitude command signal is combined with the sensed attitude and attitude rate to form the final control signal that is subsequently routed to the differential throttles, of the direct-life gas turbine engines causing the vehicle to rotate to the desired attitude, thus providing the originally commanded range rate.
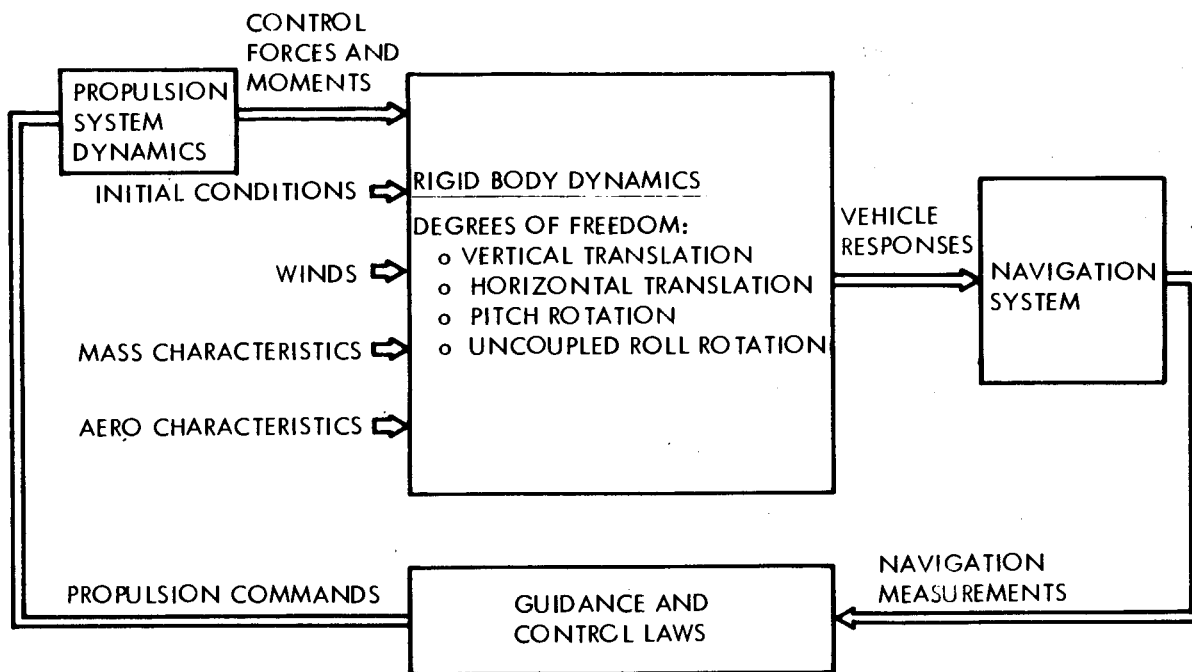
Figure 3.5-9.   Landing G&C System Digital Computer Simulation
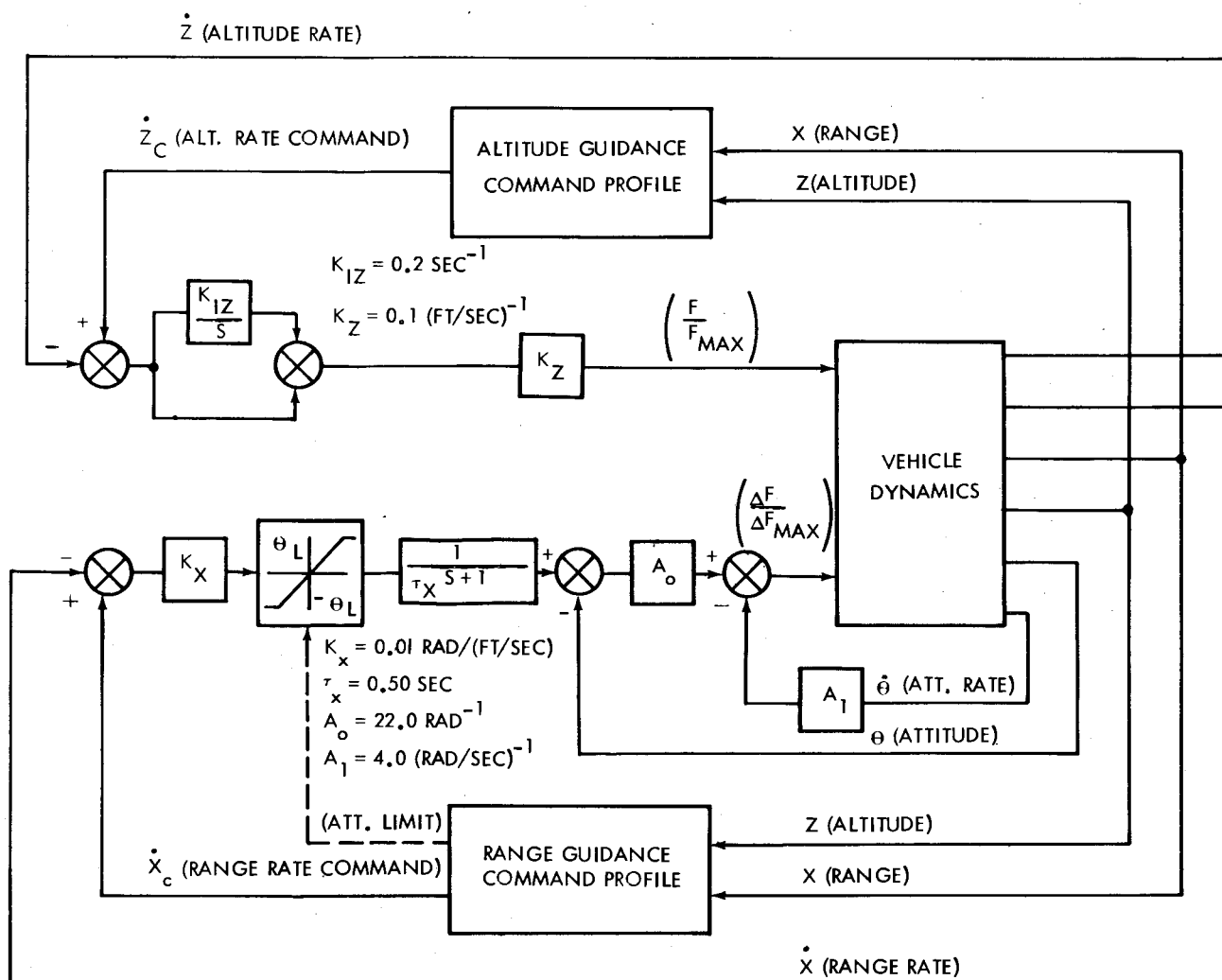
Figure 3.5-10.   Landing G&C System Functional Diagram

Guidance is achieved from a set of precomputed profiles that are stored in the guidance computer. These profiles are established to satisfy the propulsion subsystem constraints while minimizing fuel consumption. Functionally, the guidance profiles represent a set of nonlinear gain functions that relate the instantaneous measured altitude and range to the altitude rate and range rate commands.

A typical set of nominal responses for the maximum design condition is shown in figure 3.5-11. This case represents a condition where the vehicle is 4 nm from the landing pad and encounters a 95 percent speed, 99 percent shear KSC design head wind profile peaking at 12,000 ft. The 3-degree-of-freedom digital computer landing simulation was used to generate the response.
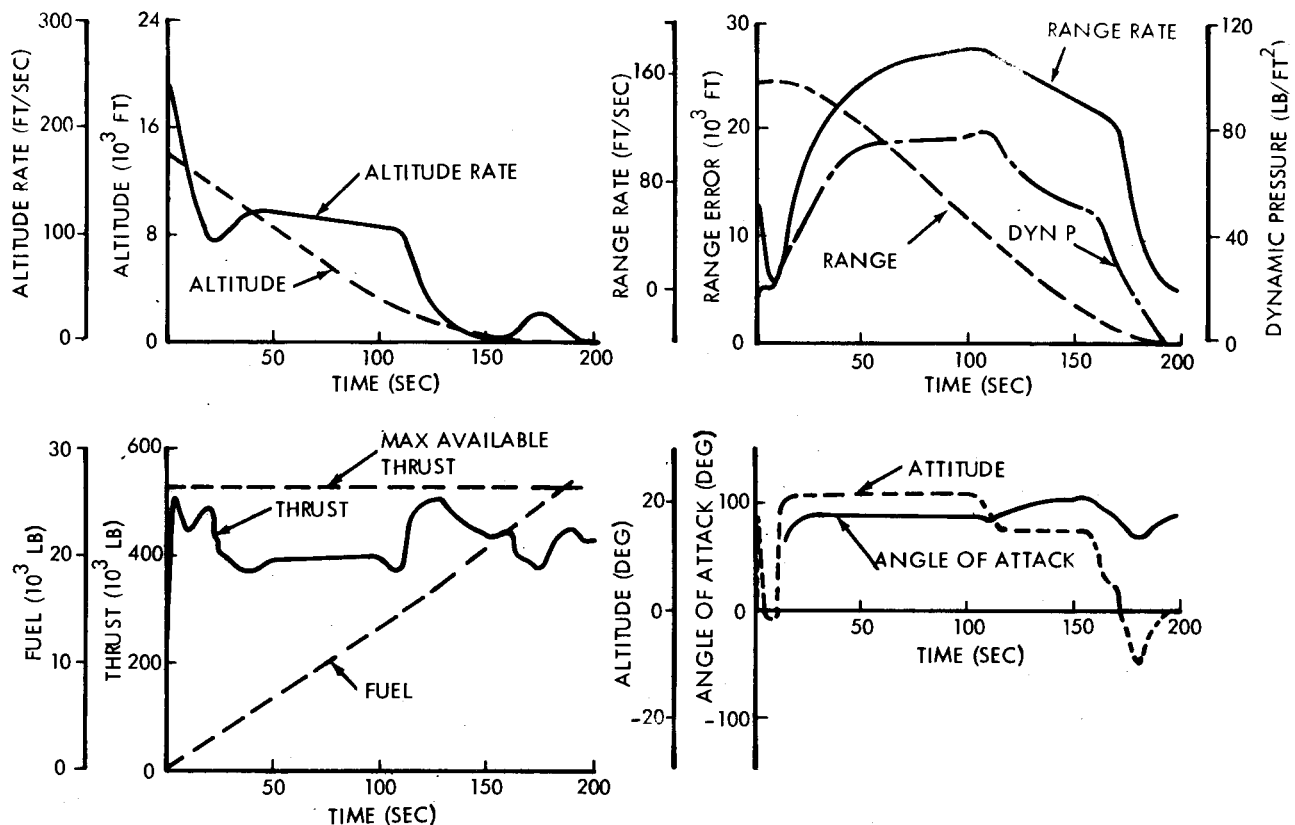
Figure 3.5-11. Typical Landing Control Responses

Controlled descent starts at 15,000 ft with touchdown occuring some 200 sec later. As the vehicle descends, its velocity vector is forced from an almost vertical direction to horizontal. At the same time the attitude is controlled to within ±22 degrees from the local vertical to ensure that the vertical propulsive forces can counteract gravitational forces. With these conditions the vehicle angle of attack ranges from zero to approximately 105 degrees. The peak aerodynamic disturbing moment during the landing maneuver has been minimized by appropriately shaping the altitude guidance command profile so that dynamic pressure is reduced to a point where the vehicle total

aerodynamic moment coefficient is maximum. This is illustrated by the dip in the dynamic pressure at approximately 10 sec after landing initiation. The resultant peak disturbing moment (not shown) for this maximum design condition is only 50 percent of the available control, indicating that adequate controllability is available. Total fuel consumption for this case is 27,900 pounds, which is used as the design fuel loading for vehicle weight computation. The peak translation velocity during the landing is 170 ft/sec referenced to the ground which is 240 ft/sec relative to the wind. The final lateral deceleration occurs when the vehicle is approximately 800 ft from the center of the landing pad. Deceleration is shown to be smooth and well damped. The attitude response during the final deceleration is well damped with the attitude error close to zero at touchdown.

The most critical phase during a fully automatic instrument landing is the final approach and touchdown. Accurate guidance, navigation, and control must be provided during this phase so that the vehicle touches down with conditions which are within the design limits of the vehicle. During the design of the guidance and control system, special emphasis was placed on achieving satisfactory touchdown characteristics by designing well damped, high accuracy control loops. Figure 3.5-12 shows the final approach trajectories for various combinations of initial range errors and winds with the assumption that perfect navigation is available. The summary table on this figure shows that the touchdown characteristics for all combinations of winds and initial conditions analyzed are well within the design requirements.

WIND / INITIAL RANGE ERROR / TOUCHDOWN CHARACTERISTIC	NO WIND		95 PERCENT HEADWIND	95 PERCENT HEADWIND	95 PERCENT TAILWIND
	0	4 NMI	0	4 NMI	4 NMI
SINK RATE (FT/SEC)	0.31	0.26	0.26	0.22	0.18
DRIFT RATE (FT/SEC)	0	0.41	0	0.35	0.48
DISTANCE FROM CENTER OF PAD (FT)	0	2.60	1.90	7.30	8.70
ATTITUDE FROM VERTICAL (DEG)	0	0.03	0	0.25	0.32

Legend:
——— { X(O) = 0 / NO WIND }
—·—· { X(O) = 0 / 95 PERCENT WIND }
— — — { X(O) = 4 NMI / NO WIND }
—o—o— { X(O) = 4 NMI / HEAD WIND }
- - - - { X(O) = 4 NMI / TAIL WIND }

ALTITUDE (FT)

RANGE TO CENTER OF PAD (FT)

Figure 3.5-12. Final Approach and Touchdown Characteristics with
Perfect Navigation

Figure 3.5-12 illustrated the landing touchdown characteristics of SERV for the ideal case of perfect navigation. During an actual landing, however, there will be some measurement errors present. A sensitivity analysis was therefore performed to establish the relationship between navigation errors and touchdown dispersions. This was accomplished by calculating a sensitivity matrix that transforms an appropriate navigation error model to a corresponding set of SERV touchdown dispersions. The 3-degree-of-freedom digital computer landing simulation that was developed during the landing studies was used to evaluate the sensitivity matrix.

Application of the sensitivity matrix method was made in analyzing a navigation scheme currently being studied by the NASA Ames Research Center. The Ames system, called RAINPAL (Recursive Aided Inertial Navigation for Precision Approach and Landing), consists of an IMU, a barometric altimeter, a set of ground based navigation aids, and employs a Kalman filter algorithm programmed in an onboard digital computer for optimally combining data from the various sources. Preliminary error models of the RAINPAL system for two different ground based navigation aids are tabulated in figure 3.5-13. Data on the left is for the precision ranging system (PRS) ground based navigation aid; the set on the right is for microwave scan beam (MSB) ground based navigation aid. The latter system is being presently considered as the future standard for commercial aviation. The 3σ landing touchdown dispersions of SERV corresponding to the two navigation error models are tabulated on figure 3.5-13, along with the maximum allowable for SERV. Note that both navigation error models provide touchdown characteristics that surpass requirements.

ASSUMED NAVIGATION ERROR MODELS

MEASUREMENT	RMS ERRORS AT TOUCHDOWN	
	PRECISION RANGING SYSTEM (PRS)	MICROWAVE SCANNING BEAM (MSB)
RANGE	1.5 FT	30 FT
RANGE RATE	0.5 FT/SEC	0.60 FT/SEC
ALTITUDE	1.5 FT	2.0 FT
ALTITUDE RATE	0.03 FT/SEC	0.03 FT/SEC
ATTITUDE	0.0466 DEG	0.0466 DEG

SERV TOUCHDOWN CHARACTERISTICS

TOUCHDOWN PARAMETER	$3-\sigma$ TOUCHDOWN DISPERSIONS FOR 95% HEADWIND/ 4 NAUT MILE INITIAL RANGE ERROR		MAX ALLOWABLE FOR SERV
	PRS	MSB	
RANGE ERROR	7.91 FT	94.7 FT	180 FT
DRIFT RATE	1.88 FT/SEC	2.58 FT/SEC	5 FT/SEC
SINK RATE	1.42 FT/SEC	1.89 FT/SEC	12 FT/SEC
ATTITUDE	0.487 DEG	0.749 DEG	2 DEG

Figure 3.5-13. Effect of Landing Navigation Errors on Touchdown Characteristics

3.5.4 ALTERNATE LANDING PROPULSION

The discussion so far has concentrated on the use of direct-lift gas turbine engines as the primary landing propulsion. However, a rocket propulsion system is an obvious candidate system and must also be considered. A comparison between the turbojet and alternate rocket engine landing propulsion system was therefore made.

For purposes of the comparison it was assumed that, using current technology guidance, navigation and control hardware, SERV would be not more than 4 miles from a vertical line above the desired landing pad when crossing the landing initiation interface. It is recognized that an advance in guidance, navigation and control capability could reduce the assumed landing interface error of 4 miles. Assessing the degree of reduction is an area for further investigation.

Figure 3.5-14 summarizes the comparison between turbojet and alternate rocket engines for the landing propulsion. Total landing system weight is shown as a function of range for the two engine systems. The bar charts to the right show a breakdown of the inert and propellant weights for the two systems at a range value of 4 miles for the turbojet engine system and a range value of 2 miles for the rocket engine system.
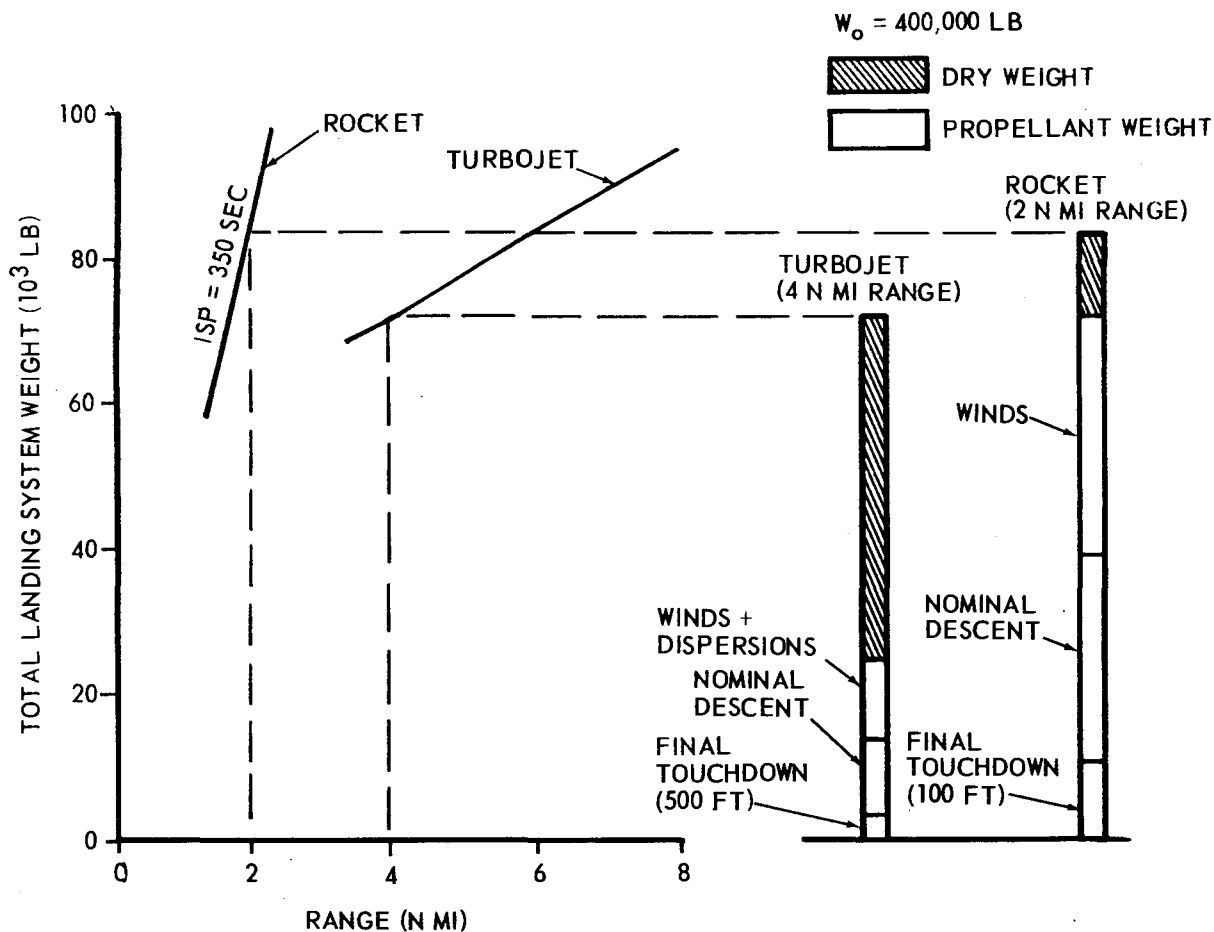
Figure 3.5-14. Rocket-Turbojet Comparison

As the bars in figure 3.5-14 indicate, dry weight (engines and associated hardware) accounts for most (approximately 66 percent) of the total weight for the turbojet system. Approximately one-third of this weight is due to the overthrust (engine out plus thrust efficiency factor) requirement. The total propellant weight for the turbojet system comprises the nominal propellant utilized during descent to 500 ft, the propellant required during vertical descent over the final 500 ft, and the propellant required to overcome winds and dispersions. This final propellant requirement comprises the delta propellant for an applied thrust factor of 68 percent, plus the RSS of the delta propellants due to winds and a lift coefficient of zero.

Total weight for the rocket engine system comprises mainly propellant (approximately 88 percent). This propellant weight requirement is optimistic with respect to the turbojet propellant requirement since no dispersions were considered, also, the vehicle was allowed to translate until an altitude of 100 ft had been achieved. Figure 3.5-14 shows that the rocket system has an advantage over the turbojet system for translation distances of less than 1.5 nm. Since attainment of landing errors of this small order is outside the current technology for this type of application, the turbojet propulsion approach was selected. Note that the turbojet system has the potential for a substantial weight reduction by the application of hydrogen fuel.

3.5.5 CONCLUSIONS

From the foregoing discussion it is concluded that an L/D = 0.3 is adequate for ranging, maneuverability, and maintenance of the ground rule for 3.0g reentry deceleration limit. Data obtained from wind tunnel tests of scale models of representative SERV configurations have demonstrated that SERV is aerodynamically stable throughout reentry and landing. The retention of lift throughout the transonic and subsonic regions is beneficial in counteracting vehicle drift due to the influence of winds. The landing maneuver can be accomplished by direct-lift gas turbine engines, even under the most adverse conditions of a 4-mile translation, 95 percent adverse winds and 1 engine out. An optimistically sized alternate rocket engine system would have approximately one-third the translation capability for equal system weight. An unmanned, fully automatic landing system has been demonstrated by simulation. In view of the aforementioned factors, the direct-lift gas turbine engines are feasible and have been selected for the recommended vehicle. However, it must be stressed that the direct-lift gas turbines need to be further developed to the thrust rating necessary for a SERV application.

Section 4

SUBSYSTEM DEFINITION

4.0 GENERAL

Subsystem design and analysis began with the baseline vehicle development (Task 1), progressed through a series of trade studies under concept evaluation (Task 3), was supported by model testing (Task 2), and concluded under the final vehicle definition (Task 4). Vehicle subsystems investigated during this course of study will be discussed here under the headings of structural, mechanical, propulsion, avionics and power. In addition, a subsystem weight summary is given by way of introduction and summary.

4.1 SUBSYSTEM WEIGHT SUMMARY

The basic structural components analyzed are indicated diagramtically on figure 4.1-1. All weight analysis results are consistent with the definitions listed here.

4.1.1 SUBSYSTEM WEIGHT COMPARISON

Table 4.1-1 presents a comparison of the final configuration with subsystem weights of the trade study baseline, the vehicle definition baseline, and the final sizing input design. Note that from vehicle to vehicle, some characteristics are varying: configuration mission description, vehicle diameter, and of course, GLOW. However, the total design analysis effort can be summarized grossly by considering the delta weight of 41,201 pounds between the initial baseline used for the trade study and the final design used as input to the final sizing. This delta represents the weight growth not only due to increased visibility into design details, but also the growth due to the incorporation of shuttle groundrules and the hybrid concept.

The 41,201-pound weight change resulted from both trade study and detailed analysis during the vehicle definition period. Figure 4.1-2 summarizes the changes by subsystems, and highlights of the analyses including the following:

1) Structural changes were due to a continuing detailed analysis throughout the study; a further breakdown of these charges is given later.

2) The types of base thermal protection were evaluated and an elastomeric ablative material was selected over the AVCOAT ablator and the coated columbium alloy reradiator.

UPPER KICK RING

UPPER LH$_2$ BULKHEAD

UPPER SHELL

CENTER KICK RING

UPPER LOX BULKHEAD

LOWER SHELL

INNER CYLINDRICAL BULKHEAD

OUTER CYLINDRICAL BULKHEAD

LOWER LOX BULKHEAD

THRUST RING

DOORS

LOWER LH$_2$ BULKHEAD

LANDING GEAR SUPPORT POINTS

REENTRY BULKHEAD
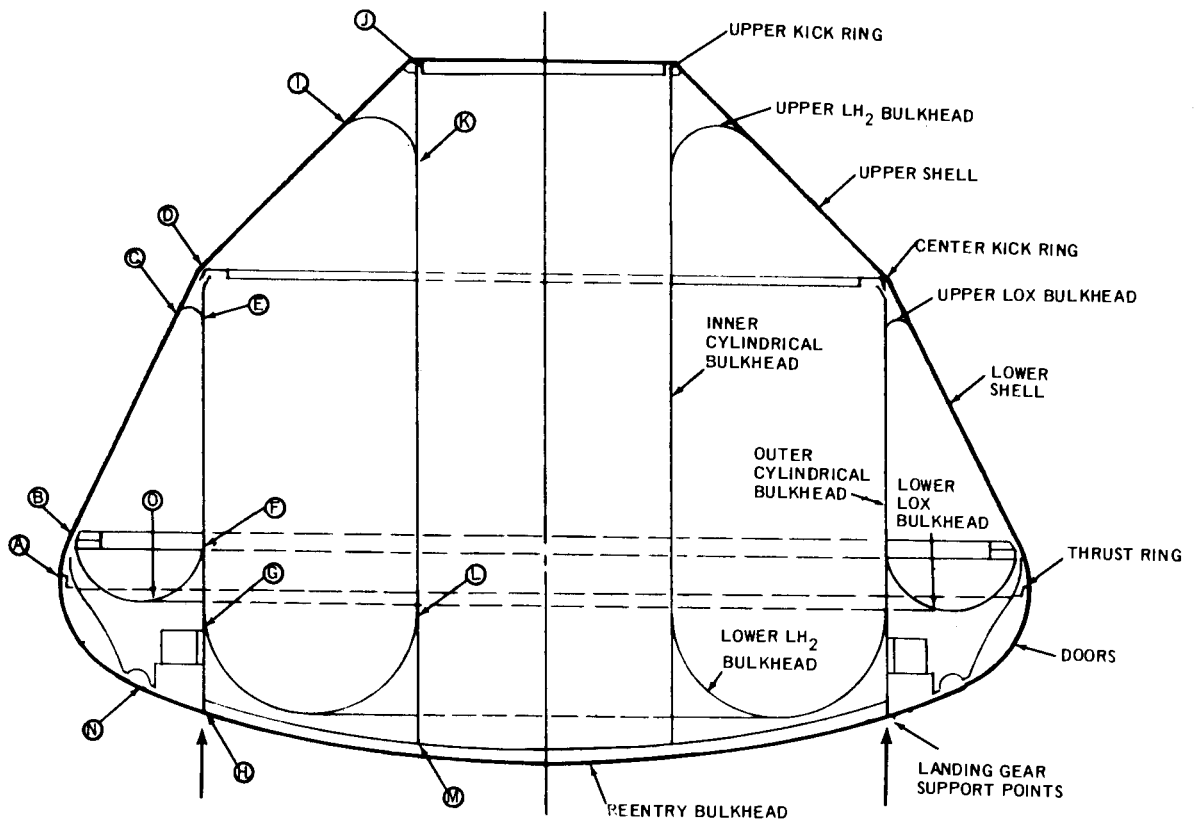
Figure 4.1-1. Baseline Structural Arrangement

Table 4.1-1. Dry Weight Comparison of Selected Vehicle Alternatives
(Pounds)

Weight Item	Task 3 Trade Studies		Task 4 Vehicle Definition Studies	
	Task 3 Baseline (9-8-70)	Final Sizing (Task 4 B/L)	Sizing Input Design	Final Sizing
Configuration Description	MURP	MURP-PM Hybrid	MURP-PM Hybrid	MURP-PM Hybrid
SERV Diameter	90	88	88	96
Primary Structure	133,531	150,349	148,297	200,018
Thermal Protection	31,636	23,208	20,438	24,695
Landing Gear	12,000	11,689	7,711	11,631
Actuators for Doors	3,000	2,997	4,419	5,405
Turbojet Engines	23,800	35,775	35,775	48,845
Turbojet Controls	2,000	2,574	2,574	3,146
Turbojet Tanks, Lines	2,000	2,036	2,036	2,490
Propellant Feed, Press.	1,200	4,227	15,076	17,348
Avionics and Power	5,000	5,834	6,681	6,681
Aerospike Engine	76,000	84,346	83,930	110,804
Auxiliary Propulsion	5,000	5,089	5,573	6,071
Aerospike Doors	10,963	11,464	11,168	12,183
Contingency (10%)	30,715	33,959	34,368	44,932
Total Dry Weight	336,845	373,547	378,046	494,249
GLOW	4,500,000	4,733,000	----	6,050,000
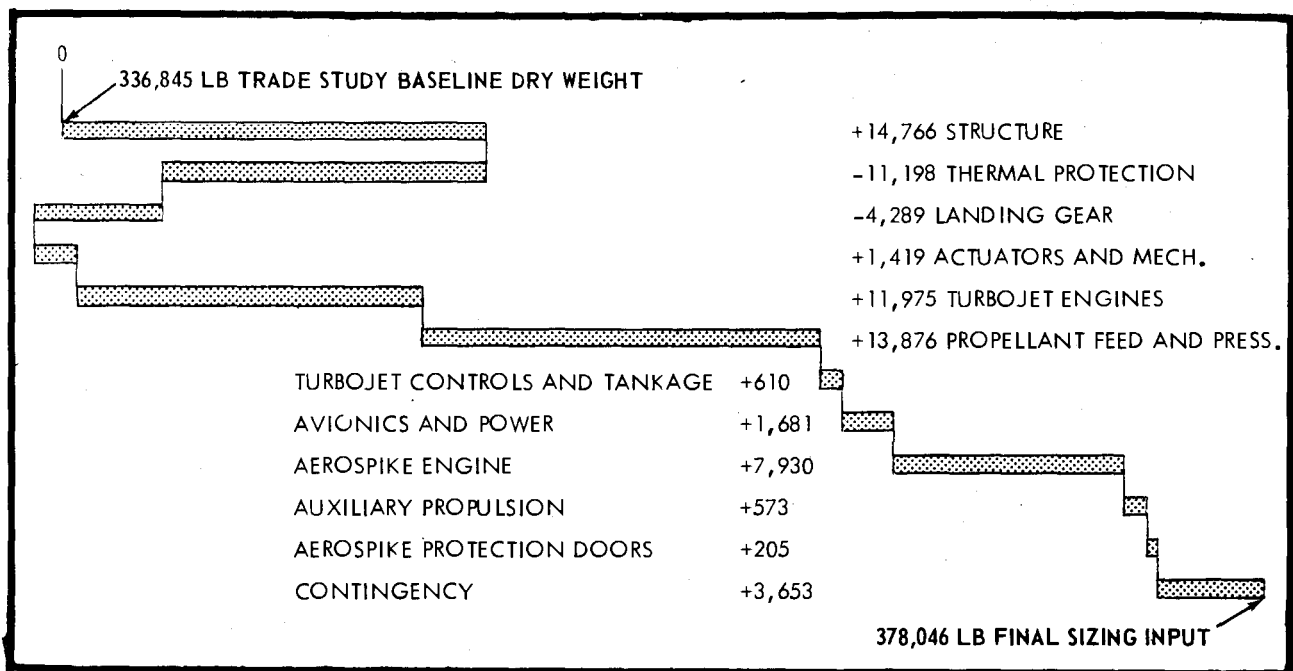
Figure 4.1-2. Subsystem Design Weight Change Summary

3) Thermal protection for the frustum sections was changed from jacketed microquartz on localized areas to Inconel welded honeycomb on all areas.

4) The revised design of the landing gear and door actuators caused their respective weight increases.

5) Reduced turbojet thrust efficiency and engine-out capability caused a substantial weight increase.

6) Better definition of propulsion subsystems and propellant feed hardware caused this weight increase.

7) The incorporation of turbopump-out capability caused the aerospike engine weight to increase.

8) Other weights increased due to better definition; it should also be noted that all weights were affected, either directly or indirectly, by dimensional and configuration changes as required throughout the study.

4.1.2 STRUCTURAL WEIGHT COMPARISON

A similar comparison of weights for the structural items identified in table 4.1-1 is presented in table 4.1-2. Here, structural analysis results may be summarized by examining the delta weight of 14,766 pounds between the initial baseline for the trade study and the final design value used as input to the final sizing.

Figure 4.1-3 summarizes changes by major assembly to yield the 14,766 pound delta:

1) Increased depth of thrust ring and incorporation of weight changes related to turbojet inlet doors, aerospike protection doors, and the joints and baffles item below.

2) The kick rings were resized after stress analysis.

3) The lower shell was reinforced due to revised analysis which included consideration of thermal gradients and discontinuity bending moments.

4) The inner and outer cylindrical bulkheads were reinforced to accommodate revised analysis including consideration of concentrated landing loads and discontinuity bending moments.

5) The lower LO_2 bulkhead and upper and lower LH_2 bulkheads were resized after stress analysis and changed from membrane to honeycomb construction to provide insulation.

6) The upper shell was reinforced to consider thermal gradients and equipment penetration.

Table 4.1-2. Structural Weight Comparison (Pounds)

Structural Item	Task 3 Trade Studies		Task 4 Vehicle Definition Studies	
	Task 3 Baseline (9-8-70)	Final Sizing (Task 4 B/L)	Sizing Input Design	Final Sizing
Configuration Description	MURP	MURP-PM Hybrid	MURP-PM Hybrid	MURP-PM Hybrid
SERV Diameter	90	88	88	96
Thrust Ring (A-B)	10,307	11,329	16,460	20,933
Kick Rings (B, D, J)	7,402	6,984	7,688	12,176
Lower Shell (B-C-D)	13,596	32,152	23,799	35,092
Outer Cylindrical Bulkhead (D-H)	31,296	30,876	37,997	50,298
Lower LO_2 Bulkhead (F-O-B)	6,550	10,179	6,820	10,114
Upper Shell (J-I-J)	11,745	8,316	12,354	20,953
Inner Cylindrical Bulkhead (J-M)	8,883	4,804	7,551	8,426
Upper LH_2 Bulkhead (J-K)	503	0	314	314
Lower LH_2 Bulkhead (L-G)	1,935	2,209	3,989	5,036
Reentry Bulkhead (H-H-N)	18,524	22,155	13,632	14,824
Lift Engine Support (N-H)	10,000	5,862	6,683	8,168
Joints, Baffles, Brkts., Etc.	12,790	15,483	11,010	13,684
Totals	133,531	150,349	148,297	200,018
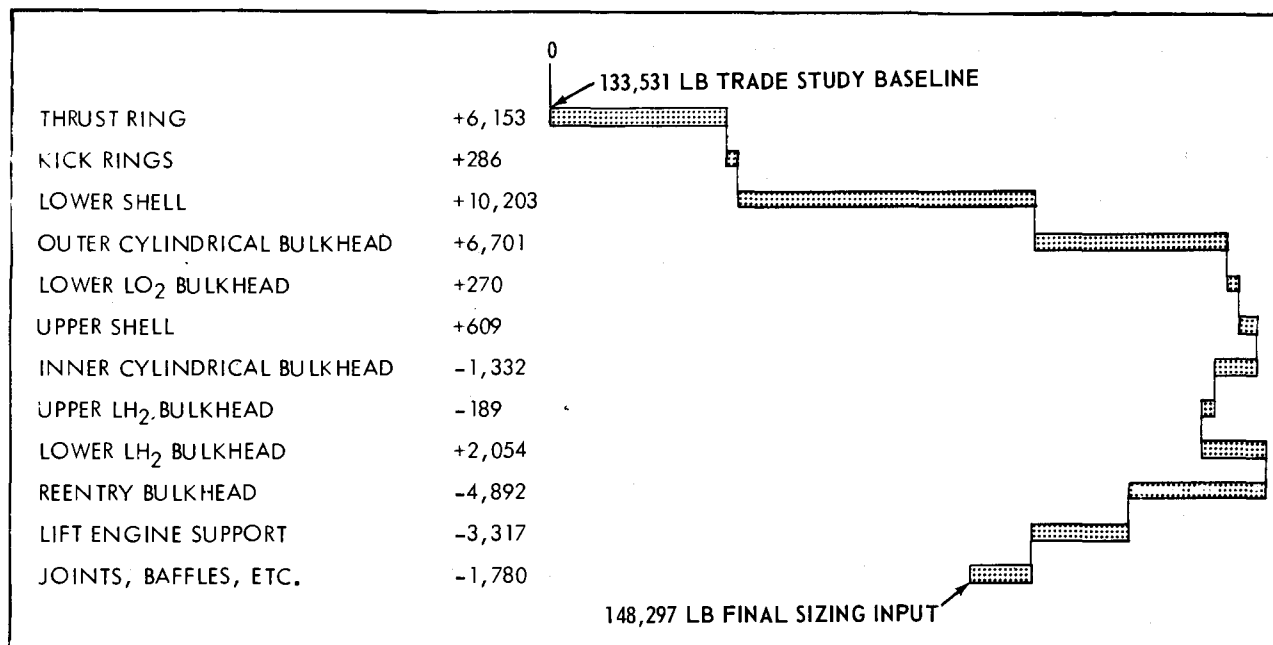
Figure 4.1-3. Structures Design Weight Change Summary

7) The reentry bulkhead was resized after stress analysis, including a lower value for dynamic load factor.

8) Lift engine supports were resized after stress analysis, and air intake ducts were added.

9) Miscellaneous weights were re-allocated from the joints and baffles item; ring-type baffles were added.

4.1.3 VEHICLE SIZING GROWTH FACTORS

In addition to establishing final configurations, the vehicle sizing program was utilized to determine the effects of parametric variations in aerodynamic characteristics, aerospike engine performance, contingency factor and inert weights on vehicle size. These effects are reflected in table 4.1-3 as resizing for propellant load and vehicle subsystem weight.

4.2 STRUCTURAL SUBSYSTEM

Major design criteria and required inputs used in the analysis of the SERV structure are summarized in table 4.2-1. The inputs were extracted from technical reference documents or calculated, utilizing study ground rules and baseline vehicle data. The structural analysis criteria were developed by cognizant personnel in a series of design review meetings and/or obtained from the "Space Shuttle Design Criteria Document". These data vary from those used during the trade studies as follows: The factor applied to the dynamic pressures on the reentry bulkhead was reduced from 1.5 to 1.1 because of use

Table 4.1-3. Vehicle Sizing Growth Factors (Fixed Payload)

INDEPENDENT VARIABLE (X)	∂GLOW/∂X	
INERT WEIGHT	+ 20.4	LB/LB
CONTINGENCY	+ 95,470	LB/PERCENT
SPECIFIC IMPULSE FOR NOMINAL THRUST	- 84,534	LB/SEC
SPECIFIC IMPULSE FOR NOMINAL FLOW RATE	-107,912	LB/SEC
THRUST FOR NOMINAL SPECIFIC IMPULSE	- 49,825	LB/PERCENT
THRUST FOR NOMINAL FLOW RATE	-503,733	LB/PERCENT
INITIAL THRUST TO WEIGHT (Δ = 0.1)	- 69,486	LB/0.1
PERCENT ULLAGE	+ 62,590	LB/PERCENT
ASCENT VELOCITY REQUIREMENT	+ 621	LB/FPS
AUXILIARY VELOCITY REQUIREMENT	+ 780	LB/FPS
DRAG	+ 14,413	LB/PERCENT
LIFT FUEL	+ 16.2	LB/LB

Table 4.2-1. Structural Analysis Approach

CRITERIA	INPUTS
• 1.4 Structural Factor of Safety • 1.1 Loading Factor Applied to Dynamic Pressures on Reentry Bulkhead (Note 1) • 3G Maximum Acceleration for Ascent and 3G Maximum Deceleration for Descent • Shock Impingement Loading Applied Over Upper Frustum • 10 Percent Weight Contingency • Landing Impact of 2G Limit, 12 FPS Vertical, at 2 Degree Attitude (Note 1) • Allowable Buckling Stresses Computed Per NASA Procedure Using Equivalent Monocoque Technique	• Ascent and Reentry Trajectory Data - Weight, Thrust, Drag - Ambient Pressure - Dynamic Pressure • Engine Performance Data - Thrust - Base Pressure • Aerodynamic Data - Local Surface Pressure Coefficient • Vehicle Configuration Data - Geometry - Dead Weight Distribution - Internal Pressure

Note 1) These criteria differ from those used in trade studies.

of actual wind tunnel data in the determination of design pressure distribution. The landing impact of a 3g limit was reduced to a 2g limit as the result of a more refined analysis of the landing phase.

4.2.1 STRUCTURAL ANALYSIS OF SHELL

The shell structure of the vehicle, which includes the upper and lower frustums and the inner and outer cylindrical bulkheads, was synthesized as a series of conical and cylindrical segments joined at circumferential node lines. Figure 4.2-1 shows the idealization of the upper frustum and is typical of the remaining shell structure. The heatshield bulkhead consisted of a series of sandwich panels supported by a spider beam assembly of major radial beams, short radial beams and cross beams. Attachment of the heatshield bulkhead to the inner and outer cylindrical bulkheads renders the complete vehicle structure redundant. In order to include the heatshield bulkhead in the math model, it was synthesized as an equivalent shell structure whose thickness and modulus of elasticity closely approximated the radial stiffness of the actual assembly.

1. MATH MODEL INCLUDES INTERACTION CAUSED BY ADJACENT SHELLS (DISCONTINUITY EFFECTS)
2. MATH MODEL SOLVES REDUNDANT LOAD PATHS ON BASIS OF RELATIVE STIFFNESS
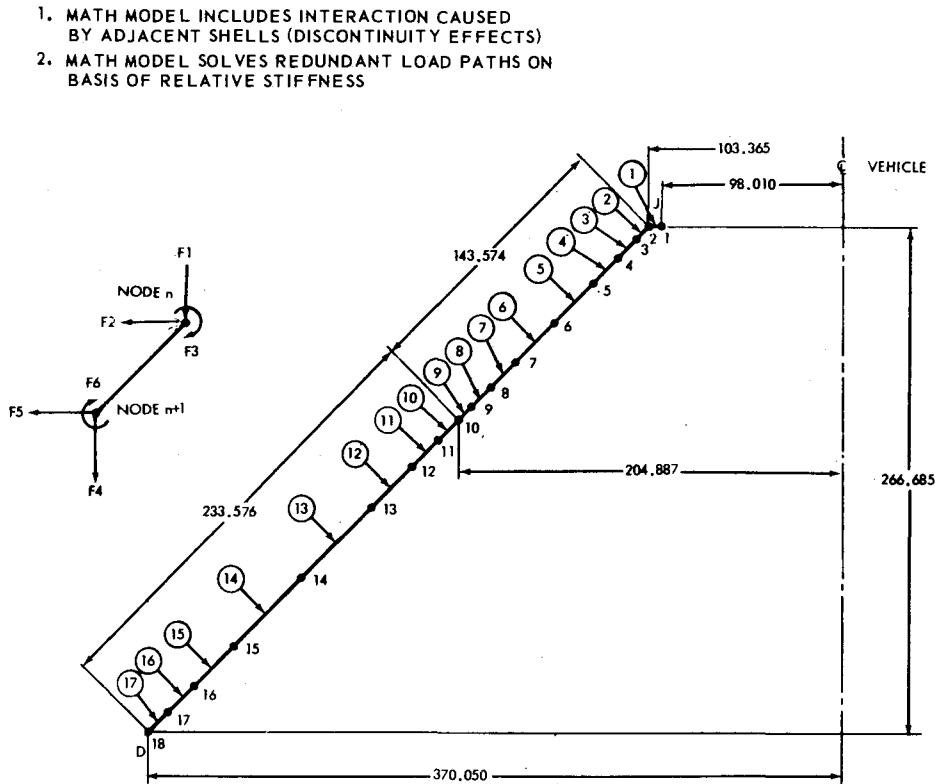
Figure 4.2-1. Math Model Idealization of Upper Frustum

The computer program was used to analyze an axisymmetric shell structure by the finite stiffness method. A stiffness matrix for each segment is constructed, based on the six degrees of freedom illustrated in the auxiliary sketch of figure 4.2-1, and on the simple plate characteristics which are equivalent to the actual sandwich. These segmental stiffness matrices are then assembled, in the same manner as the actual structure is

connected, to produce a total stiffness matrix for the vehicle. The stiffness matrix is then inverted, resulting in the vehicle flexibility matrix. A load column is then constructed corresponding to each design condition (or critical mission time point) for which the vehicle is to be analyzed. Multiplying the flexibility matrix by the load column results in a compatible set of nodal deflections for this landing. The deflections at the nodes forming the end boundaries of an individual segment are then extracted and multiplied by the segmental stiffness matrix. The result is a set of internal loads acting on the segment.

There are two major advantages gained by the application of the finite stiffness method to the analysis of the SERV primary structure. First, the discontinuity effects arising from the connection of two dissimilar shells of revolution; i.e., the upper frustum to the inner cylindrical bulkhead, are fully evaluated in each shell provided the nodal spacing in each shell, adjacent to the joint, is kept small enough to define the rapidly damped bending moment distribution. Second, since loads are distributed as a function of component stiffnesses, unique solutions are obtained for redundant structures.

Figure 4.2-2 presents the longitudinal normal frequencies for the SERV vehicle which was derived from a dynamic model constructed by adding the two toroidal lower tank bulkheads to the math model previously discussed. The dynamic model had a total of 116 degrees of freedom and was used to investigate four mass conditions for the free-free case, a fully loaded vehicle at liftoff (T = 0), the vehicle at the maximum dynamic pressure time point (T = 77 sec), the maximum longitudinal acceleration time point (T = 138 sec) and the vehicle with propellant tanks empty. The fully loaded vehicle was also investigated for an on-pad condition. Figure 4.2-2 illustrates the mode shape for a full vehicle in the free-free condition at an omega of 13.154 radians per second, and is presented as a typical example of the results. In general, it was found that the membrane bulkhead was quite flexible compared to the primary structure and that the bulkhead modes predominate at the lower frequencies. Figure 4.2-3 shows the results of a preliminary appraisal of the structural/liquid dynamic model which reveals no significant payload structural gain factor for a sinusoidal forcing function at the thrust vector. Examination of the frequency/mode shape data, such as illustrated in figure 4.2-2, also showed no significant payload displacement relative to the tank bulkheads. Nothing was found in this very preliminary type analysis to indicate that the SERV configuration would be susceptible to POGO type instability, but a much more detailed analysis is recommended for future study.

In all cases, the sizing of the shell structure previously discussed is based on the use of room temperature material properties. However, the weight of the thermal protective system required to keep the structure at room temperature would be prohibitive. Figure 4.2-4 illustrates the method employed in arriving at the combination of thermal protective system weight vs structural weight increase due to an actual thermal gradient that would minimize the increase in total vehicle weight.

The diagram at the left of figure 4.2-4 illustrates the points on the lower frustum at which the analysis was made. These points reflect changes in face thickness. Using theory developed for long sandwich cylinders, the meridional and hoop thermal stresses in both the inner and outer faces of the sandwich were calculated for a given temperature

| MODE | FREE - FREE | | | | SUPPORTED |
	FULL t = 0	MAX Q t = 77	MAX.ACCEL t = 138	EMPTY	FULL t = 0
1	4.904	5.916	7.405	82.155	4.893
2	8.252	9.955	12.462	123.507	8.196
3	10.276	12.215	15.053	132.122	10.269
4	13.154	15.748	19.471	139.423	11.281
5	16.209	19.345	23.812	218.161	15.889
6	19.721	23.555	29.030	219.653	17.890
7	22.711	27.347	34.124	231.731	20.976
8	29.399	35.282	43.583	271.782	28.542
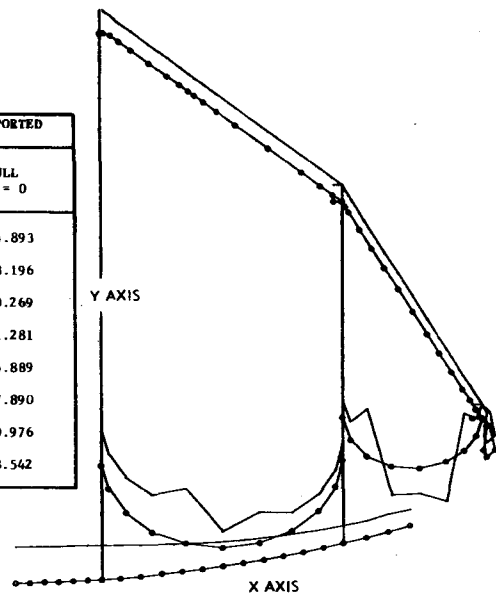
Figure 4.2-2. Frequencies and Mode Shapes
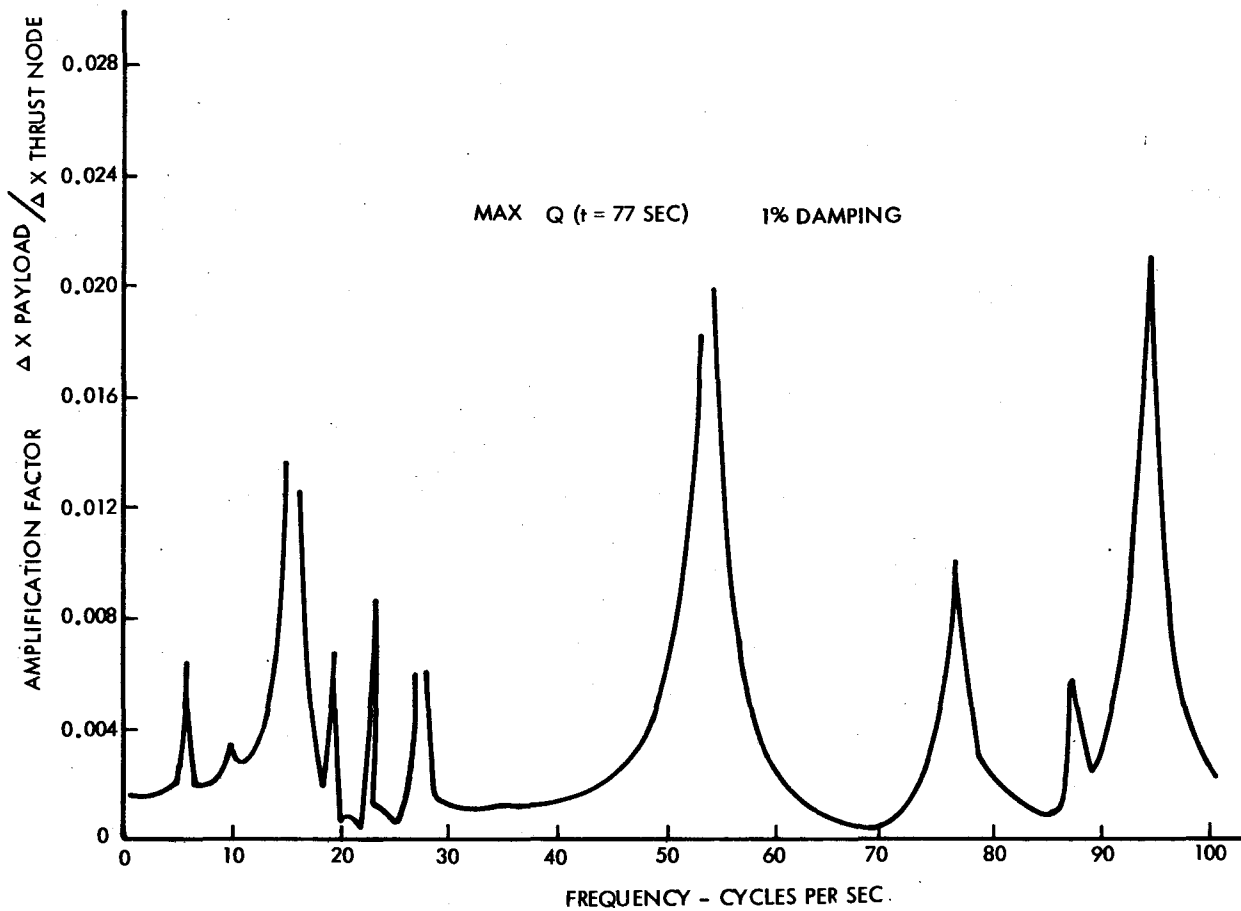
Figure 4.2-3. Payload Frequency Response
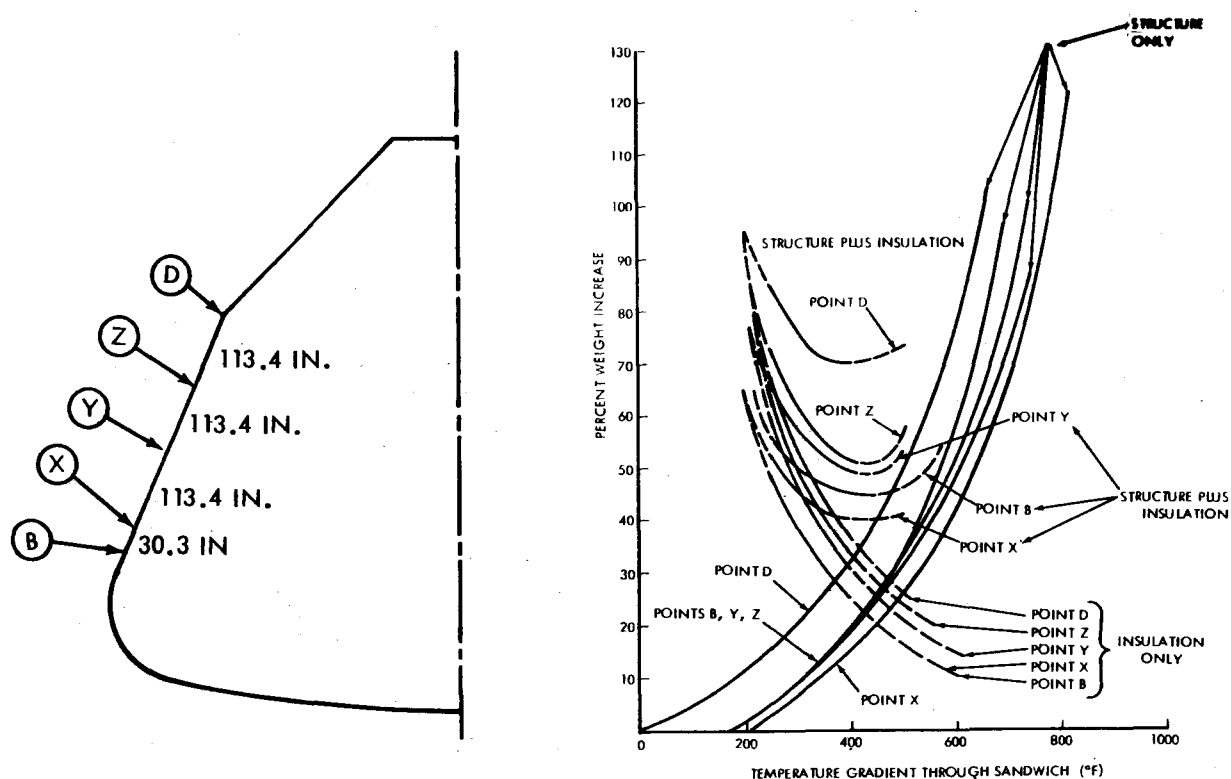
Figure 4.2-4. Thermal Gradient Effects

gradient. The difference between the minimum allowable stress and the thermal stress is thus equal to the magnitude of the stress that is available to carry primary airframe loads. For a given ascent design condition, for which the internal loads were known, the required thickness of each face could then be calculated. The percentage increase in sandwich weight of the hot sandwich over that at room temperature was then determined. Repeating this procedure for various temperature gradients provided one curve as shown in figure 4.2-4 under the "structure only" label. Only the worst case portions of the curves were drawn, so when in some cases the failure mode changed from tension to intercell buckling, a discontinuity in the slope of the curve appears as in that for Point Y.

The weight of the thermal protection system, calculated as a percentage of the unit weight of the primary sandwich structure, was also determined in terms of the temperature gradient permitted to exist in the primary sandwich structure. These curves are presented in figure 4.2-4 under the "insulation only" label.

At any value of temperature gradient, the percentage weight of the combined thermal protection system and the structure was evaluated and plotted as the fish hook curves under the "structure plus insulation" label. The minimum total vehicle weight increase obviously results when the "structure plus insulation" curve is at the lowest point. In general, it can be seen that, for the lower frustum, this occurs when only that amount of insulation is provided which results in a temperature gradient in the structure of approximately 400°F.

4-10

Data from analyses such as is illustrated in figure 4.2-4 was used to estimate the weight of the thermal insulation system and the required structure in the upper and lower frustum for subsequent use in the vehicle sizing program.

Each of the primary structural components of the vehicle, with the exception of the heat shield bulkhead, was sized on the basis of overall stability (figure 4.2-5). Due to the refinement in analysis made possible by use of the math model, the depth of analyses of the shell structure was increased. The effects can be seen in the added structural detail shown in figure 4.2-5. The local areas in which the foil thickness of the core is other than the earlier target thickness of 0.0020 inch reflect regions where high transverse shear loadings due to shell discontinuity effects has made it necessary to increase core strength. These same areas, without exception, also exhibit increases in face thickness when compared to neighboring regions. These increases in face thickness were also dictated by discontinuity effects.

• INCONEL 718 SANDWICH PANEL
• SQUARE CORE CELL

LOCA-TION	PANEL THICKNESS (IN.)	FACE SHEET THICKNESS (IN.)	CORE SHEET THICKNESS (IN.)	CORE CELL SIZE (IN.)
1	1.60	0.026	0.0025	0.500
2	1.60	0.018	0.0020	0.500
3	4.00	0.020	0.0020	0.500
4	2.70	0.038	0.0030	0.500
5	2.70	0.020	0.0020	0.500
6	2.70	0.018	0.0020	0.500
7	2.70	0.020	0.0020	0.500
8	2.70	0.027	0.0020	0.500
9	5.00	0.024	0.0020	0.500
10	5.00	0.036	0.0020	0.500
11	5.00	0.050	0.0020	0.500
12	0.680	0.014	0.0020	0.500
13	0.680	0.016	0.0020	0.500
14	0.680	0.014	0.0020	0.500
15	0.375	0.030	0.0040	0.500
16	0.375	0.010	0.0020	0.500
17	3.40	0.010	0.0020	0.500
18	3.80	0.010	0.0020	0.500
19	0.375	0.014	0.0035	0.500
20	0.375	0.010	0.0020	0.500
21	1.00	0.014	0.0020	0.750
22	1.00	0.014	0.0020	0.375
23	1.00	0.006	0.0020	0.750
24	1.00	0.006	0.0020	0.750

Figure 4.2-5. SERV Structural Arrangement

4.2.2 STRUCTURAL ANALYSIS OF REENTRY HEAT SHIELD

The heat shield assembly consists of Honeycomb panels supported by a spider beam arrangement of structural beams. The heat shield configuration with the panel design pressures superimposed is shown on the left of figure 4.2-6. The panel design pressures were calculated by averaging the node point pressures which were calculated using pressure coefficient data extracted from the preliminary aerodynamic criteria generated for use in the sizing program. Using these pressures, the Honeycomb panels were idealized as circular sectors and rectangular shapes. The assumed pressure distribution at

the structural beams is shown at the right of figure 4.2-6. A 500°F operating temperature was considered in the panel analysis. A 200°F temperature gradient across the panels yielded a 10% weight penalty.

PANEL DESIGN PRESSURES   PRESSURE DISTRUBUTION TO BEAMS
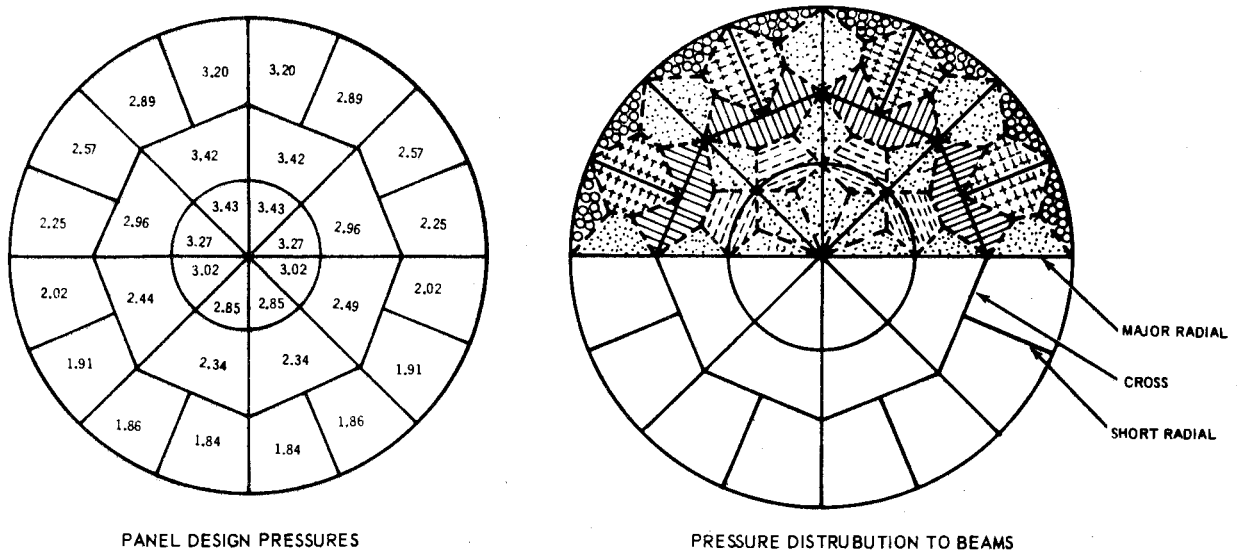
Figure 4.2-6.   Reentry Heat Shield Pressure Distribution

Figure 4.2-7 illustrates the reentry heatshield beam structure and presents panel thickness details of interest.

- PH15-7 Mo WELDED SANDWICH PANEL
- 0.50-IN. SQUARE CORE CELL
- 0.002-IN. CORE SHEET THICKNESS

PANEL NO.	PANEL THICKNESS (IN.)	FACE SHEET THICKNESS (IN.)
1,21	1.55	0.010
2,22	2.12	0.015
3,24	1.72	0.015
4,23	1.63	0.015
5,17	1.69	0.010
6,18	2.49	0.015
7,20	2.19	0.015
8,19	1.92	0.015
9,13	1.77	0.010
10,14	2.85	0.015
11,16	2.73	0.015
12,15	2.46	0.015
25,29	1.47	0.010
26,30	1.98	0.015
27,32	1.58	0.015
28,31	1.58	0.015
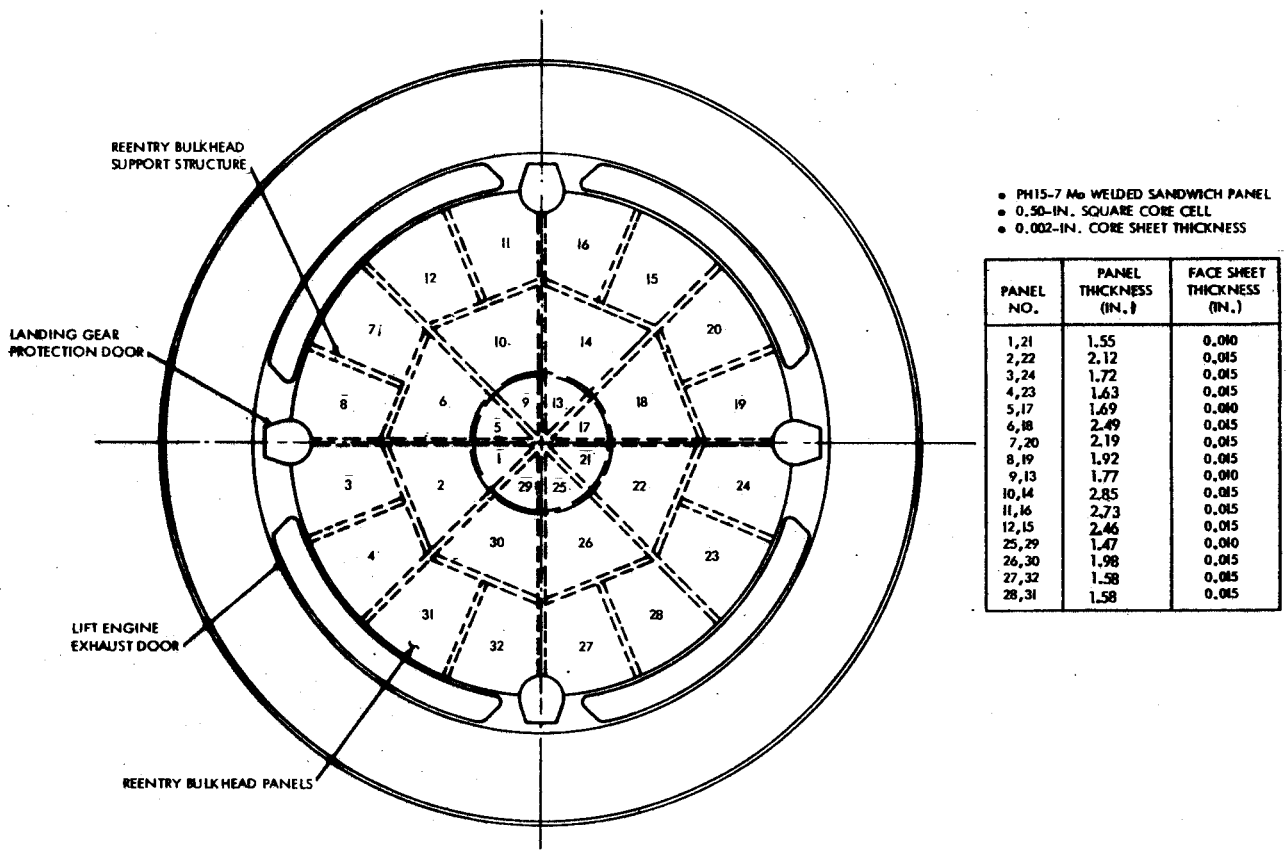
Figure 4.2-7.   Reentry Heat Shield Structural Arrangement

4-12

4.3 MECHANICAL SUBSYSTEMS

The method of actuation and sealing of the aerospike protection doors and the gas turbine inlet and exhaust doors are discussed in this section. Details of the four landing gear assemblies are also presented.

4.3.1 DOOR ACTUATION AND SEALING

The aerospike door system (figure 4.3-1) comprises 16 doors arranged circumferentially around the SERV. Each door interfaces with the vehicle at the forward and aft ends, and with adjacent doors at the sides. Sixteen linear actuators are positioned at the optimized one third door length point, with one actuator located at each door interface. Actuation of the mechanism generates circumferentially in-line loads along the door diameter. This axial load is sufficient in magnitude to effect a radial inboard or outboard force to overcome the flight load at the time point in question. The result is an inboard or outboard door movement caused by a diameter change at the actuator line. Support beams to take the axial loads generated by the actuation mechanism in opening and closing the doors are installed circumferentially in line with the actuator forming a hoop. The aerospike door actuation system is formed by the actuator/beam combination and is essentially an expanding hoop when opening, and a shrinking hoop when closing.

LINEAR ACTUATOR
ASSEMBLY

AEROSPIKE DOOR
(TYPICAL 16 PLACES)

LOAD SUPPORT BEAM
(TYPICAL)

AFT VIEW OF SERV LOOKING FORWARD

DOOR CLOSED

DOOR OPEN
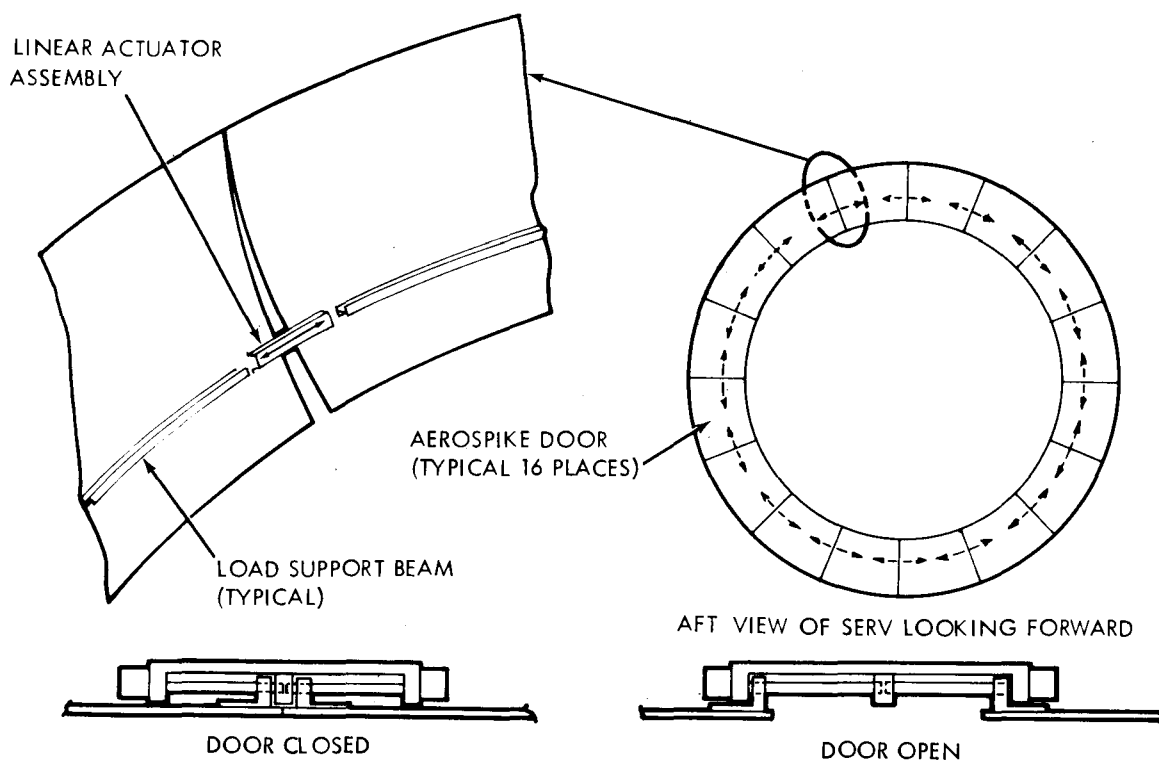
Figure 4.3-1. Aerospike Door Actuation

A high temperature silicone seal (RTV 560) , in combination with the door geometry and positive locks, is employed to effect the aerospike door seal (See figure 4.3-2.). The door-to-door interface seal is made by employing a tongue and groove design such that when the door is drawn to the closed position the silicone is compressed and wedged to the conformity of the door. The door forward hinge seal is accomplished by the door forward edge compressing the silicone seal (installed on the vehicle structure) as the door approaches the closed position. The silicone seal in this case is a continuous band installed on the vehicle structure at the door forward interface. The door aft interface lock and seal arrangement includes a high temperature silicone seal along the aft end and inboard corner of the door panel. The SERV structure is designed to receive the door by implementing a groove and step design to ensure a seal over any imperfections or uneveness in the seated interface between the door and the structure. All of the door seal configurations have the wedging and compressing characteristics to effect a positive seal over imperfections in the interface structure. A positive lock and seal compression effect on the aft interface is accomplished by means of a spring lock actuation device installed in a structure cavity. As the door closes, a trunion attached to the door structure engages with the locking device, activating the spring and causing the door to be snugged into place. Six locking devices per door ensures a uniform interface seal.
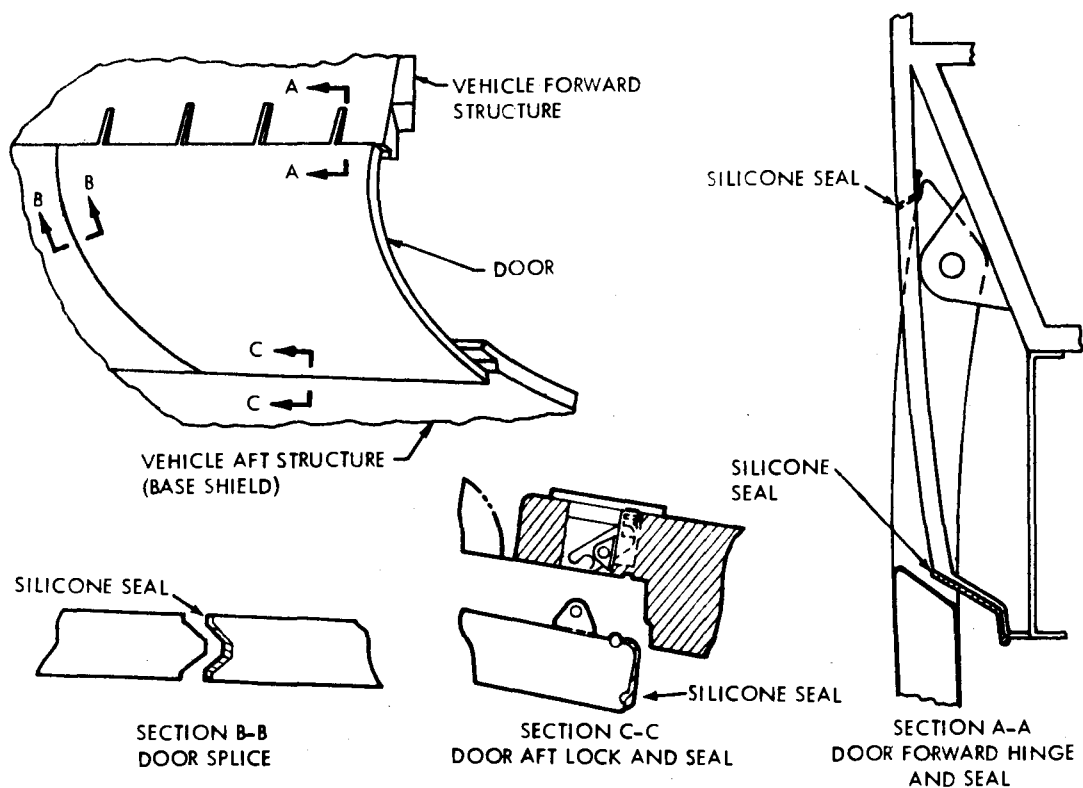
Figure 4.3-2. Aerospike Door Sealing

The lift engine air intake doors are located in the thrust ring forward of the aerospike engine. A spring system is combined with solenoid activation to accomplish door opening (figure 4.3-3). Solenoids activate a spring loaded cannister that releases positive door locks, thrusting the door open to air flow. Air flow causes the door to open to the fully extended position, the opening speed being controlled by a snubber device. The snubber device consists of a screw jack rod with a ratchet and shock absorbing lock to prevent the door from closing or slamming open. Silicone seals (RTV560) are employed on the perimeter of the door frame. The typical frame and door interface is set at a 45-degree slope with a step groove to ensure compression of the silicone seal in effecting a proper fit over any small structural imperfections.
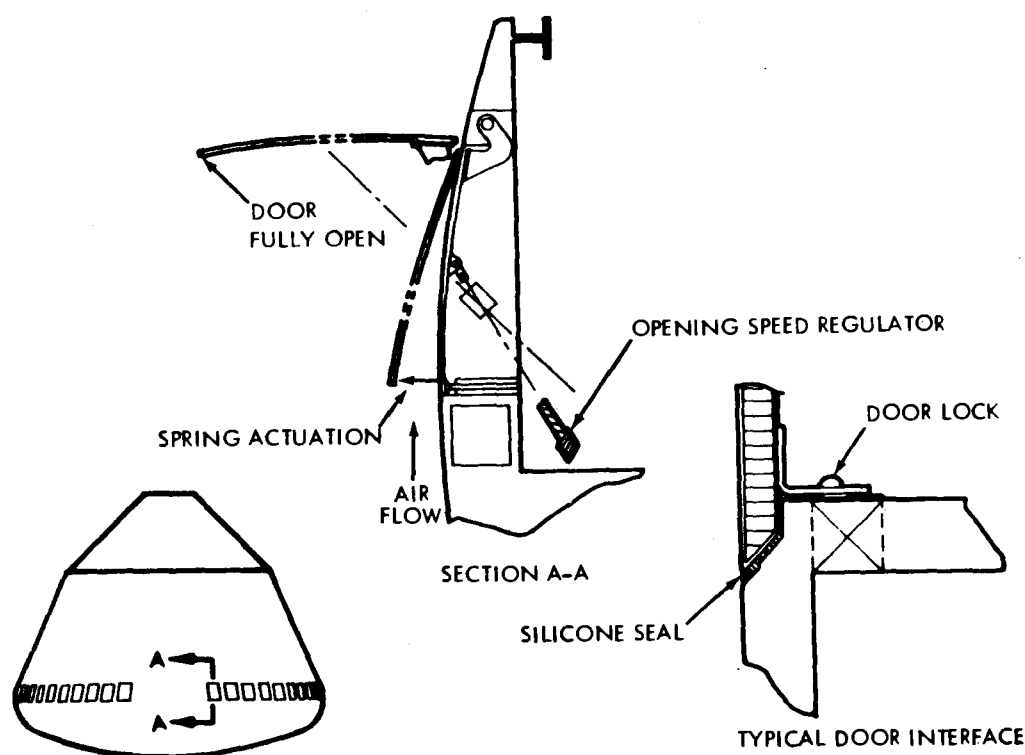
Figure 4.3-3.   Actuation and Sealing of Lift Engine Air Intake Doors

The four lift engine exhaust doors employed for four banks of lift engines are located in the reentry base shield radially equidistant in four quadrants (See figure 4.3-4.). Electrically powered screw jacks are used to push the door downward into the air flow, maintaining an even plane. A cable pulley system subsequently causes each door to move laterally inboard on a track system, exposing the lift engine banks. Four one-half horse-power motors and two one horsepower motors per bank are employed for the door downward and inboard movements. A silicone seal (RTV560) is installed along the door perimeter and aft corner and interfaces with the vehicle at a 15-degree stepped slope. Positive locking action is employed by a spring latching system that lifts the door against the seal interface thereby effecting a compressing wedging action.

DOOR OPEN
(TYPICAL 4 PLACES)

SECTION A-A

DOOR OPEN

LOCK ASSEMBLY

SILICONE SEAL

VIEW AFT ON SERV, LOOKING FORWARD
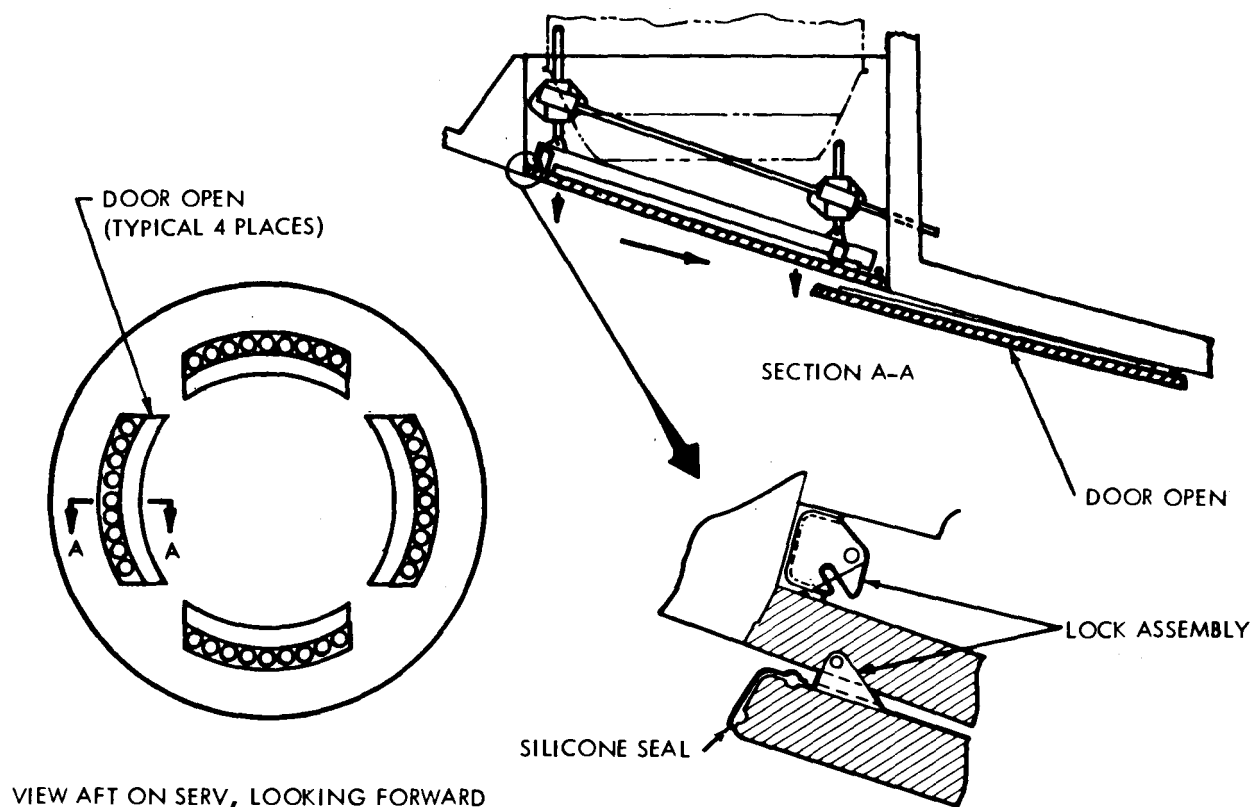
Figure 4. 3-4. Actuation and Sealing of Lift Engine Exhaust Doors

4.3.2 LANDING GEAR/DOOR SUBSYSTEM

The selected landing gear system is essentially a linear actuator arrangement enclosed in a canister mounted in the LO_2/LH_2 common skirt. (See figure 4.3-5.) The system is actuated mechanically and effects opening of the base shield door and extension of the gear housing. An electric motor provides mechanical power. After full housing extension, a hydraulic accumulator replenishes the shock absorber cylinder, causing it to extend to the active position giving full extension to the landing gear assembly. At touchdown, oil is bled back into the accumulator by means of the shock stroke. The gear is designed to accept a 2g deceleration, and a 12-ft/sec vertical velocity, at a 2-degree attitude. Gear assembly support is achieved by locating the main gear housing (canister) within the SERV outer cylindrical bulkhead skirt. The skirt takes the vertical load and a percentage of the resulting moment. An attachment is also made to the side wall of the main gear housing by means of a structural tie to the base shield support beams. This provides the remaining resistance to gear moment at touchdown and support for the base shield beams during flight.

TANK SKIRT

LANDING GEAR HOUSING

HINGE SPRING AND LOCK ASSY

HYDRAULIC ACCUMULATOR

LANDING GEAR STOWED

BASE SHIELD AND GEAR SUPPORT STRUCTURE

LH₂ TANK

DOOR (ACTUATED BY GEAR EXTENSION)

18-INCH SHOCK STROKE

LANDING GEAR EXTENDED
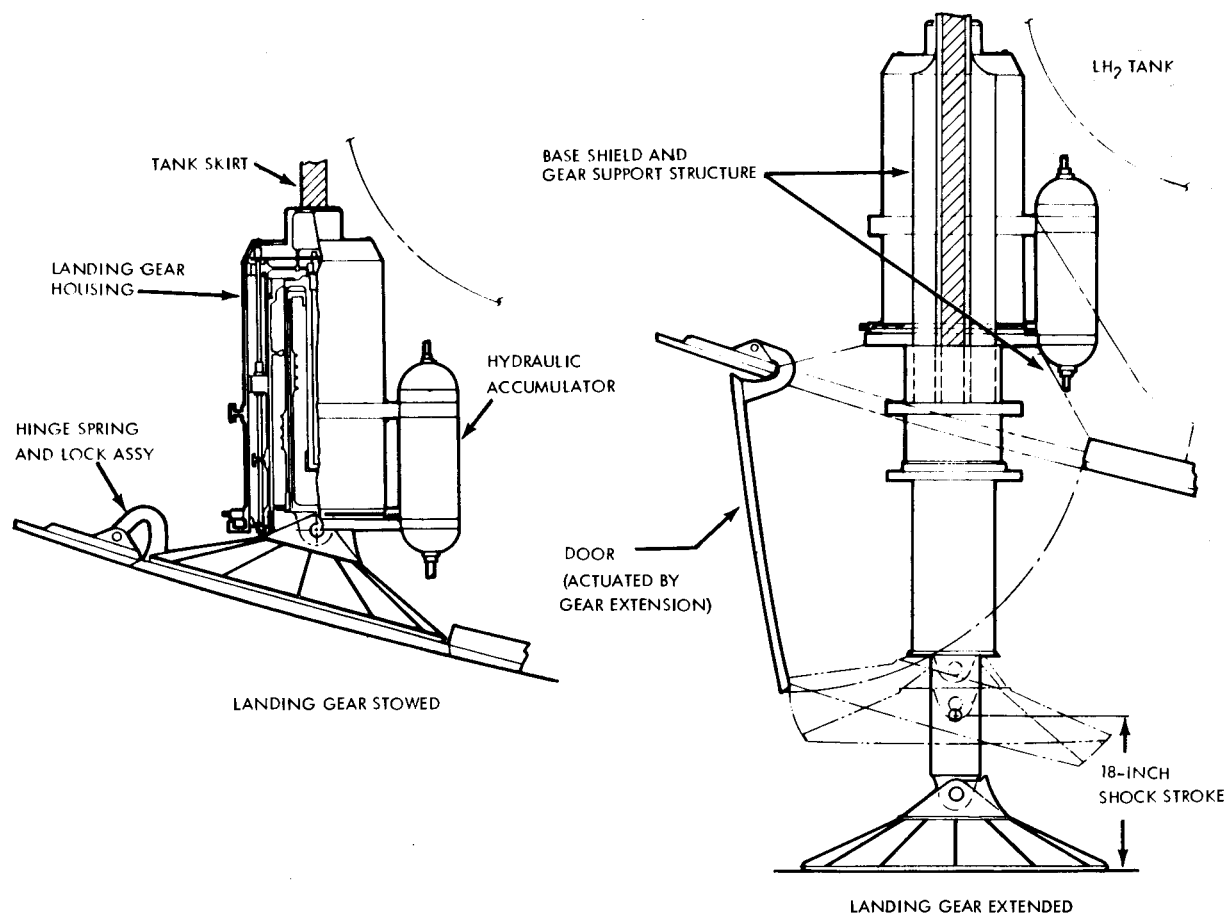
Figure 4.3-5. Landing Gear/Door Subsystem

4.4 PROPULSION SUBSYSTEMS

Design and analysis of the propulsion subsystems were performed in sufficient detail to support the investigation of the key feasibility issue of weights. Six subsystems have been identified and the first four make up the ascent main propulsion subsystem group:

1) Twelve-module aerospike engine
2) Main propellant feed, fill and drain
3) Main propellant pressurization and vent
4) Main propellant recirculation and engine purge

5) Auxiliary propulsion
6) Landing main propulsion
7) Alternate ascent propulsion

In addition, use of high-pressure bell engines as an alternate ascent propulsion subsystem was investigated.

4.4.1 ASCENT MAIN PROPULSION

The four ascent main propulsion subsystems are shown in figure 4.4-1. As described previously, the aerospike engine has a sea-level thrust of 7.45 million pounds and spec-

4-17

ific impulse values of 348 sec and 467 sec at sea level and vacuum, respectively. The 12-module engine has several special features including interconnection of engine modules on the high pressure side of the turbopumps and a turbopump over-speed capability to provide for turbopump failures without deterioration in engine performance. In addition, the engine is capable of throttling to a minimum thrust level of 18 percent of nominal and differential throttling of ± 15 percent without exceeding minimum thrust level. (The SERV flight trajectory limits vehicle acceleration to 3g, which requires primary throttling of the aerospike engine to approximately 20 percent of nominal thrust.)
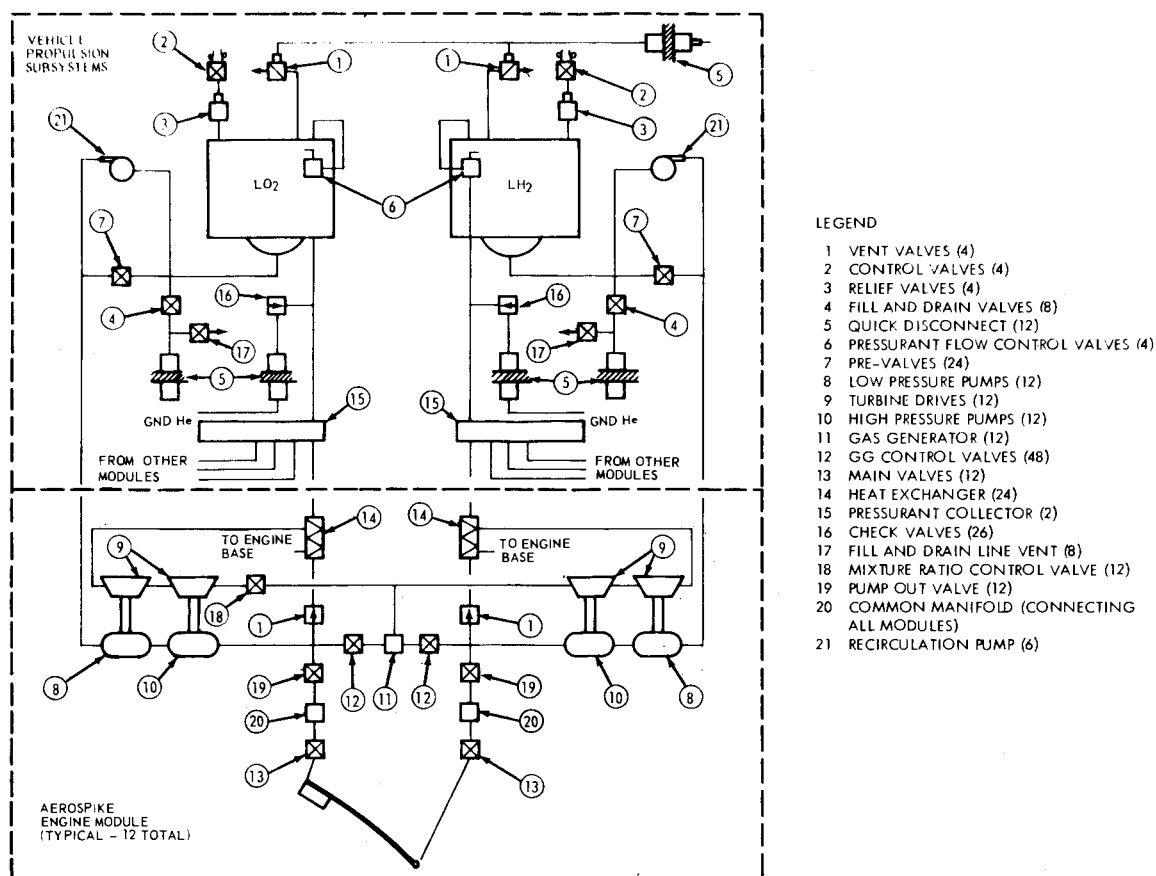
Figure 4.4-1. Schematic Diagram of the Ascent Main Propulsion

Propellants flow to the 12 modules from 24 sumps, 12 in each of the main tanks. Level sensors are provided in each tank at several locations to ensure a fuel-rich depletion cutoff. However, this provision is a backup because normal cutoff (fuel rich) is commanded when orbital velocity is attained. Fluid residuals include propellants trapped in engine lines, main feed lines and recirculation subsystem lines, as well as liquid residuals and pressure gases in the main tanks. All hydrogen liquid residuals are vented in orbit while maintaining tank pressure at 5 psia. Oxygen liquid residual is allowed to boil off and elevate the oxidizer tank pressure to 15 psia, which results in an increase in pressurant weight between burnout and reentry; the

remaining oxygen liquid residual is vented in orbit. (The APS contains a sufficient quantity if hydrogen to re-pressurize the main fuel tanks during reentry and landing, when it is transferred into the pressurant category.)

Prevalves are located in each feed line to eliminate the possibility of draining either main propellant tank in the event of a feed line rupture and to allow for propellant shutoff in the event of a turbopump failure. A double-redundant recirculation system is installed on each main tank for propellant conditioning during launch operations. Propellant fill and drain is provided by means of four lines for each propellant. Double-redundant valving is provided to vent the fill lines during flight. The aerospike engine is provided with an inert gas purge prior to introducing liquid propellants . Purge gas is supplied from the same high-pressure helium supply used to fill a pressurant tank in the APS.

The pressure and pressurant requirements for the Task 4 baseline vehicle were used to size the pressurization subsystem, a constant gauge pressure system at 5 psig for LH_2 and 10 psig for LO_2. The autogenous concept was chosen for each propellant; this concept utilizes heat exchangers in main engine turbine exhaust lines, a gaseous pressurant collector, redundant distribution lines and flow control valves located at the pressurant distribution locations at the top of each tank.

4.4.2 AUXILIARY PROPULSION

The auxiliary propulsion subsystem (figure 4.4-2) serves multiple functions as follows:

- Ascent roll control
- Orbit circularization
- On-orbit station keeping
- Orbit-to-orbit maneuvering
- Attitude control for orbit-to-orbit maneuvering

- Deorbit
- Reentry attitude control
- Main propellant tank repressurization during reentry
- Propellant supply for fuel cells

The subsystem is made up of four basic assemblies: propellant tankage, pressurization and acquisition; propellant conditioning; propellant distribution; and thrusters. All components except for tankage, distribution lines and thrusters are triply redundant since crew safety is dependent on its operation. Each component function will be operational after two failures of that component.

Performance and propellant requirements for the APS are based on a thruster I_s of 460 sec and an equivalent system I_s of 400 sec. APS propellant tankage is located on the interior of the SERV main propellant tanks. A gaseous helium pressurant is incorporated for the oxidizer, while an autogenous hydrogen pressurant is employed. Hydrogen pressurant conditioning is accomplished by coiling tubes around the propellant conditioning gas generator to vaporize the cryogen. Approximately 2 percent of the hydrogen is required as pressurant.

1. CONNECTIONS TO TWO ADDITIONAL IDENTICAL PROPELLANT CONDITIONING UNITS, ONE DOUBLY ISOLATED, ONE SINGLY ISOLATED
2. CONNECTION TO GH$_2$ PRESSURANT COLLECTOR
3. FUEL CELL PROPELLANT SUPPLY CONNECTIONS
4. LO$_2$ STORAGE
5. LH$_2$ STORAGE
6. VALVE ASSEMBLY (TYP)
7. REGULATOR ASSEMBLY (TYP)
8. HELIUM PRESSURANT STORAGE
9. RELIEF VALVE (TYP)
10. ISOLATION VALVES (TYP)
11. SHUTOFF VALVE FOR CONDITIONING UNIT (TYP)
12. TURBOPUMP ASSEMBLY (TYP)
13. HEAT EXCHANGER (TYP)
14. GAS GENERATOR (TYP)
15. GAS GENERATOR CONTROL VALVE (TYP)
16. NON-BURNING PROPULSIVE VENT
17. NON-PROPULSIVE VENT
18. GASEOUS OXYGEN ACCUMULATOR
19. GASEOUS HYDROGEN ACCUMULATOR
20. THRUSTOR CONTROL VALVE, FILTER AND ISOLATION ASSY (TYP)
21. THRUSTOR (TYP)
22. CONDITIONING UNIT START ACCUMULATOR (TYP)
23. CHECK VALVE ASSEMBLY (TYP)
24. HYDROGEN PRESSURIZATION LOOP

Figure 4.4-2. Schematic Diagram of the Auxiliary Propulsion Subsystem

Each APS propellant conditioning assembly consists of two sets of independent gas generators, one feeding a turbopump and the other providing hot gases for input to a heat exchanger for vaporizing and heating the cryogenically stored propellant. The turbine outlet gases are also used as secondary inputs to the heat exchanger. Oxidizer and fuel conditioners operate independently on a demand basis when the propellant accumulator pressure drops below a specified minimum value. Propellant distribution is accomplished via high pressure accumulators and ring line distributors.

APS thrusters are located in four modules of five nozzles at equidistant points around the maximum vehicle diameter. Two thrusters in each module are pointed forward, parallel to the vehicle longitudinal axis, one is pointed downward and the remaining two oppose each other in a tangential direction for roll control. Redundant operation is supplied for all axis maneuvers in pitch, yaw or roll. The eight forward-facing thrusters (two in each module) are used to provide the impulse necessary for orbital maneuvers and SERV deorbit.

A connecting link with redundant valving is supplied between the APS gaseous hydrogen accumulator and the main tank gaseous hydrogen pressurant collector. During reentry, the APS hydrogen conditioner is utilized to provide pressurant for repressurization of the main hydrogen tank.

Additional connecting links join the APS gaseous propellant accumulators and vehicle fuel cell units with redundant regulators and valving. Fuel cell propellant supplies are stored in the APS tanks.

4.4.3   LANDING MAIN PROPULSION

This subsystem (figure 4.4-3) is made up of turbojet lift engines and associated tankage, feed lines, and start and control equipment.

①	FUEL TANK
②	PRESSURANT TANK
③	REGULATOR ASSEMBLY
④	PRESSURE RELIEF VALVE
⑤	VALVE ASSEMBLY
⑥	QUICK DISCONNECT
⑦	FUEL TRANSFER LINE
⑧	SECONDARY TANKAGE FOR FUEL (FOR CG OFFSET SHIFT)
⑨	FUEL DISTRIBUTION MANIFOLD
⑩	ENGINE THROTTLE VALVE
⑪	THROTTLE CONTROLLER ASSEMBLY
⑫	TURBOJET LIFT ENGINE
⑬	STARTER ASSEMBLY
⑭	CHECK VALVE
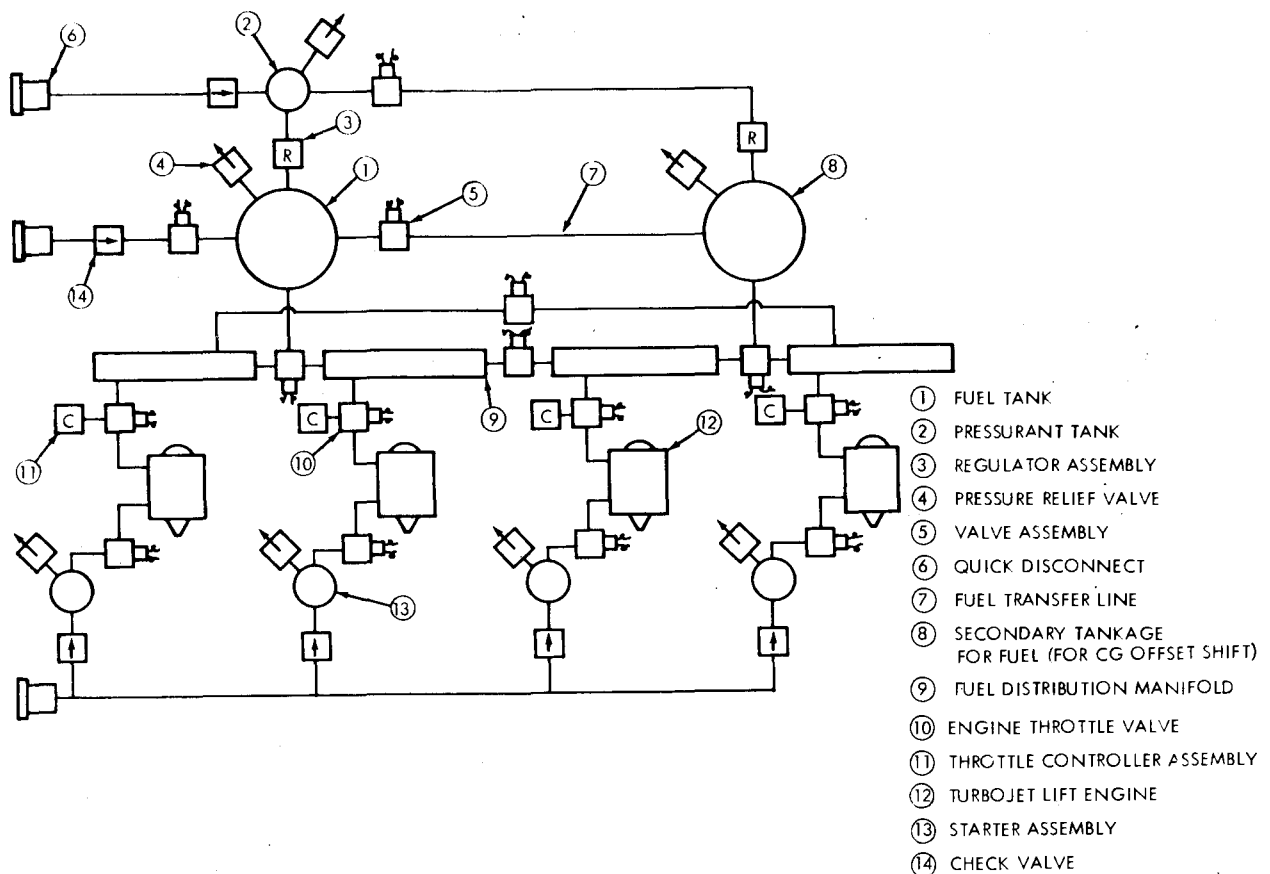
Figure 4.4-3. Schematic Diagram of the Landing Main Propulsion Subsystem

The turbojet lift engines identified for SERV are based on development work done by the Detroit Diesel Allison Division of General Motors Corporation in collaboration with Rolls-Royce.   An engine with a thrust of 10,000 to 25,000 pounds and a thrust-to-weight factor of 17 to 20 is within present technology capabilities.

Jet engine thrust requirements are based on worst operating conditions for translation by differential throttling through maximum opposing winds with one engine out and maximum aerodynamic forces.   This worst condition requires a thrust equal to 116.8 percent of SERV weight and occurs during a portion of the flight when approximately 80 percent of the loaded jet fuel is still on board.   A thrust efficiency factor of 80 percent is also applied to account for inlet pressure loss and air temperature effects.

Jet fuel and tankage requirements are based on flight simulation for the worst operation conditions as defined in the foregoing paragraph; an all-nominal flight would

leave a jet fuel residual of approximately 12,000 pounds. Fuel tankage is arranged so that all of the fuel is on one side of the vehicle at the beginning of reentry, thereby supplying an additional cg offset, and can be moved to the opposite side prior to the landing phase to minimize thrust unbalance requirements. Fuel transfer is provided via 6-inch lines with a tank pressure driving force.

The fuel transfer lines serve as fuel distribution lines during engine operation, with feeder lines to each engine that are flow controlled by electro-pneumatic devices.

4.4.4 ALTERNATE ASCENT PROPULSION

One of the trade study tasks was the identification of a SERV configuration propelled to orbit by high pressure bell engines as an alternate ascent propulsion method. The general features of the alternate SERV are shown in figure 4.4-4. Apart from adaptation of the high-pressure bell engines there are other departures from the aerospike propelled version. These differences include: relocation of the direct-lift gas turbine engines; the method of air intake and routing of air to the direct-lift gas turbines; and a reduced number of doors and associated mechanisms. However, the most significant change is in the method of transferring thrust loads into the structure. (See figure 4.4-5). The depth of analysis performed on this alternate configuration was limited by available study resources and it is recommended that a more detailed analysis be performed to positively establish the potential of the configuration.
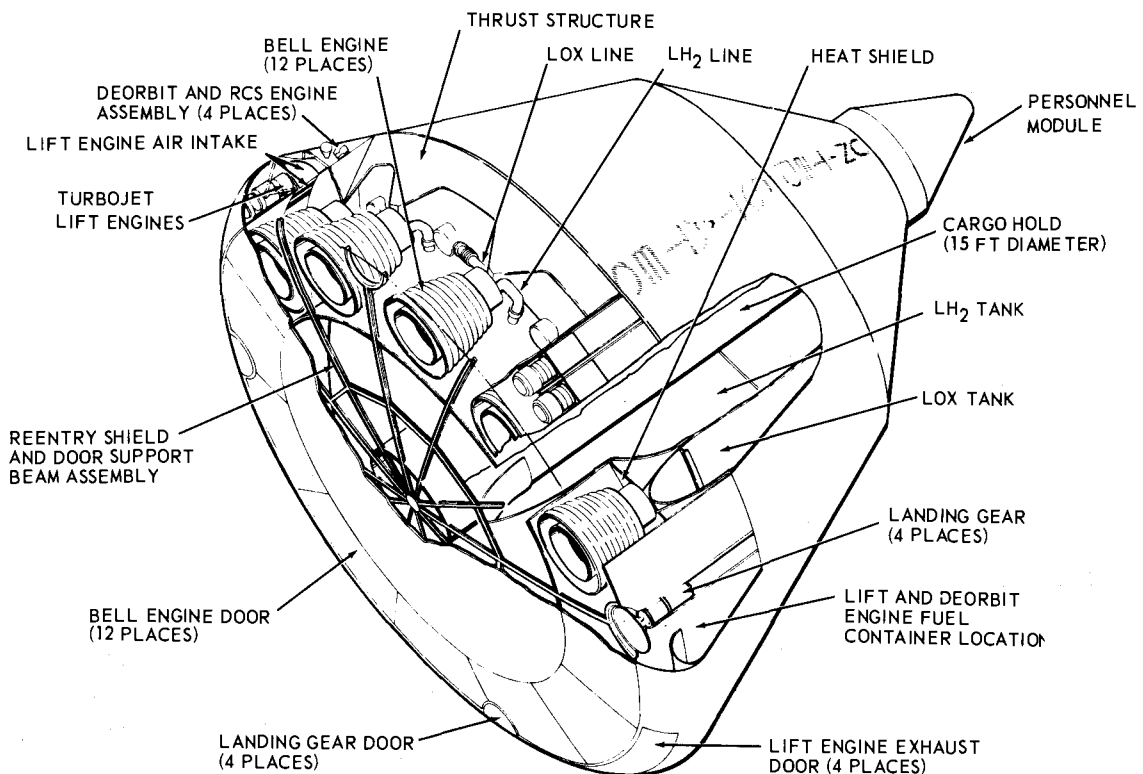
Figure 4.4-4. Vehicle Arrangement with Bell Engine Ascent Propulsion
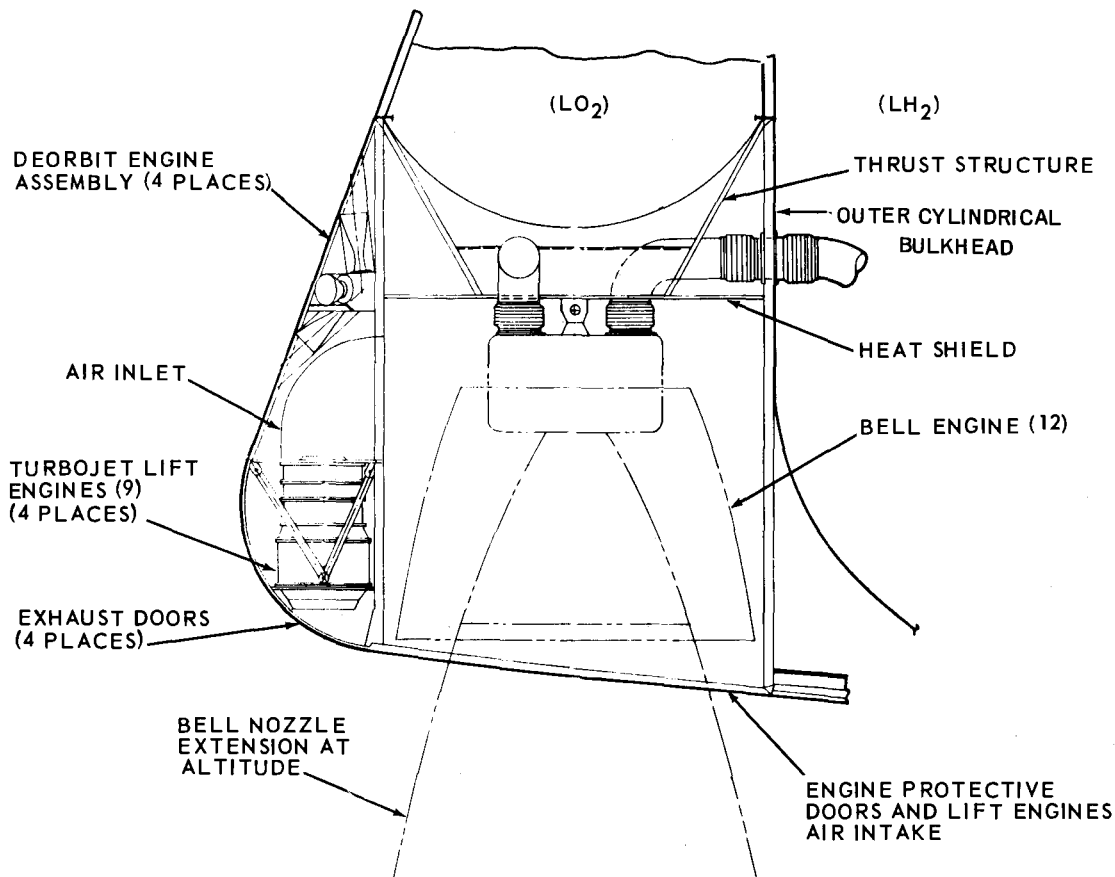
Figure 4.4-5. Engine Compartment Arrangement

4.5 AVIONIC AND POWER SUBSYSTEMS

The SERV integrated avionic subsystem (IAS) includes all vehicle operational subsystems as on integrated scheme with an on-board digital computer as the focal point of operation. (See figure 4.5-1.) Most of the IAS components considered for this system are either a direct fallout of the Saturn/Apollo program or are available off-the-shelf. No major development is required to design the components not presently available since current technology is sufficient. Error analyses have shown that the selected components for IAS are capable of meeting the imposed SERV performance accuracy requirements for flight and landing.

A gimballed platform has been selected because of the large amount of experience with such platforms. Sun sensors, star trackers and horizon seekers will be used to provide attitude reference while SERV is in orbit.

The IAS subsystem is subdivided into the following functional elements:

- Guidance and Navigation
- Vehicle Flight Control
- Data Management
- Communications
- Power Generation and Control

DATA
MANAGEMENT
- 331 LB
- 207 W

—————— GUIDANCE AND NAVIGATION ——————

DATA
MANAGEMENT
(CONTINUED)

- 587 LB
- 1425 W

——————— FLIGHT CONTROL ———————

- 45 LB
- 27 W

| LASER RADAR REFLECTOR |

| ORBIT MAN-EUVER RCS ENGINE THRUST CONTROL |

| CENTRAL PROCESSOR AND MEMORY |

| CENTRAL PROCESSOR AND MEMORY |

| INERTIAL REFERENCE AND ELECTRONICS |

| LOW GRAVITY SENSORS |

| HORIZON SEEKERS |

| RADAR TRANS-PONDERS |

| ASCENT ENGINE ACTUATION AND THROTTLE CONTROLS |

| DESCENT ENGINE ACTUATION AND THROTTLE CONTROLS |

| DAU |

| STAR TRACKER AND SUN SENSOR |

| DAU |

| LANDING RADAR |

| DIGITAL CONTROLLER |

| RATE GYRO ACCELEROM-ETERS |

| DAU |

| ON-BOARD EXECUTIVE COMPUTER INTERFACE AND BUS CONTROL |

| ON-BOARD COMPUTER INTERFACE AND BUS CONTROL |

DATA BUS

| DAU |

| FLIGHT LOG RECORDER |

| DAU |

| RF DATA LINK TO SPACECRAFT |

| DAU |

SECONDARY POWER

PRIMARY POWER

EMERGENCY POWER

| POWER CONDITIONING |

| POWER DISTRIBUTION AND TRANSFER |

| COMMAND LINK DECODER |

| HARDWIRE LINK TO SPACECRAFT DISPLAY AND DATA ENTRY KEYBOARD WITH MANUAL OVERRIDE CAPABILITY |

| SERV SUBSYSTEMS |

| GSE POWER SOURCE |

| PRIMARY AND EMERGENCY POWER SOURCES |

| UPLINK RECEIVER |

| PCM/TM DOWNLINK TRANS-MITTER |

| HARDWIRE LINK TO GSE FOR PREFLIGHT AND POSTFLIGHT CHECKOUT DISPLAY |

◄——— POWER GENERATION AND CONTROL ———►

- 5304 LB
- 518 KWH

◄————————— COMMUNICATION —————————►

- 131 LB
- 45 W

Figure 4.5-1. Functional Diagram of Avionic and Power Subsystems

The functional relationship of these elements is shown on figure 4.5-1.

The data management (DM) subsystem includes a digital computer, signal interface units, a data distribution network and a digital recorder.

The data analysis unit (DAU) scheme of interfacing can be considered a form of data compression since each of the estimated 60 DAU's will monitor an assigned group of transducers or subsystems for limit comparison. Normally the only data transmitted from the DAU to the DM Computer would be an out-of-tolerance condition of a flight critical measurement.

An operational communications subsystem will provide SERV with tracking capability for rendezvous and landing, command link for transmission and navigation updates, vehicle status data transmission for remote display, and remote link for vehicle subsystem control.

The RF links required can be implemented using existing aerospace qualified RF communications equipment.

The power subsystem block diagram, figure 4.5-2, shows the overall concept. This subsystem supplies: 1) power from the auxiliary source for heavy, short-duration loads; 2) power from the normal source for continuous or intermittent, moderate loads; and 3) power from the emergency source for peak normal or emergency loads.

● TOTAL DRY WEIGHT – 5304 LB
● TOTAL ENERGY – 518 KWH

RATING SOURCE	S-S (KW)	PEAK (KW)
NORMAL-DC	20	40
AUXILIARY-AC	134	600
EMERGENCY-DC	3	6
TOTAL	157	646
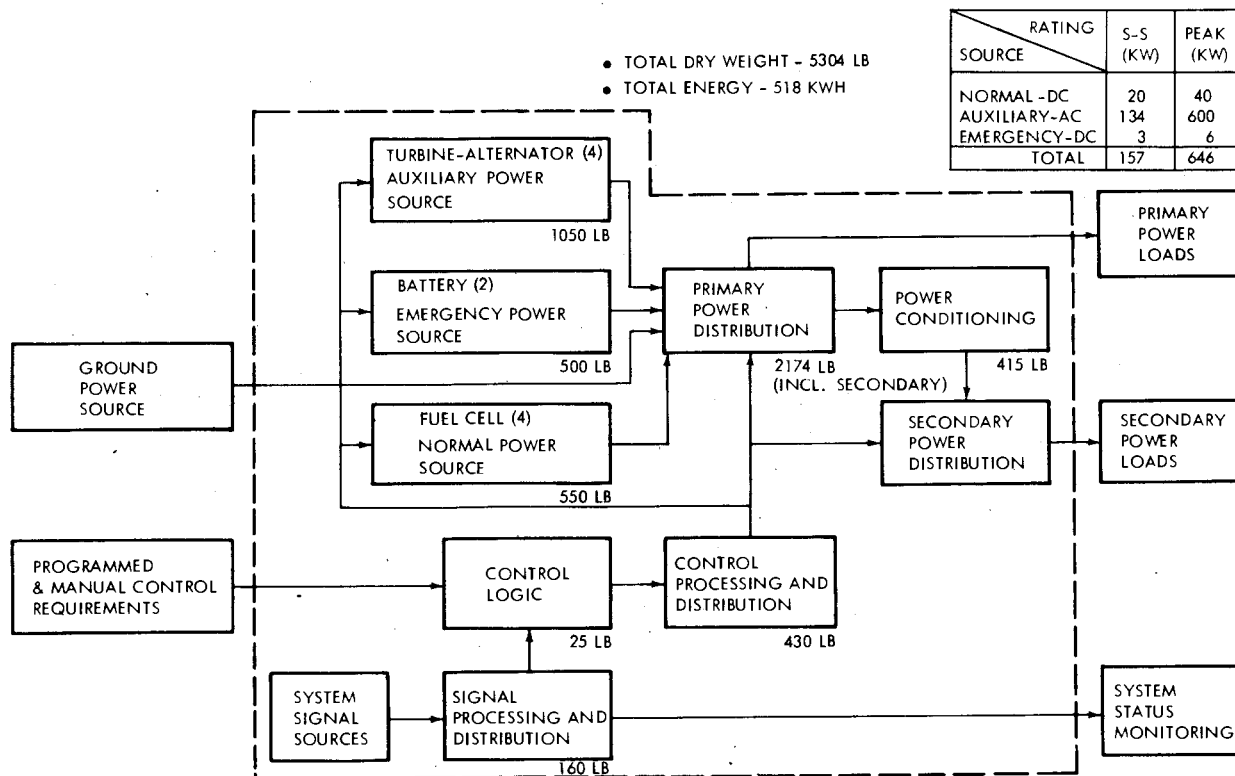
Figure 4.5-2. Functional Diagram of Power Subsystem

The primary and secondary power distribution networks includes overload protection devices, buses, bus switching devices, load switching devices, bus transfer devices, and cables.

The power conditioning components include inverters, dc-to-dc converters, regulators, etc., necessary to provide the proper voltages and frequencies to the various loads.

The control processing and distribution network distributes control signals to the various devices of the power distribution network. The network accepts digital multiplexed signals from the internal control logic and the external on-board computer, and provides appropriate signals to power-handling components.

Provisions will be included for connection of a ground power source that will be capable of supplying all power necessary for preflight operations on the ground. While in orbit, the SERV power subsystem is self-supporting and power from external sources is not required.

The weights of the power subsystem components are shown in figure 4.5-2. The power subsystem weight includes plumbing, charge and control units, installation hardware and allowance for structural supports.

4.5.1 NAVIGATION ERRORS

Figure 4.5-3 shows the error ellipses in the downrange and crossrange plane for two different times of IMU update. The worse case (1200 sec before deorbit) shows a downrange error of 1.88 nm and a crossrange error of 2.45 nm. The figure shows that if update can be delayed to 240 sec before deorbit, then the errors can be reduced by approximately one-half.

Further improvement can be made by reducing the IMU navigational error, which is a major contributor to the total error. One of the two large sources of IMU error is that caused by the accelerometer bias. If the processing of accelerometer data is delayed until just before deorbit (with the exception of the time during reentry) the IMU error can be significantly reduced. Similar improvements could be made if PIGA type accelerometers were to be used, since this type causes bias errors which are an order of magnitude smaller than those specified for the Honeywell platform. Figure 4.5-3 shows a comparison of the error ellipses and indicates that in both the downrange and crossrange, IMU errors can be reduced by almost 0.5 nm.

Table 4.5-1 presents a summary of an error analysis of the SERV guidance and navigation (G&N) system based on the standard 110 nm reference orbit.

The major sources of landing error which cannot be nulled by maneuvering can be attributed to:

- Inertial measurement navigational errors due to the IMU hardware tolerances. This source is a major contributor to navigation error.
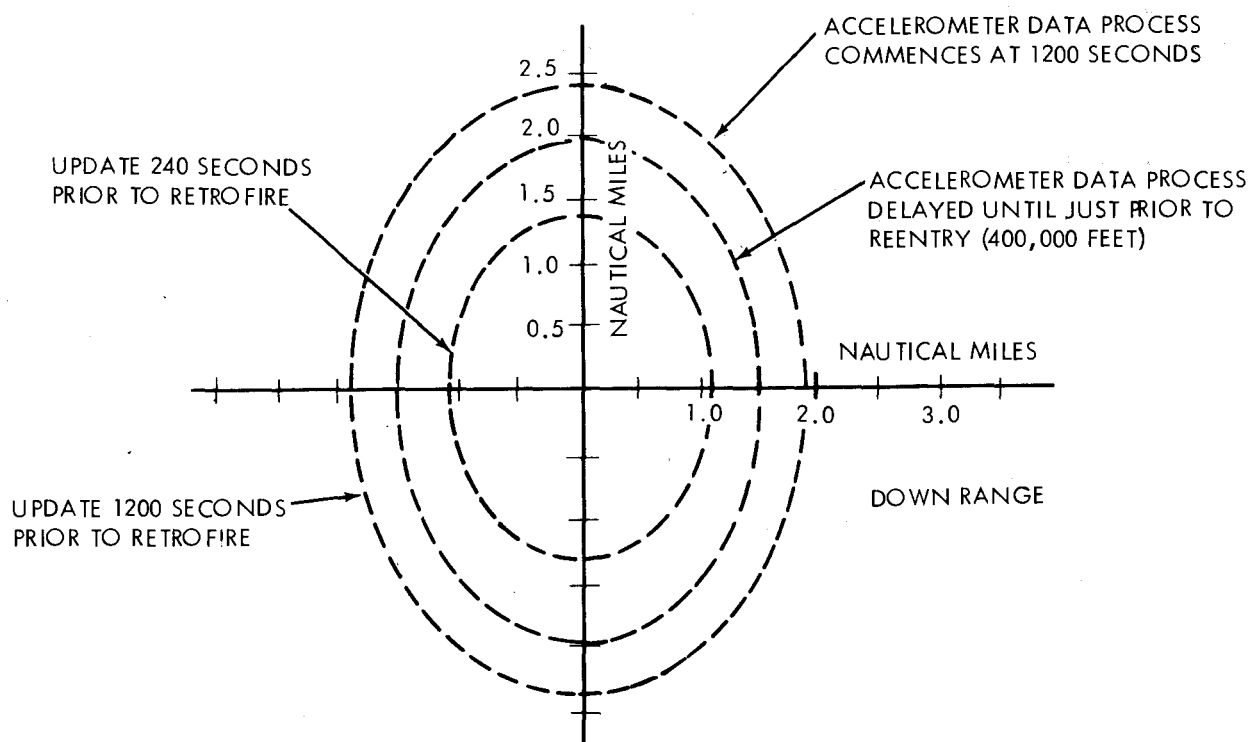
Figure 4.5-3. Navigation Hardware Error Ellipses vs "Time of IMU Update"

Table 4.5-1. SERV Reentry Error Summary

(3σ Range Error at 25,000 ft altitude)

Error Source	Range Errors (NM) for IMU Update			
	(1) 20 Minutes Prior to Deorbit		(2) At 168,000-Ft Altitude	
	Downrange	Crossrange	Downrange	Crossrange
Tracking Radar	0.26	0.86	0.01	0.01
Navigation IMU	1.88	2.47	0.12	0.12
Guidance/Steering (Est)	1.50	1.50	1.50	1.50
(a) RSS Totals	2.42	3.02	1.51	1.51
(b) Navigation Computation	0.20	0.02	0.20	0.02
Arithmetic Sum of (a) and (b)	2.62	3.04	1.71	1.53

- Initial state vector errors (position and velocity) of SERV orbit at the time of last update. The magnitude of these errors considered the Manned Space Flight Network (MSFN) for ground updating.

- Guidance or Steering laws used.

- Bias-type navigation errors resulting from the numerical integration techniques used in the computer navigation logic.

Each of these error sources are listed in column 1 of table 4.5-1. An alternate method exists for determining the initial state vectors for the orbit parameters in orbit navigation.

Based on present state-of-the-art accuracy of vertical reference sensors such as horizon seekers, the navigational error to 25,000 ft will exceed the 4 nm landing maneuver capability. As a result, a supplement is required for this navigational scheme. Orbit state vectors are measured by onboard equipment of SERV and used by the IMU to navigate from deorbit to the reentry interface. When SERV appears near the horizon from the landing site, a ground radar tracks it to establish position. Upon coming out of communications blackout, a radar uplink relays position information to SERV that is designed to reduce the existing navigational errors to within the required ± 4 nm by the time the landing phase commences (25,000 ft altitude).

If a method for on-orbit navigation is used whose system errors are less than the SERV maneuver capability, SERV can come within 3σ values of 1.71 nm downrange and 1.53 nm crossrange. Table 4.5-1 summarises all error sources.

Column 2 of table 4.5-1 shows the increase in landing accuracy that results if an update of state variables is made using ground tracking located at the landing pad. The update would be made after SERV emerges from the communications blackout region.

4.5.2 DATA ANALYSIS UNIT

A data management technique to reduce data handling in the SERV computers was identified in this study as the Data Analysis Unit (DAU). (See figure 4.5-4.) The DAU is capable of:

1) Asynchronously monitoring all the test points assigned to it in a repeating cycle at the DAU clock rate.

2) Making boundary limit comparisons on each measured test point. These comparisons will include high and low limits as well as the action response time within which a measurement should complete its action when stimulated; e.g., thrust buildup of an engine or speed variations of a turbine alternator.

3) Issuance, to the onboard computer, of failure flags when boundary limits are exceeded. These flags would be of varying priority levels to allow for flagging, on a priority basis, of selected measurements related to potential vehicle failure.
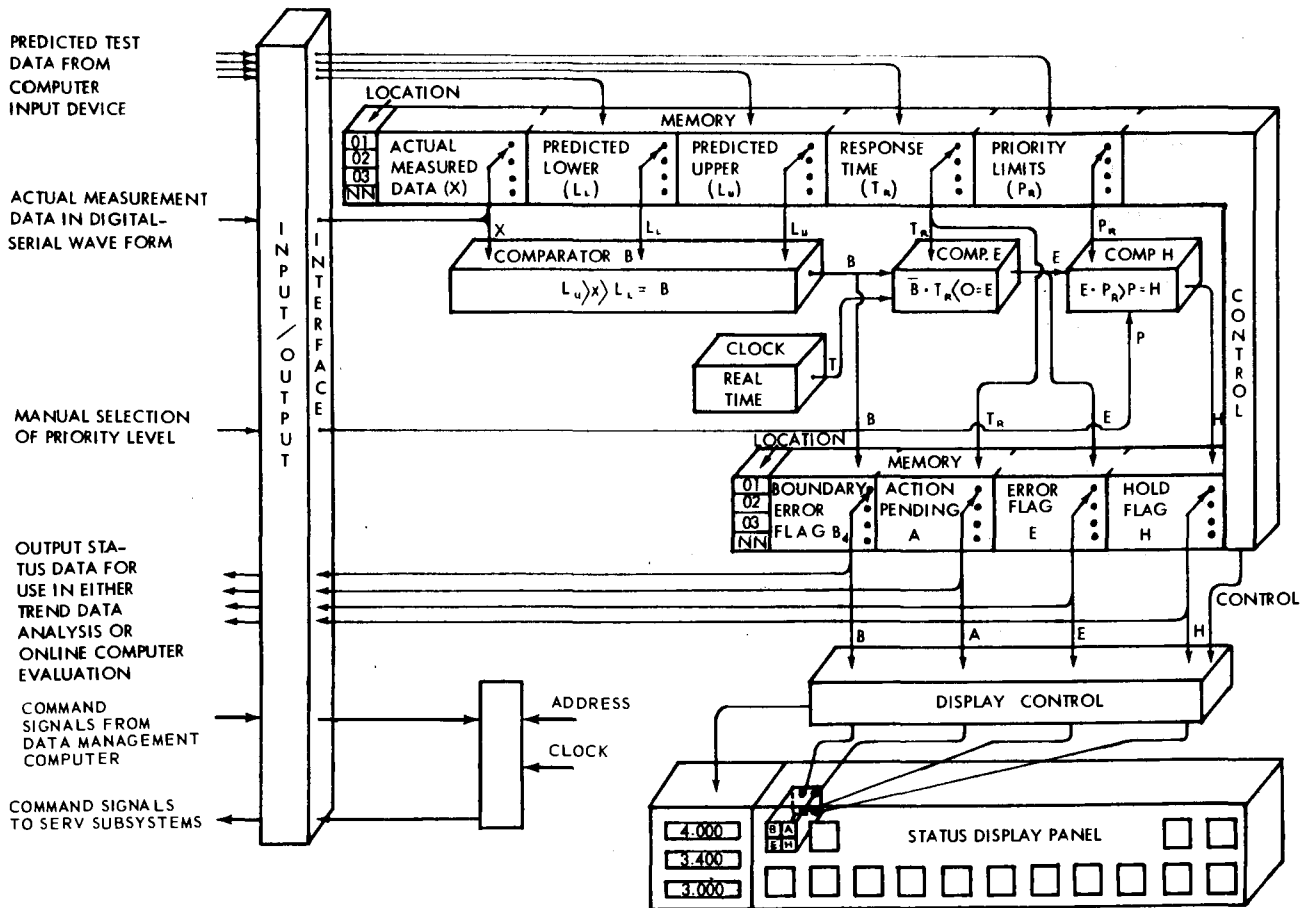
Figure 4.5-4. Data Analysis Unit (DAU)

The technique of reporting black box failures by exception to the main computer can be considered as a form of data compression.

The DAU memory is addressable from a keyboard or from the onboard computer. Changes to the measurement boundary limits can be made to reflect changes in vehicle mission assignment or in vehicle operational status. Thus, checkout evaluation criteria can be entered into the DAU memory to be compatible with their respective operational phases. A schematic of the DAU is shown in figure 4.5-4.

4.6 RELIABILITY

A reliability goal was established to gain some insight into any potential reliability problems that could cause a major perturbation in the SERV study, (See figure 4.6-1). This goal was budgeted to the subsystems so that individual measures of desired reliability performance would be available with which to evaluate the reliability characteristics of each subsystem. A reliability goal was chosen that would be both realistic and cost effective; the goal of 0.990 satisfied both of these criteria.

The 0.990 SERV reliability goal has been allocated to three major mission phases.
(Note that in a series operation: 0.996 x 0.996 x 0.997 = 0.990.)

The mission phase reliability was, in turn, further allocated to principal subsystems required during the mission phases. An allocation then becomes a subsystem goal. Note in figure 4.6-1 that current reliability estimates for the aerospike and the turbo-jet, respectively, is below the allocated requirement. This requirement is based on no turbopump-out and no engine-out capability. The studies show that no reliability problems are foreseen in achieving the goals on the other subsystems shown in figure 4.6-1.

Table 4.6-1 compares the allocated reliability (goals); the estimated reliability which can be attained using the Rocketdyne and Allison values with no turbopump-out and no engine-out, and the estimated reliability again using Rocketdyne and Allison values with turbopump-out and engine-out capability. The effect and importance of designing SERV with turbopump-out and engine-out capability shows that the goals can be met and these engine subsystems are designed with this capability incorporated.

* ESTIMATED RELIABILITY
FOR SINGLE MODULE = 0.9975
FROM NR DATA

** ESTIMATED RELIABILITY
FOR SINGLE TURBOJET = 0.9996
FROM ALLISON DATA
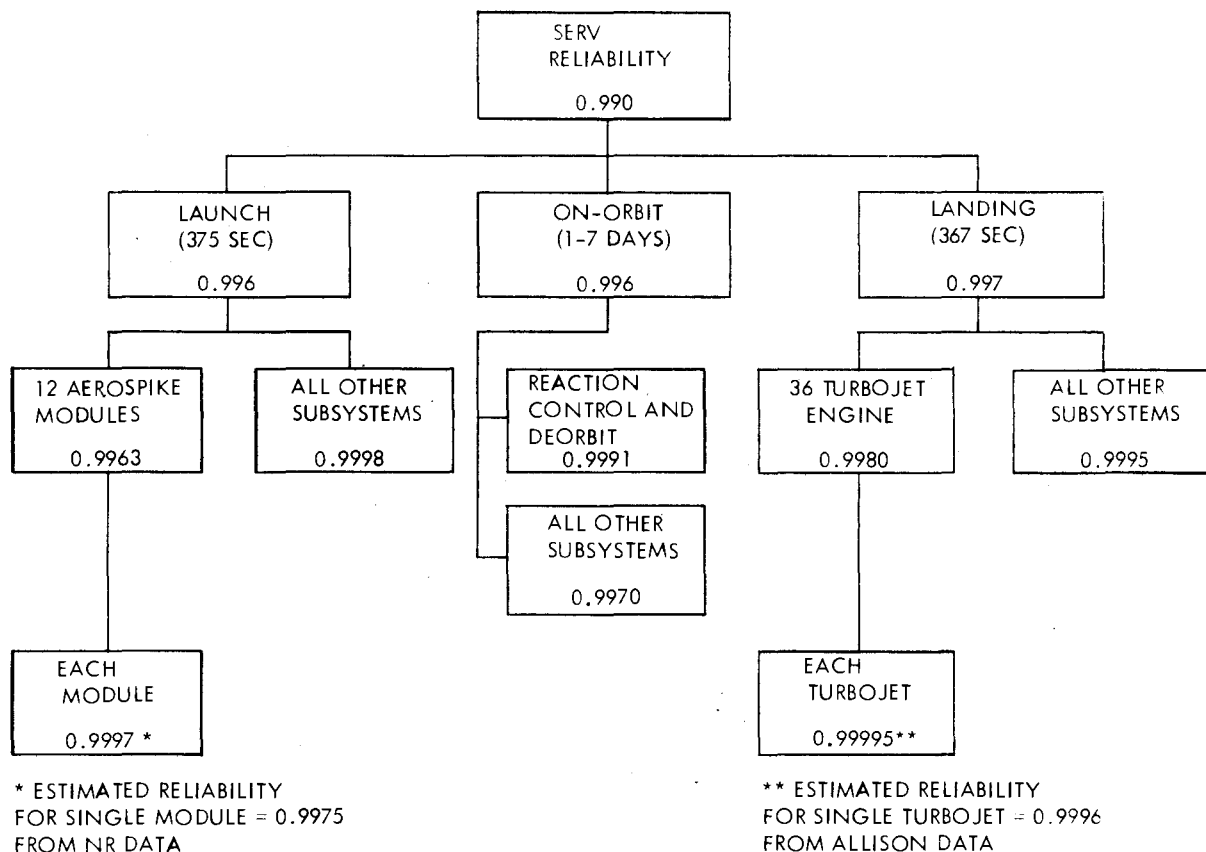
Figure 4.6-1. Allocated Reliability by Mission Phase and by Subsystems

Table 4.6-1. Comparison of Estimated SERV Reliability With and
Without Turbopump-Out and Engine-Out Capability

RELIABILITY	LAUNCH	ON-ORBIT	LANDING	TOTAL
ALLOCATED	0.9960	0.9960	0.9970	0.990
ESTIMATED NO TURBOPUMP-OUT AND TURBOJET ENGINE-OUT CAPABILITY	0.9690	0.9960	0.9853	0.950
ESTIMATED WITH TURBOPUMP-OUT AND TURBOJET ENGINE-OUT CAPABILITY	0.9997	0.9960	0.9988	0.994

4.7 SYSTEMS SAFETY EVALUATION

A system safety evaluation was performed on the SERV vehicle in order to determine
if any major hazards were inherent in the SERV design concept. All situations were
evaluated which, in the course of completing a typical mission cycle, could lead to
potential hazards to the SERV vehicle, its crew and passengers, or ground personnel.
For completeness, all phases of the SERV mission from liftoff to touchdown were con-
sidered, including hazards associated with operations and interfaces with the PM and
MURP, the cargo module, and the space station.

A gross hazards evaluation was prepared in matrix form as illustrated in figure 4.7-1.
A total of 85 operational events were tabulated. Each event identifies the safety hazard
that can occur, the possible cause of the hazard, the effect to personnel and/or hardware,
the hazard detection measure, and the hazard reduction measure.

No hazards were found to exist which could not be reduced or eliminated by present
state of the art technology. The majority of the hazards identified are classified into
three general categories: operational/procedural hazards, hardware oriented hazards,
or hazards caused by human error. Hazards caused by human error are minimized by
the proper selection of personnel skills and careful attention to operational procedures
and detail designs. Hardware oriented hazards are minimized by adherence to proper
design practice and by the incorporation of effective failure detection and personnel
abort systems.

I T E M	OPERATIONAL EVENT	HAZARD	POSSIBLE CAUSE	EFFECT	HAZARD DETECTION MEASURES	HAZARD REDUCTION MEASURES
3.4	Peak dynamic pressure (Max Q)	Failure of SERV or PM/MURP structure due to overstress imposed by maximum dynamic pressure-fire/explosion.	Loss of attitude reference. TVC hard-over. Loss of control error signal. Loss of inertial platform.	Personnel death or injury from loss of atmosphere, vehicle breakup, over-pressure	Stress sensor moni-tors life support system monitor and automatic warning systems	Provide PM/MURP with separate chamber, (with redundant life support system) don space suits, provide PM/MURP with high Q abort capability.
3.5	Monitor ascent acceleration	ACCELERATION in excess of 3G	Uncontrolled engine burn	Abort mission	Accelerometer sen-sors, monitors	Automatic thrust controls to limit acceleration to tolerable levels. PM/MURP has high acceleration abort capability.
3.6	Monitor SERV and PM MURP systems status	EXPLOSION FIRE Explosive decompression	Meteor penetration	Crew and passengers	Very little warning for	Provide meteorite shields in
3.7	Attain required velocity	PROPULSION MALFUNCTION	Rupture or str failure of prop propulsion plu system			
3.8	SERV Engine shutdown	SERV engine system or instrumentation system malfunction	Fuel propellan inoperative or engine shutdow base			
3.9	Close Aerospike Doors	Doors fail to close	Malfunctioning mechanism			
3.10	Personnel abort for PM/MURP	Abort system fails to operate or mal-function.	Separation bolts released. Abo thrusters not op			

- 85 EVENTS EXAMINED

- ALL HAZARDS IDENTIFIED CAN BE REDUCED TO ACCEPTABLE LEVEL OR CAN BE ELIMINATED

Figure 4.7-1.   Gross Hazards Evaluation

Section 5

OPERATIONS

5.0 GENERAL

The major manufacturing, transportation, and launch operations are briefly reviewed in this section.

5.1 MANUFACTURING OPERATIONS

The structural fabrication, assembly, checkout and preparation for shipment will be performed at MAF in buildings 103, 110 (VAB), and 420, Stations 1 through 4. Fabrication of structural components and subassemblies such as rings, support beams, inner cylindrical bulkhead, landing gear assembly, doors, reentry bulkhead panels and cargo containers will be conducted in building 103. Building 110 is used to develop the outer cylindrical bulkhead and the lower and upper outer shell structure. The inner and outer cylindrical bulkheads and the lower and upper outer conical shell subassemblies are fabricated of steel honeycomb panels welded together on a building block approach as a complete circular subassembly. The LO_2 and LH_2 lower bulkheads will be developed as circular segments prior to mainstream assembly. In addition to circular external work platforms, internal suspended work platforms and tooling are required as illustrated in operations 600, 800, 1000 and 1400 of figure 5.1-1.

All subassemblies in buildings 103 and 110 are transferred to building 420, Station 1 for the final assembly as depicted in the mainstream flow sequence, figure 5.1-1. The vehicle is then moved to Station 2 for pressure test and cleaning. The LH_2 tank is filled with sealed styrofoam balls and gas pressure tested in conjunction with the LO_2 tank, which is partially filled with demineralized water to simulate propellant weight and reduce gaseous volume. The vehicle is returned to Station 1 for installation of the lower and upper thermal protection shells over the existing structural shell. The vehicle is transferred to Station 3 for the installation of electromechanical-hydraulic and avionic and propulsion systems, and final assembly activities. At the completion of these activities the vehicle is moved to Station 4 for checkout, weight, CG and optical alignment operations prior to preparation for shipment activities.

Total time period for typical manufacture of a vehicle is 93 weeks.

The major external facility modification at MAF, see figure 5.1-2, is minimal and limited to enlarging the existing 4-cell building 420 both vertically and horizontally for final assembly, test and checkout. Other external modifications are: widening

OPERATION 100 – SUPPORT BEAM AND LANDING
GEAR ASSEMBLY

OPERATION 250 – INNER CYLINDRICAL
BULKHEAD ASSEMBLY

OPERATION 300 –MATING INNER CYLINDER
BULKHEAD AND THRUST
RING

OPERATION 400 – MATING OUTER CYLINDER
BULKHEAD

OPERATION 600 – LH₂ LOWER BULKHEAD
INSTALLATION

OPERATION 800 – LO₂ LOWER BULKHEAD
TO OUTER CYLINDER BULKHEAD

WEEK 24

OPERATION 50 – THRUST RING ASSEMBLY

OPERATION 360 – OUTER CYLINDRICAL BULKHEAD
ASSEMBLY

OPERATION 900 – INSTALL LIFT ENGINE
MODULES

OPERATION 1800 – INSTALLATION OF SHELL TPS
OPERATION 2000, 3000 AND 4000 – SYSTEM INSTALLATION AND FINAL
ASSEMBLY

OPERATION 5000 – CHECKOUT, WEIGHT, CENTER
OF GRAVITY

OPERATION 6000 – PREP FOR SHIP

WEEK 93

ALKALINE CLEANSER
NITRIC ACID
SOLVENT

OPERATION 1600 – CLEANING, LEAK TEST AND PRESSURE TEST

WEEK 60

OPERATION 1400 – UPPER SHELL
OPERATION 1300 – INSTALL PROPELLANT TANK INTERIORS
OPERATION 1300–10 – INSTALL RETRO TANKAGE
OPERATION 1300–20 – INSTALL PRESSURIZATION SYSTEM

OPERATION 1000 – INSTALL LOWER SHELL

OPERATION 1250 – UPPER SHELL

OPERATION 950 – LOWER SHELL

Figure 5.1-1.   Manufacturing Sequence
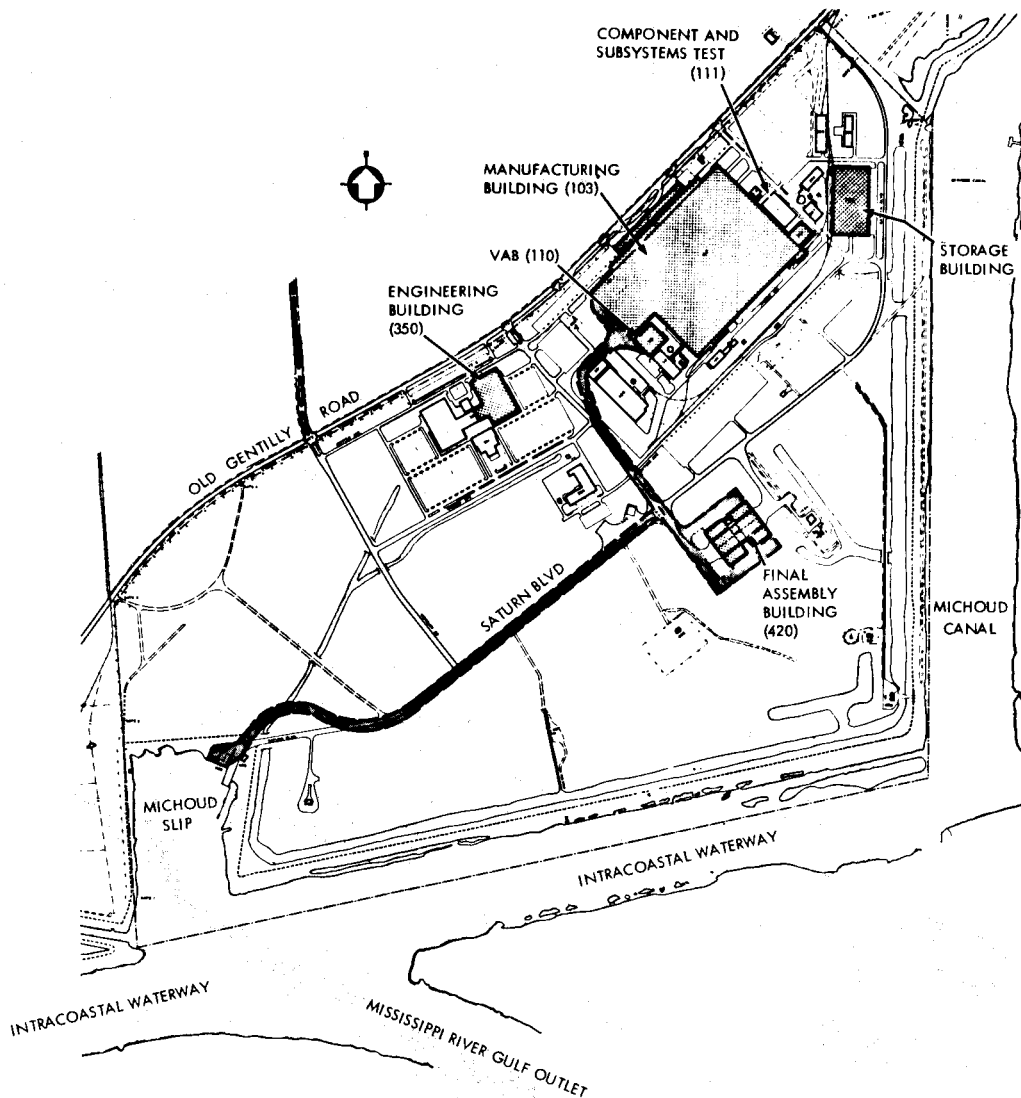
Figure 5.1-2. SERV Manufacturing Site Plan

Saturn Blvd from building 420 to the Michoud Slip, widening of the route between buildings 103, 110 (VAB) and 420, and widening one dock at the Michoud Slip. Modifications to all other buildings involve internal rearrangement only.

Delivery of subcontractor/vendor items can be performed by road, water or spur rail directly to the MAF. The proximity to each other of engineering, manufacture, test and ship loading facilities is notable.

5.2 TRANSPORTATION

Figure 5.2-1 shows the SERV being transported on the Bay-class vessel owned by the West India Shipping Company. The vessel is 266 feet long with a 51 foot beam and can be ballasted to draw 6-12 feet of water. The pin-on type sponsons would increase the

vehicle width to 89 feet; therefore the vessel can still pass through the locks and bascule bridges between the MAF and KSC-VAB dock with no route modifications or offloading of cargo. The pin-on sponsons are presently under consideration for other applications by the West India Shipping Company. The vessel deck can presently accept the point loading from the landing gear. However, if the SERV diameter is in excess of 88 feet, it will be supported by a transportation ring (similar to the launch ring), which can pivot vehicles up to 96 feet diameter through 22 degrees to produce an effective width of 89 feet to facilitate passage through the bascule bridge and locks at KSC.

Transportation of SERV by commercial carrier was the selected method because the total estimated transportation costs by this method was found to be considerably less than the total estimated cost of modifying, maintaining and manning an existing NASA shuttle barge.
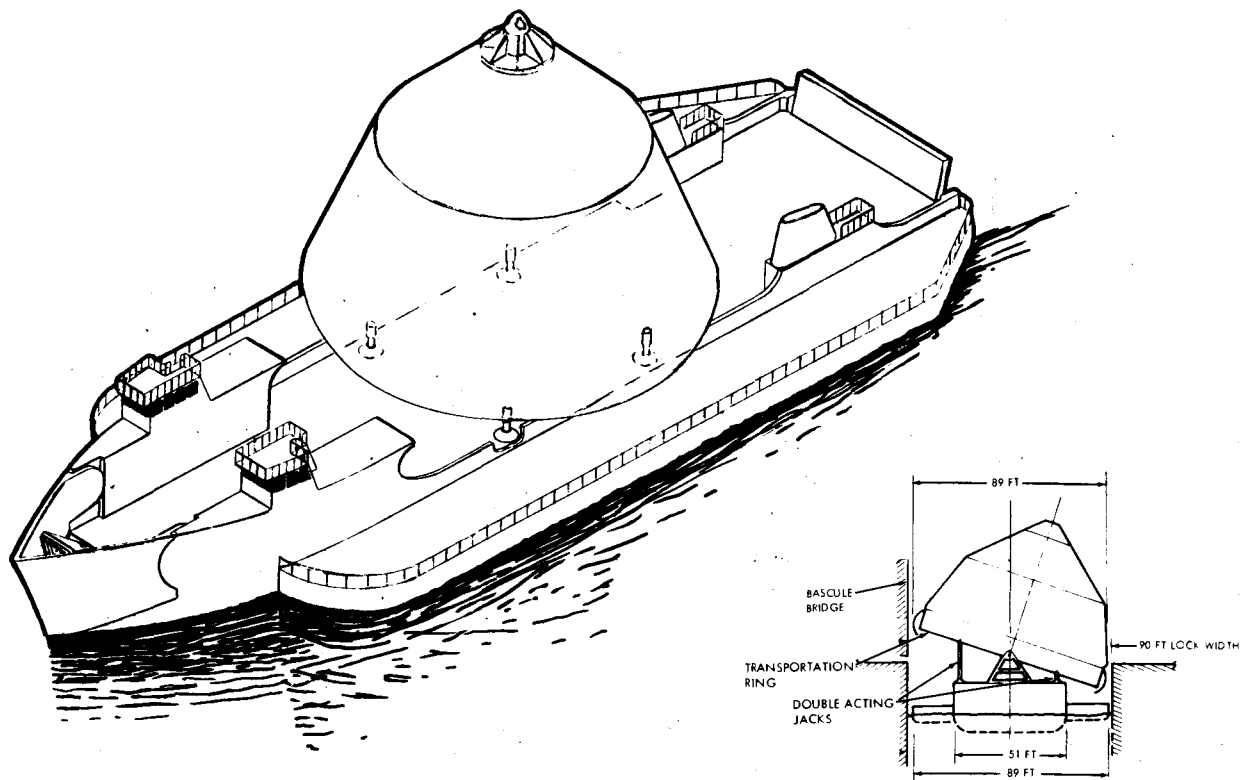
Figure 5.2-1. Bay Class Vessel Transporter

5.3 LAUNCH OPERATIONS

The baseline ground operations approach involves the area between the VAB and launch pads A and B at LC-39. (See figure 5.3-1.) SERV vehicles up to 96 foot diameter can be delivered from MAF through the Port Canaveral 90-foot-wide locks and bascule bridges via the Banana River to the VAB dock. SERV vehicles in excess of 88 feet in

diameter can be transported by tilting the SERV as deck cargo on a Bay-class vessel to reduce the effective width. This route will also be used for the delivery of the Personnel Modules and Cargo Modules, the latter using modified S-IB stage transporters for overland movement to and from existing barges.

Figure 5.3-1. KSC Operations

The baseline ground operations approach identifies twin 500-1000 foot diameter landing pads for the SERV adjacent to the crawlerway and 1.75 miles from the VAB and LC-39. The 4-mile-radius circle identifies the target area at 25,000 feet altitude. The winged MURP spacecraft will land at the existing 10,000-foot landing strip. Transportation of

the relatively small MURP spacecraft from the landing strip back to the VAB poses no problems as this vehicle can be tractor towed on existing highways at off-peak congestion hours. The use of the existing VAB for cargo and vehicle assembly, dispersal, storage, servicing and refurbishment provides proximity to road, rail, sea, and air methods of transportation from all parts of the nation.

The flow chart, figure 5.3-2, identifies the major facilities and operations involved in the selected operational approach, with special emphasis on the turnaround cycle. Delivery of the test and operational SERV vehicles from MAF to KSC is by a Bay-class vessel. A 200-ton-capacity barge crane is used to off-load SERV onto the operational wheel type transporter which is then tractor drawn to the VAB.

Following SERV landing in proximity to the VAB and after cooldown, deactivation, and personnel and priority cargo removal operations have been performed, SERV is loaded onto the wheeled transporter used previously for delivery from MAF. The loading of SERV onto the transporter is achieved by positioning dollies under the landing gear pads and winching SERV up ramps onto the transporter for delivery to the VAB high bay.

Figure 5.3-2 identifies major sequential operations required in preparation for vehicle storage, or recycling for launch. The platform enclosure that can be raised and lowered to encompass the SERV assembly in the VAB high bay provides a ready means for personnel access to all levels during disassembly, servicing, refurbishment and assembly, regardless of the launch configuration required. During configuration disassembly and assembly operations, hoist capability is provided by an existing 250-ton traveling bridge crane in the VAB. A new LUT and existing crawler-tractor (CT) provide the transportation system to LC-39 in a manner similar to the Saturn V.

The SERV storage, servicing and vehicle assembly and disassembly operations are performed in the VAB high bay area. The cargo module, MURP and Personnel Module, storage, servicing, assembly, and disassembly of cargo are performed in the low bay area. The MURP spacecraft would be tractor towed from the strip via the Orsino Causeway to the VAB low bay for recycling to storage or relaunch as required.

● LOAD BARGE AT MAF

DELIVERY

● TRANSPORT TO.
KSC ATLANTIC DOCK/VAB DOCK (AS REQ'D)

● OFF-LOAD AND TRANSPORT
TO VAB HIGH BAY

OPERATIONAL

LANDING
WITH OR WITHOUT PM

● LAND SERV
ON PAD

● PERSONNEL
EGRESS

● DEACTIVATE

● LOAD AND
TRANSPORT
TO VAB HIGH
BAY

● LOWER PLATFORM ENCLOSURE

● REMOVE CARGO AND/OR
PERSONNEL MODULE AND
TRANSFER TO LOW BAY

● HEAT SHIELD REFURBISH

● SERVICING AND
CHECKOUT

● VEHICLE MATING WITH
MURP OR PM

● INTEGRATED CHECKOUT

● CT/LUT
TRANSPORTS
MATED
VEHICLE TO
LC-39

● LUT
INSTALLATION
ON PAD

● LOAD
PROPELLANTS

● LOAD
PERSONNEL
(IF REQ)

● CHECKOUT
AND LAUNCH

VAB
LOW BAY

DELIVERY AND
OPERATIONAL

MURP LANDS
ON SKID STRIP

● TOW TO VAB
LOW BAY

● MURP – SERVICE, REFURBISH AND CHECKOUT

● CARGO MODULE – LOAD AND UNLOAD

● PERSONNEL MODULE – SERVICE AND REFURBISH

Figure 5.3-2. SERV Spacecraft Ground Operations

Section 6

PROGRAM PLAN

6.0 GENERAL

The final vehicle configuration, supporting flight technology analyses, subsystems, and operations have been discussed in previous sections. In this section, scheduling activities for implementation of the SERV space shuttle are presented, together with the associated ROM cost.

6.1 PROGRAM SCHEDULE

The program schedule, figure 6.1-1, is a projection of activities for those elements having a major impact on the initiation of the program, through the first manned orbital flight (FMOF). The schedule shows a 12-month phase B study commencing in the last quarter of CY 1971, followed by phases C and D starting at the beginning of CY 1973, with 90 percent engineering release at the end of CY 1974 and 100 percent release 10 months later. Facility modifications are identified at MAF and KSC. Modifications of MAF facilities are scheduled for the start of CY 1973, with the emphasis directed toward the modification, tooling and fixtures for building 420. Modifications of KSC facilities can be delayed a year after the start of MAF modifications.

It is proposed to build one structural test vehicle (STV-1) which will be used for handling and transportation equipment checkout, a mode and frequency test, and a static loads and life cycle test followed by a test to destruction. These tests will be conducted at KSC and will take approximately 20 months to complete.

A static fire vehicle (SF-1) will be used in the program for propellant load, cold flow and static fire tests. Turbojets and other subsystems will not be installed. The tests, of 15 months duration, will be conducted at KSC and after completion the vehicle will be overhauled, refitted and cycled as a production vehicle.

6.2 MANUFACTURING SCHEDULE

The manufacturing schedule, figure 6.2-1, shows fabrication and assembly commencing in the third quarter of CY 1974. This schedule identifies the period of activity associated with each mainline component and subassembly operation to be performed either in buildings 103 and 110 at MAF or at a subcontractor's facility. Major assembly or installation displayed as an extension to each line (bar) operation are followed by checkout, weighing, center of gravity (CG) checks, and preparation for shipment. These activities are all performed in appropriate stations within building 420.

Figure 6.1-1. SERV Program Schedule

SUBASSEMBLY
MAJOR ASSEMBLY/INSTALLATION

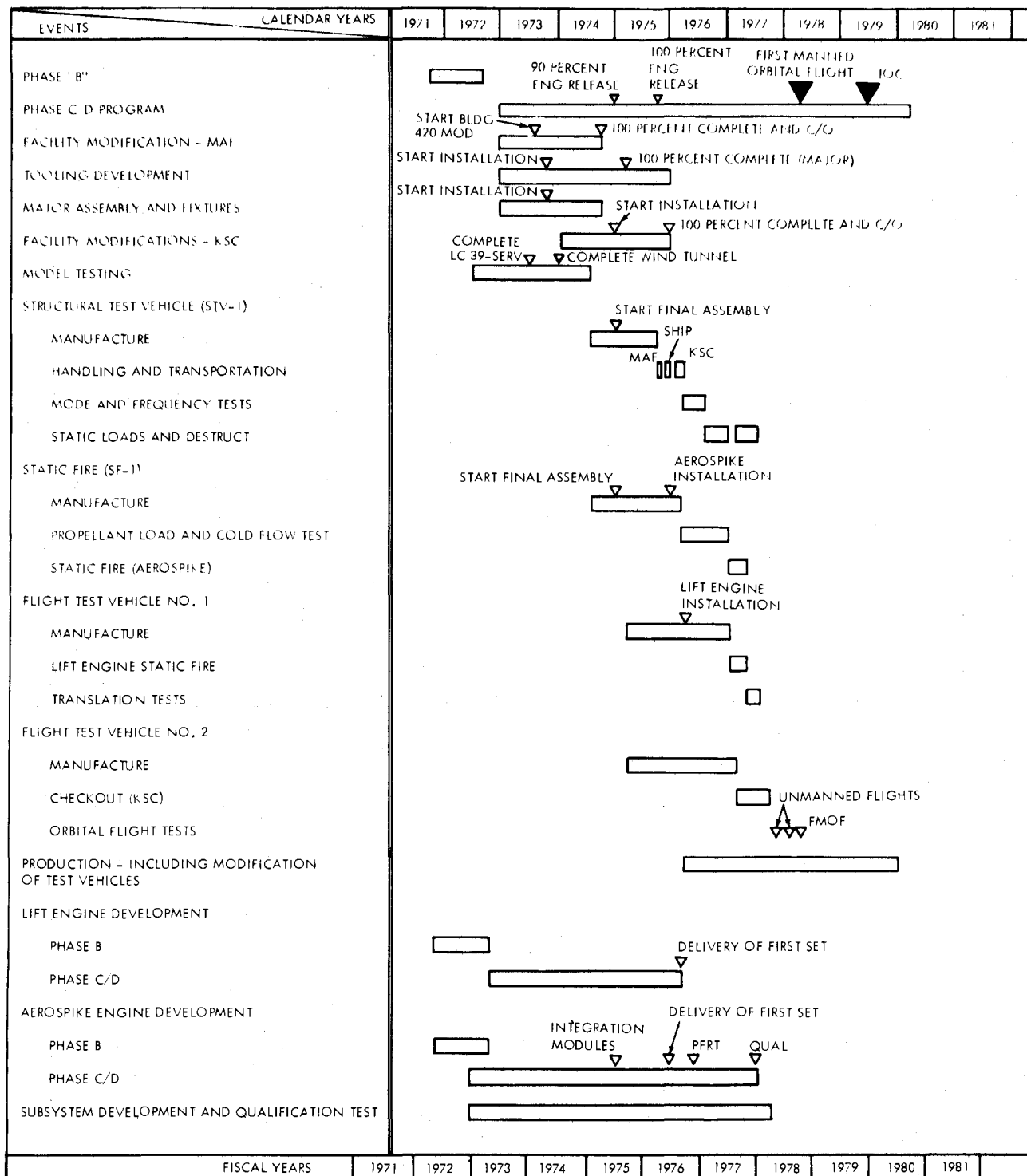| OPERATION NO.	OPERATION	VEHICLE IDENTITY	CY 1974		CY 1975		CY 1976		CY 1977		CY 1978		CY 1979	
			1	2	1	2	1	2	1	2	1	2	1	2
300	ASSY SUPPORT BEAM, THRUST RING	STV-1	(1A)*											
400	INSTALL OUTER CYL BULKHEAD		(1A)											
600-800	INSTALL LH$_2$ AND LO$_2$ LOWER BULKHEADS		(1A)											
1000-1400	INSTALL UPPER AND LOWER SHELLS		(1A)											
1600	PRESSURE TEST AND CLEAN			(2)										
1800	INSTALL TPS - LOWER AND UPPER SHELL			(1A)										
2000-3000	SYSTEMS INSTALL. (DOORS-PANELS)		(3)											
5000-6000	CHECKOUT, WEIGHT, C.G., PREP FOR SHIP.			(4)										
300	ASSY SUPPORT BEAM, THRUST RING	SF-1	(1B)											
400	INSTALL. OUTER CYL BULKHEAD		(1B)											
600-800	INSTALL LH$_2$ AND LO$_2$ LOWER BULKHEADS		(1B)											
1000-1400	INSTALL UPPER AND LOWER SHELLS		(1B)											
1600	PRESSURE TEST AND CLEAN			(2)										
2000-3000	SYSTEM INSTALL (AEROSPIKE, DOORS, PANELS)		(3)											
5000-6000	CHECKOUT, WEIGHT, C.G., PREP. FOR SHIP.			(4)										
300	ASSY SUPPORT BEAM, THRUST RING	FLT. TEST NO. 1			(1A)									
400	INSTALL OUTER CYL BULKHEAD				(1A)									
600-800	INSTALL LH$_2$ AND LO$_2$ LOWER BULKHEADS				(1A)									
900	INSTALL LIFT ENGINE MODULES				(1A)									
1000-1400	INSTALL UPPER AND LOWER SHELLS					(1A)								
1600	PRESSURE TEST AND CLEAN					(2)								
2000-3000	SYSTEMS INSTALL (DOORS-PANELS)						(3)							
5000-6000	CHECKOUT, WEIGHTS, C.G., PREP. FOR SHIP.						(4)							
300	ASSY SUPPORT BEAM, THRUST RING	FLT. TEST NO. 2			(1B)									
400	INSTALL OUTER CYL BULKHEAD				(1B)									
600-800	INSTALL LH$_2$ AND LO$_2$ LOWER BULKHEADS				(1B)									
900	INSTALL LIFT ENGINE MODULES					(1B)								
1000-1400	INSTALL UPPER AND LOWER SHELL					(1B)								
1600	PRESSURE TEST AND CLEAN					(2)								
1800	INSTALL TPS - LOWER AND UPPER SHELL					(1B)								
2000-4000	SYSTEMS INSTALLATION						(3)							
5000-6000	CHECKOUT, WEIGHT, C.G., PREP. FOR SHIP.						(4)							
300	ASSY SUPPORT BEAM, THRUST RING	OPERATIONAL NO. 1					(1A)							
400	INSTALL OUTER CYL BULKHEAD						(1A)							
600-800	INSTALL LH$_2$ AND LO$_2$ LOWER BULKHEADS						(1A)							
900	INSTALL LIFT ENGINE MODULES						(1A)							
1000-1400	INSTALL UPPER AND LOWER SHELL							(1A)						
1600	PRESSURE TEST AND CLEAN							(2)						
1800	INSTALL TPS LOWER AND UPPER SHELL							(1A)						
2000-4000	SYSTEMS INSTALLATION							(3)						
5000-6000	CHECKOUT, WEIGHT, C.G., PREP. FOR SHIP.							(4)						
900	INSTALL LIFT ENGINE MODULE	OPERATIONAL NO. 2							(1A/B)					
1600	PRESSURE TEST AND CLEAN								(2)					
1800	INSTALL TPS LOWER AND UPPER SHELL								(1A/B)					
2000-4000	SYSTEMS INSTALLATION								(3)					
5000-6000	CHECKOUT, WEIGHT, C.G., PREP FOR SHIP.	(EX SF-1)								(4)				
1600	PRESSURE TEST AND CLEAN	OPERATIONAL NO. 3 (EX-FLT TEST NO. 1)								(2)				
2000-4000	SYSTEMS INSTALLATION									(3)				
5000-6000	CHECKOUT, WEIGHT, C.G., PREP. FOR SHIP.										(4)			
	REMOVE TEST INSTALLATIONS (KSC)	OPERATIONAL NO. 4 (EX-FLT TEST NO. 2)										■		
	CHECKOUT (KSC)											■		

NOTE:

( )* DENOTES STATION NUMBER OF OPERATION IN BUILDING 420 AT MAF
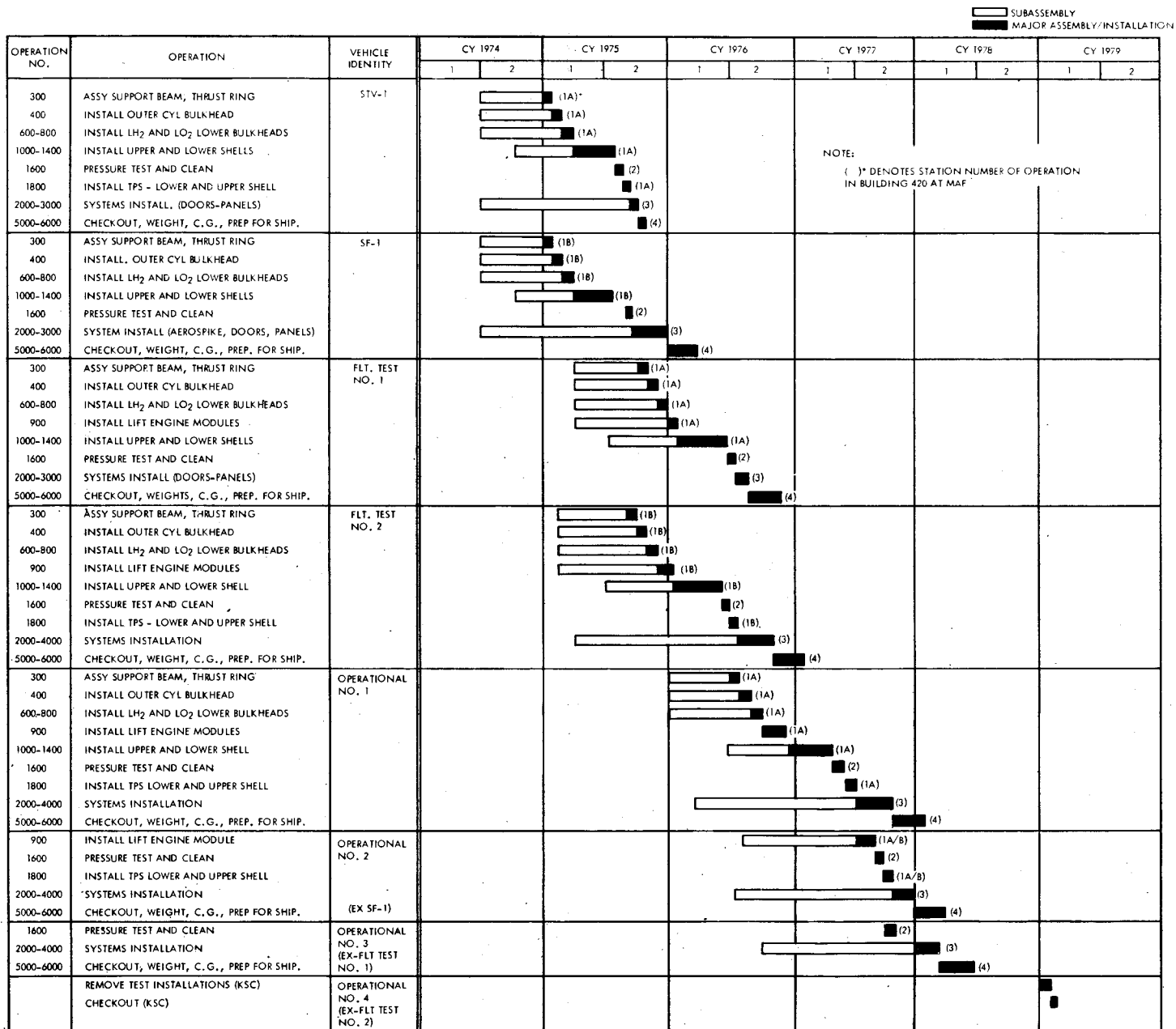
Figure 6.2-1. Manufacturing Schedule

6.3 VEHICLE TEST SCHEDULE

The vehicle test schedule, figure 6.3-1, is divided into the following seven major activities: 1) R&D tests; 2) model tests; 3) structural test vehicle (STV-1); 4) static fire vehicle (SF-1); 5) flight test vehicle No. 1 (FT-1); 6) flight test vehicle No. 2 (FT-2); and 7) component qualification.

6.4 FACILITY MASTER SCHEDULE

Figure 6.4-1 shows the major facility modifications at MAF and KSC. At MAF, the major item is the modification and installation of equipment in building 420. Commencing at the beginning of CY 1973, building 420 is scheduled for completion in the last quarter of CY 1974, approximately 2 months prior to final structural assembly of the first test vehicle, STV-1.

All other facility modifications at MAF are scheduled to be complete at least 3 months before their use.

Because of their size and also because they are required in the movement of vehicles between stations in building 420, the SERV transporters will be assembled at MAF. These transporters will be available approximately 2 months prior to the need to move STV-1 from station 1 to station 2. Inter-facility transportation will be performed by a commercial carrier using existing equipment. The major facility items at KSC to be modified are the VAB, LC-39A and LC-39B, and the LUT.

PROGRAM	LOCATION	VEHICLE	CY 72	CY 73	CY 74	CY 75	CY 76	CY 77	CY 78	CY 79	CY 80
R&D TESTS	VARIOUS										
• SUBSYSTEMS											
• AEROSPIKE											
• LIFT ENGINES											
MODEL TESTS											
• LC-39/SERV	MAF/KSC										
• SERV WIND TUNNEL	VARIOUS										
• RF RADIATION	KSC										
STRUCTURAL TEST VEHICLE		ST-1									
• HANDLING AND TRANSPORT	MAF-KSC										
• MODE AND FREQUENCY	KSC-VAB										
• LIFE CYCLE AND STATIC LOADS	KSC-VAB										
• DESTRUCT	KSC-VAB										
STATIC FIRE VEHICLE		SF-1									
• PROPELLANT LOAD AND COLD FLOW	KSC-LC39										
• STATIC FIRE	KSC-LC39										
FLIGHT TEST VEHICLE NO. 1		FT-1									
• LIFT ENGINE STATIC TESTS	KSC-LC39										
• TRANSLATION TESTS	KSC-LANDING PADS										
FLIGHT TEST VEHICLE NO. 2		FT-2									
• INTEGRATED ORBITAL FLIGHTS	KSC-LC39										
COMPONENT QUALIFICATION	VARIOUS										

Figure 6.3-1. Vehicle Test Schedule

IDENTITY	CY 1973				CY 1974				CY 1975			
	1	2	3	4	1	2	3	4	1	2	3	4

DESIGN AND PROCURE

FABRICATE, INSTALL, TEST AND FINAL ACCEPTANCE

MICHOUD
- BUILDING 420
- ROTARY TABLES (5)
- 150-TON CRANE WITH TELESCOPE WELD FIXTURE (2)
- PNEUMATIC, HYDROSTATIC AND CLEAN FACILITY
- WEIGHT AND C.G. CHECK EQUIP.
- RELOCATE EXISTING EQUIPMENT WITHIN MAF
- SPECIAL FOUNDATIONS - EQUIPMENT AND TOOLING
- VARIOUS CRANE MODIFICATIONS
- ROAD AND DOCK MODIFICATIONS
- NEW FACILITY ITEMS, SPECIAL EQUIPMENT AND TOOLING WITHIN MAF
- SERV TRANSPORTER (3)

KSC
- VERTICAL ASSEMBLY BUILDING
- LAUNCH COMPLEX 39A AND B
- LANDING PADS (2), STRIP AND GSE
- CRAWLERWAY (SERVICE ROAD)
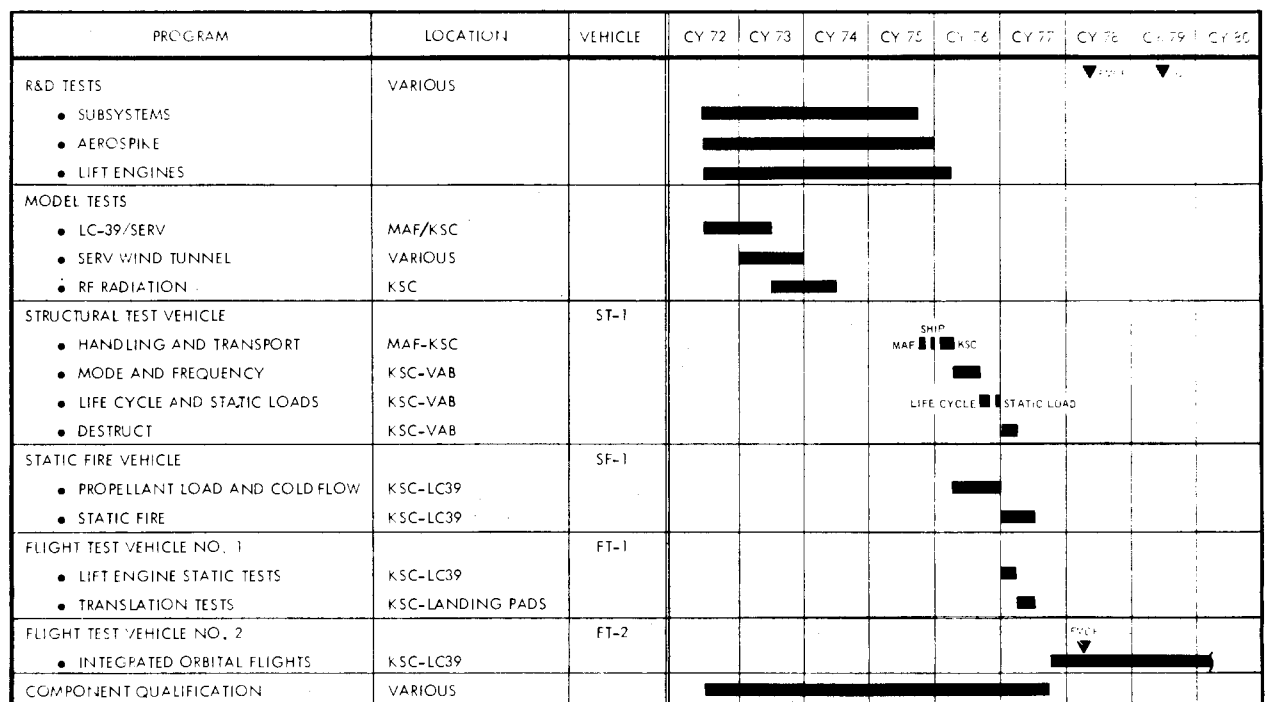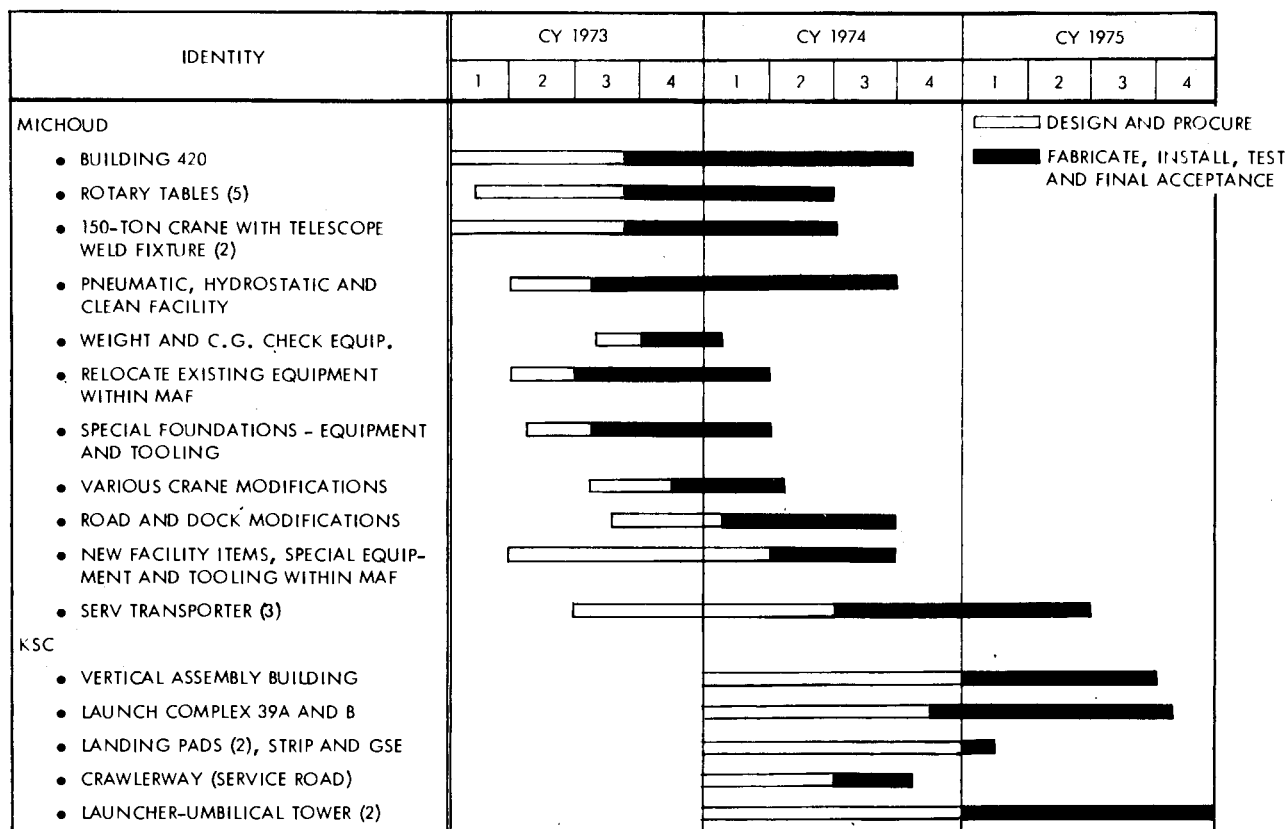- LAUNCHER-UMBILICAL TOWER (2)

Figure 6.4-1. Facility Schedule

The start of final assembly in stations 1A and 1B and the subsequent movement of vehicles through stations 2, 3 and 4 are critical to the overall schedule. Delays in scheduled occupancy affects subsequent vehicle movement. Relief to this schedule is possible because the initial vehicles do not require all systems to be installed for their respective test program. This reduces individual assembly time compared to the installation requirements for testing later vehicles. For example, STV-1 requires minimum system installation, SF-1 does not require lift engine installation, and flight test vehicle No. 1 (FT-1) does not initially require aerospike modules. Note that scheduling to modify a test vehicle by final installation of systems to an operational standard is influenced by when that particular vehicle has completed its test program.

It is planned to return vehicles SF-1 and FT-1 to MAF for removal of test equipment, and after installation completion they will become operational vehicles 2 and 3, respectively. FT-2 has all systems installed prior to leaving MAF and will not return to MAF; test instrumentation will be removed at KSC. After removal of instrumentation the vehicle becomes operational vehicle No. 4.

The first flight test vehicle (FT-1) will be fitted with turbojets and associated subsystems and used for horizontal and vertical translation flight tests at KSC. An aerospike engine will not be installed in this vehicle. The translation tests are scheduled to take 6 months and will be completed 3 months before the completion of checkout of the first

orbital flight vehicle. Following satisfactory completion of the horizontal and vertical translation tests, the vehicle will be returned to MAF for recycling as a production vehicle.

The second flight test vehicle (FT-2) will be utilized for orbital flight test and will be delivered to KSC 12 months prior to the first manned orbital flight. Prior to the first manned flight, two unmanned orbital test flights will be accomplished.

Throughout the aforementioned development period, subsystem and component development and qualification tests will be performed at MAF and other government and sub-contractor facilities.

The critical path for the schedule is as follows: 1) complete model tests; 2) initiate MAF and building 420 modifications; 3) commence installment of major tooling and fixtures; 4) MAF facility complete and checked out; 5) 90 percent engineering release, start final assembly of structural test vehicle (STV-1) and static fire test vehicle (SF-1) and start facility installation at KSC; 6) 100 percent installation of major tooling at MAF; 7) 100 percent engineering release and shipment of STV-1; 8) delivery and installation of first aerospike engine modules; 9) delivery and installation of first direct lift gas turbine engines; 10) completion of vehicle static loads, static fire, translation tests and completion of subsystem development and qualification tests; 11) two unmanned orbital flights prior to FMOF; and 12) manned/unmanned flights prior to IOC.

6.5 COSTS

ROM costs were developed for key cost categories of interest. Figure 6.5-1 illustrates SERV shuttle program cumulative costs for the SERV only, SERV-PM and SERV-MURP. The cumulative cost curves also show program cost in percent discount rate in accordance with Bureau of the Budget Circular No. A-94, dated June 26, 1969. The program cost distribution is presented in figure 6.5-2. The effect of launch rate on operations cost is presented in table 6.5-1 and the typical cost per flight for a 445-flight program is presented in table 6.5-2. The first unit cost for SERV itemized by WBS is shown in table 6.5-3.

6.6 PROGRAM COST BREAKDOWN

A typical breakdown of the SERV Shuttle Program cost is presented in figure 6.6-1; high cost areas are presented in table 6.6-1. The table identifies the high cost areas by WBS element, percentage of total program cost, and the cost drivers of the WBS element; all other elements have lower percentage costs. Note that the five RDT&E high cost areas identified account for 28.06 percent of the program cost and this represents 49 percent of the total RDT&E cost. (See figure 6.6-1.) Restated, five areas account for approximately 48 percent of the program RDT&E cost.
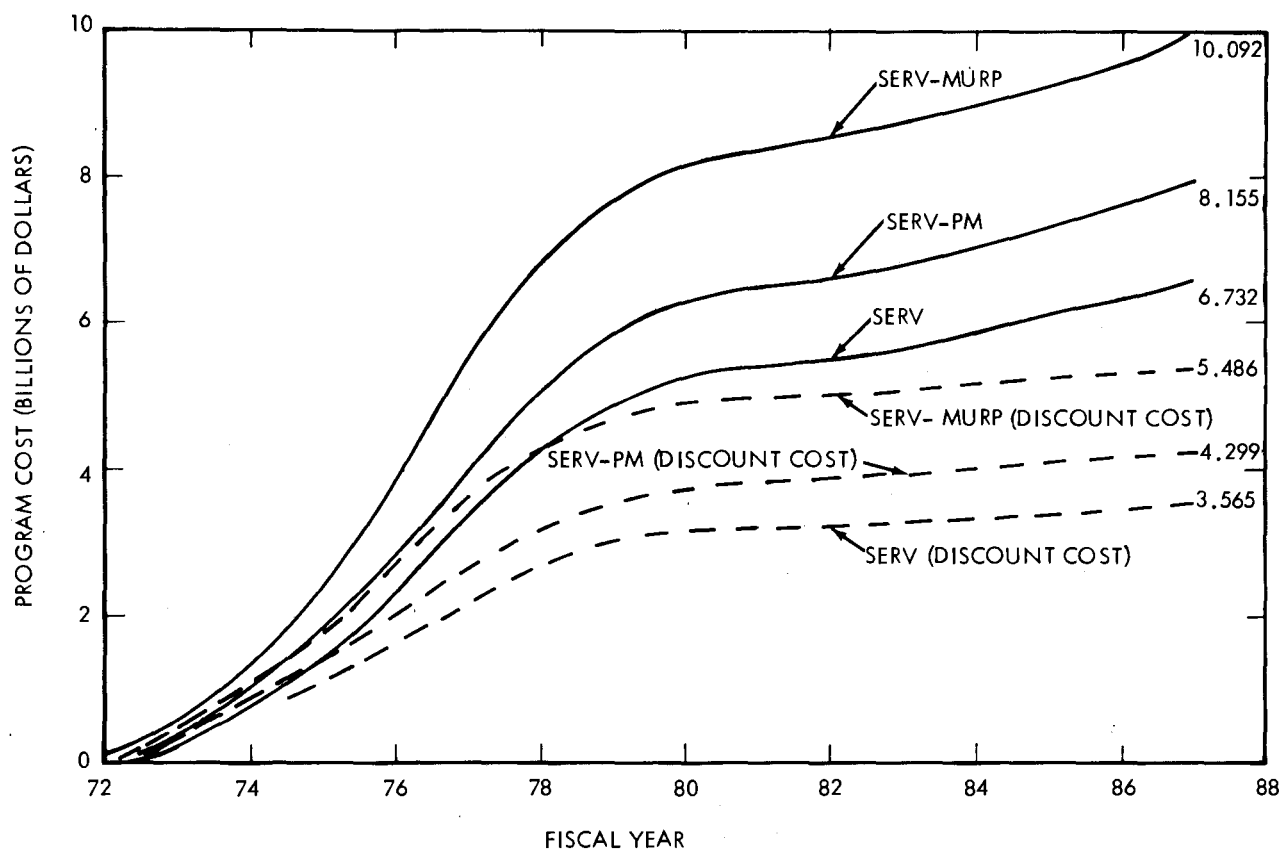
Figure 6.5-1. SERV Shuttle Program Cumulative Cost

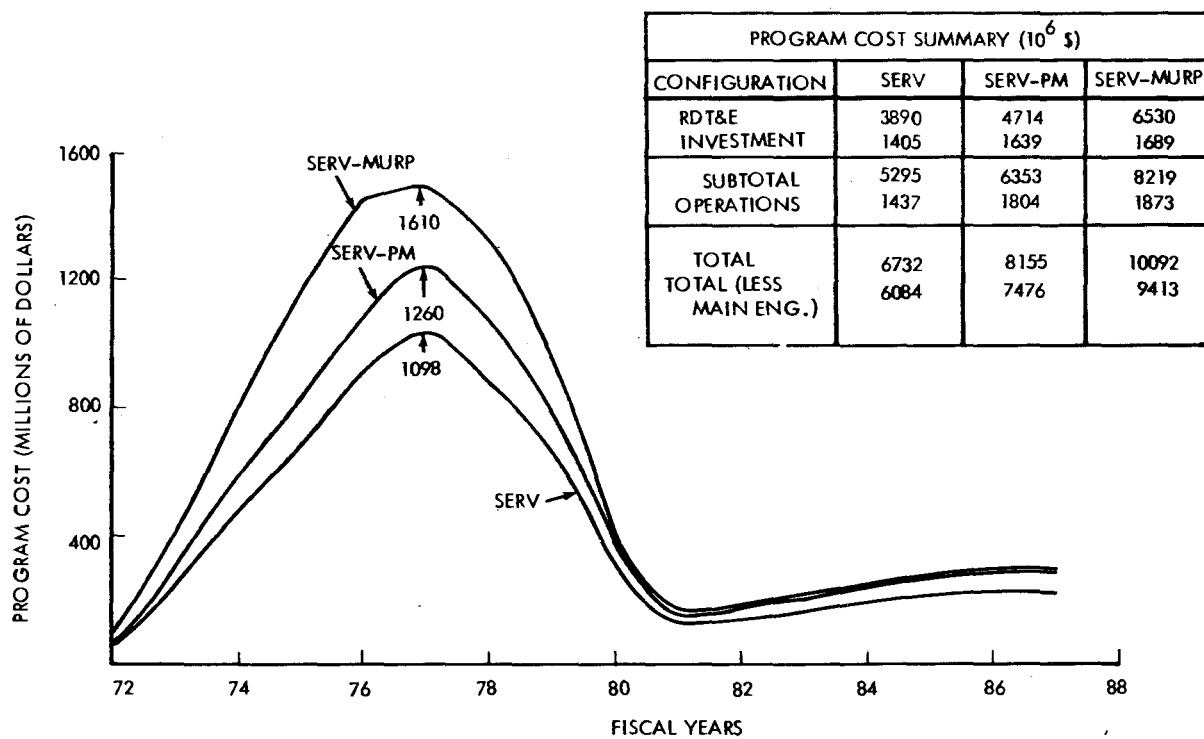| PROGRAM COST SUMMARY (10^6 $)			
CONFIGURATION	SERV	SERV-PM	SERV-MURP
RDT&E INVESTMENT	3890 1405	4714 1639	6530 1689
SUBTOTAL OPERATIONS	5295 1437	6353 1804	8219 1873
TOTAL TOTAL (LESS MAIN ENG.)	6732 6084	8155 7476	10092 9413

Figure 6.5-2. Program Cost Distribution

Table 6.5-1. Effect of Launch Rate on Operations Cost

NUMBER OF LAUNCHES IN LAST YEAR	TOTAL LAUNCHES IN TEN YEAR PROGRAM	TOTAL COST FOR 10 YEAR PROGRAM		TOTAL OPERATIONS COST PER FLIGHT	
		SERV-MURP	SERV-PM	SERV-MURP	SERV-PM
10	100	765.0	760.0	7.65	7.60
25	220	1147.8	1111.6	5.21	5.05
50	365	1615.5	1557.2	4.43	4.27
75	445	1873.9	1803.9	4.21	4.05

(MILLIONS OF 1971 DOLLARS)

Table 6.5-2. Typical Cost Per Flight

Typical Cost Per Flight (445-Flight Program)	SERV-MURP	SERV-PM
Operations	4.21	4.05
Fleet Amortization	0.86	0.83
Total ($M/FLT)	5.07	4.88

(Millions of 1971 Dollars)

Table 6.5-3. SERV First Unit Cost

WBS Item		Totals
Propulsion		
Aerospike Engine	60.0	
Lift Engines	29.5	
Attitude Control	8.5	
		98.0
Avionics		
Guidance and Navigation	8.0	
Instrumentation	5.6	
Communications	1.4	
		14.8
Airframe		
Structures and TPS	202.0	
Landing	1.0	
		203.0
Power		
Electrical	22.7	
Hydraulic and Pneumatic	2.1	
		24.8
Assembly and Checkout		9.5
First Unit Cost Total		350.1

(Millions of 1971 Dollars)

RDT&E
58 PERCENT
($4714M)

OPERATIONS
22 PERCENT
($1804M)
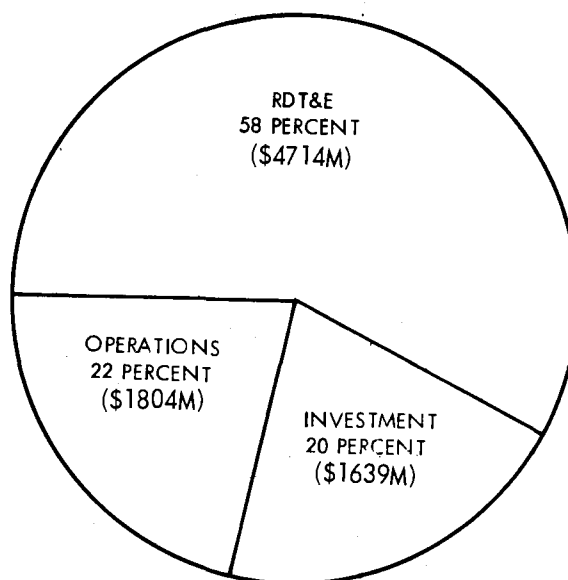
INVESTMENT
20 PERCENT
($1639M)

Figure 6.6-1. Typical Breakdown of SERV Shuttle Program Cost

Table 6.6-1. SERV Shuttle Program High Cost Areas

Area	Percentage of Total Program Cost	Cost Drivers
SERV Flight Test - RDT&E	8.21	Months in flight test program, number of test flights, test hardware.
Structures - RDT&E	7.58	Development of sandwich fabrication, EBW welding and non-destructive testing techniques.
Main Engines - RDT&E	6.82	Engine thrust, chamber pressure, specific impulse.
Structures - Investment	4.20	Fabrication of sandwich.
Ground Test - RDT&E	3.19	Structural testing, hot firing, wind tunnel testing.
Program System Engr - RDT&E	2.26	Engineering support to integration and development activities.

Section 7

CONCLUSIONS AND RECOMMENDATIONS

7.0 GENERAL

The study objectives were accomplished as follows:

- An appropriate SERV configuration has been selected.
- The feasibility of the SERV aerospike engine has been determined.
- Definitive design and weight analyses have been performed.

7.1 VEHICLE CONFIGURATIONS

The study commenced with an initial baseline SERV-MURP configuration, as shown in figure 1.2-2. Through trade studies, wind tunnel model tests, and a definitive design analysis, the initial baseline was developed into the SERV hybrid configuration shown in figure 2.3-2 and this configuration is presented as a mature outgrowth of the initial SERV concept and sized to meet the requirements of a space station mission in accordance with the initial study ground rules.

7.2 FEASIBILITY ISSUE CONCLUSIONS

The potential of SERV was shown in figure 1.3-1 to be keyed to six feasibility issues. Each of these issues has been examined and, within the limitations of the study, it is concluded that:

- The feasibility of aerospike performance for SERV application has been confirmed within the limitations of the cold flow tests.

- Key weight factors on which the success of an SSTO depends have been confirmed by structural and subsystem analyses.

- The ascent and reentry aerodynamic characteristics have been established by wind tunnel tests.

- The selected TPS consists of a honeycomb forebody shell (non-load-carrying) and a low-density elastomeric, ablative heat shield.

- SERV is controllable by differential throttling during ascent and stable throughout descent from deorbit to touchdown.

- A 4-mile target radius at the 25,000 ft landing interface is adequate with suitable position update 240 sec prior to deorbit, and again when emerging from the blackout zone.

- An automatic landing principle with turbojet lift engines is feasible.

In addition to the above conclusions on the key feasibility issues, the following supporting conclusions were determined:

- A capability for intact abort and abort for crew survival has been identified.

- Manufacture at MAF and launch from KSC is feasible with minimal facility change.

7.3 RECOMMENDATIONS

This study has shown the influence of structural and subsystem weights on SSTO performance and further in-depth investigation of SERV should be undertaken in the critical areas as follows:

- Configuration external shape, internal arrangement, and subsystems should be further optimized to reduce GLOW.

- Alternate methods of construction should be considered, with particular reference to the influence of thermal gradients and the weight integration of non-load-carrying TPS with the primary structure.

- All subsystem weights should be substantiated by increased depth of analysis.

- The reentry and landing concept should be examined in greater depth, including integration of Apollo reentry techniques and performance of detailed hardware error and trajectory perturbation analyses.

It is also recommended that the aforementioned in-depth investigation be supported by further studies of the integral aerospike engine and direct lift turbojet engines.

7.4 STUDY LIMITATIONS

The basic study approach was directed toward establishing SERV concept feasibility and the most significant conclusions are not affected by any study limitations. However, two limitations are worth noting:

- As the study progressed, it became evident that the study ground rules were not all applicable nor advantageous to a

SSTO which requires a different method of operation to that of a two-stage concept. For example, the most restrictive limitation was the identification of a MURP-size winged orbiter (spacecraft) as an alternate payload. A smaller and lighter spacecraft would result in a smaller SERV; SERV does not require a winged spacecraft as large or as heavy as the MURP.

- The influence of the turbojet lift engine performance has an important influence on vehicle landed weight and it is essential that more definitive data, supported by appropriate wind tunnel tests, be provided in support of further study effort.